

Motion Correction in Magnetic Resonance Imaging Using the Signal of Free-Induction-Decay

THÈSE N° 6963 (2016)

PRÉSENTÉE LE 6 JUIN 2016

À LA FACULTÉ DES SCIENCES DE BASE

LABORATOIRE LEENAARDS-JEANTET D'IMAGERIE FONCTIONNELLE ET MÉTABOLIQUE

PROGRAMME DOCTORAL EN GÉNIE ÉLECTRIQUE

ÉCOLE POLYTECHNIQUE FÉDÉRALE DE LAUSANNE

POUR L'OBTENTION DU GRADE DE DOCTEUR ÈS SCIENCES

PAR

Maryna Volodimirivna WASZAK

acceptée sur proposition du jury:

Prof. D. Van De Ville, président du jury
Prof. R. Gruetter, Dr G. Krüger, directeurs de thèse
Dr M. Zaitsev, rapporteur
Prof. M. Stuber, rapporteur
Prof. J.-Ph. Thiran, rapporteur



ÉCOLE POLYTECHNIQUE
FÉDÉRALE DE LAUSANNE

Suisse
2016

Für alle Bären dieser Welt.

Acknowledgement

From Alessandro Daducci I got the one important piece of information that there might be an open PhD position at the so called 'Siemens group' at the CIBM if not because of him I would have never known and of course have never written to Gunnar Krueger asking about that opportunity - thank you Alessandro for that. Gunnar Krueger was very fast at replying to my request and we met already only couple of days later. He invited me to come to introduce myself at a group meeting and a month later I have started to work on this project. Gunnar was very supportive in most of my ideas during this work but also guided me through them such that I wouldn't lose my focus. I would like to also thank Tobias Kober for showing to me how to operate the scanner and the art of IDEA programming and introducing me to the world of motion correction. I am grateful to you, Bénédicte Maréchal, for being such a great role model – a woman, mother, an engineer and a successful researcher - I hope I will be able to reach up to your standards. Thanks to you Alexis Roche I am now a bit more knowledgeable in statistics and know that there is more in life reaching significance. Tom Hilbert, you helped me during my first steps in ICE programming and were always there when I had troubles accessing the servers. Moreover, your head was the best for testing my motion correction sequence I wished all subjects' heads were more like yours. Cristina Granziera – you introduced me to the delicious Italian wines and cuisine and also entrusted me to watch over your wonderful daughters. Pavel Falkovskiy, I could always rely on you when it came to the numerous tests of our motion correction sequence. It is a pleasure to know you as colleague and a friend. Davide Piccini through you I learned that there are more body parts that can be visualized by MRI. Thank you for your efforts of fostering collaboration between the 'cardiac people' and the 'Siemens group' by organizing the cross team meetings. Guillaume Bonnier you have shared your precious patient data with me, thank you for listening to my motion correction problems. You had always some suggestions which were out of the box. Thank you Kieran O'Brien for being a constant motivation to do some sports during the lunch breaks and healthy eating culture. Mário João Oliveira, thank you for being such a patient colleague and subject. You never said no to a scan although I never managed to run my sequence on you. Pascal Forny and Théo Galy-Fajou, you were not only great interns but also awesome subjects even though I sometimes had problems fitting all your hair Théo into the head coil :).

I am grateful to you, Rolf Gruetter, for kindly agreeing to be my thesis director even though your time is scarce through having to look after so many PhD students. Thank you Reto Meuli for not only providing the funds for this work but also together with Malik Babaker and Frank Tobalem the expertise in advising me from a medical perspective. Meritxell Bach, I would like

Acknowledgements

to thank you for sharing your expertise on how to write an ethics application and getting it approved easily.

Alexander Loktyushin, I would like to thank you for our great collaboration. I enjoyed working with you. That is how science can be great fun when it allows to meet people like you. Dylan Tisdall and Andre van der Kouwe, it was a great pleasure discussing with you one of my projects. I am grateful to you for sharing your experience with me.

Michael Herbst, Maxim Zaitsev, and Benjamin Knowles thank you guys for our fruitful collaboration. I always enjoyed coming to your site in Freiburg.

Onur Afacan, Burak Erem it was fun collaborating with you. I hope our project will be continued also after my graduation.

Last but not least I would like to thank my husband, friend and life companion Sebastian Waszak.

Lausanne, March 6, 2016

M. W.

Abstract

Magnetic resonance imaging (MRI) is highly susceptible to subject's motion and can significantly degrade image quality. In brain MRI exams, involuntary head movements can affect the sampled k-space data. Such unintended alterations may result in visible image artifacts such as blurring, ghosting and others, and therefore potentially disqualify the image from diagnostic purposes. Methods to characterize motion in order to mitigate its impact on image quality exist and range from MR sequence based techniques to scanner independent tracking systems. Although, many motion detection and correction strategies have been proposed in the past, a universal solution to the problem does not exist yet. The work of this thesis was focused on the exploitation of the motion information from a multi-channel Free Induction Decay Navigator (FID) to develop and to optimize motion detection and correction methods in structural brain MRI. After a short introduction to the motion problem in MRI the fundamental methodology behind FID based motion detection is presented and used in this thesis. Considerable work has already been done in the field of motion correction for MRI that is summarized by reviewing the most recent literature, which allowed to reveal some pitfalls in the present approaches and to demonstrate the motivation behind an FID-based method for motion correction in MRI. The first study was conducted to demonstrate that substantial motion information is contained in the multi-channel FID signal, whereby the FID signal is correlated with motion parameters that were obtained from a highly accurate optical tracking system. This work was able to confirm the theoretical foundations from the Biot-Savart law, however, also revealed that a pure FID-based method is not sufficient to exactly calculate the underlying motion trajectory. It is speculated that scanner and subject related information might lead to a closed form solution, yet it was not possible to derive one due to a high dimensionality of the motion problem. Therefore, two alternative approaches were developed to utilize the FID signal for motion detection and correction in MRI. First, a prospective motion correction strategy for an MP-RAGE sequence is demonstrated, whereby the FID signal is used to trigger a prospective motion correction mechanism. The second alternative approach describes how the FID signal can be used to evaluate the quality of an already acquired image and how the FID signal can be used as an optimizer for an autofocusing based retrospective motion correction technique.

Key words: Structural MRI, FID navigator, motion detection, motion correction

Zusammenfassung

Magnetresonanztomographie (MRT) ist sehr anfällig für Bewegung, wodurch die Bildqualität erheblich beeinträchtigt werden kann. Unwillkürliche Kopfbewegungen während einer MRT-Untersuchungen können sich negativ auf die gesammelten Daten auswirken. Solche unbeabsichtigte Inkonsistenzen im k-Raum können als Bildartefakte wie Unschärfe oder Geisterbilder in Erscheinung treten und das Bild von Diagnosezwecken disqualifizieren. Methoden, um Bewegung und ihre Auswirkungen auf die Bildqualität zu mindern, existieren und reichen von MR basierten Techniken zu sequenz- und scannerunabhängigen Trackingsystemen. Obwohl viele Bewegungserkennungs- und Korrekturstrategien in der Vergangenheit vorgeschlagen worden sind, ist eine universelle Lösung für das Problem noch nicht in Sicht. Diese Arbeit konzentrierte sich auf die Ausschöpfung der Bewegungsinformation eines Mehrkanal-FID-Navigators (FID) mit dem Ziel eine entsprechende Methode zu entwickeln, um Bewegungserkennungs- und Korrekturverfahren in struktureller MRT zu optimieren. Nach einer kurzen Einführung in die Problematik von Bewegung in der Magnetresonanztomographie, wird die Methodologie der FID-basierten Bewegungserkennung dargestellt, welche dieser Arbeit zur Grunde liegt. Substanzielle Arbeit auf dem Gebiet der Bewegungskorrektur in der MRT wurde bereits durchgeführt, die wir durch eine Betrachtung der neuesten Literatur sowie einiger erwähnenswerter, bereits etablierter Methoden präsentieren. Dies ermöglichte einige Fallstricke in den vorliegenden Ansätzen zu offenbaren und die Motivation für die Verwendung der FID-basierten Methode darzulegen. Um zu zeigen, dass beträchtliche Bewegungsinformation in dem Mehrkanal-FID-Signal enthalten ist, wurde eine Studie durchgeführt, in der das FID-Signal mit Bewegungsparametern korreliert wurden, die von einem hochgenauen optischen Trackingsystem stammen. Diese Studie hat es ermöglicht die Theorie zu bestätigen, aber auch gezeigt, dass nur das FID-Signal alleine nicht ausreicht, um die Bewegungsparameter exakt zu bestimmen. Es kann spekuliert werden, dass scanner- und sequenzabhängige Informationen zu einer analytisch geschlossenen Lösung führen können, aber es war noch nicht möglich solch eine Lösung zu präsentieren. Daher wurde untersucht wie das FID-Signal auf eine andere Art verwendet werden kann, um Bewegung in der MRT zu detektieren und zu korrigieren. Es wurde eine prospektive Bewegungskorrekturstrategie für eine MP-RAGE-Sequenz vorgeschlagen, wo die FID-Signale verwendet werden, um einen Bewegungskorrekturmechanismus zu triggern. In einem anderen Ansatz wird vorgeschlagen die FID-Signale als Qualitätsmaß für bereits akquirierte Bilder zu verwenden. Ausserdem konnte gezeigt werden, dass das FID-Signal auch zur Optimierung eines retrospektiven Bewegungskorrekturverfahren verwendet werden kann.

Acknowledgements

Stichwörter: Strukturelle MRT, FID-Navigator, Bewegungsdetektion, Bewegungskorrektur

Contents

Acknowledgement	i
Abstract (English/Deutsch)	iii
Contents	vii
List of figures	xi
List of tables	xiii
1 Preface	1
1.1 Objectives and Overview of this Thesis	1
1.2 Main Contributions	2
2 Introduction	3
2.1 Free Induction Decay and Motion	3
2.2 Motion Effects in Magnetic Resonance Imaging	5
2.3 Clinical Impact of Motion in MRI	6
3 State of the Art and Problem Statement	7
3.1 Prospective Motion Correction	8
3.2 Retrospective Motion Correction	10
3.3 Problem Statement and Motivation	11
4 Accuracy and Precision of Head Motion Information in Multi-Channel Free Induction Decay Navigators for Magnetic Resonance Imaging	13
4.1 Introduction	14
4.2 Methods	15
4.2.1 Motion and FID Signals	15
4.2.2 Experimental Set-Up and Data Acquisition	17
4.3 Results	18
4.3.1 FID Navigator Signal-to-Noise Ratio and Steady-State	18
4.3.2 Accuracy and Precision of Motion Prediction Based on FID Navigator Data	19
4.3.3 FID Navigator Signal Stability	21

Contents

4.3.4	The Ability of the Linear Model to Extrapolate Between Different Motion Types	23
4.3.5	Minimal Training Data Requirements	25
4.3.6	Inter-Scan and Inter-Subject Model Differences	27
4.4	Discussion	28
4.4.1	Prediction Accuracy of the Multi-Channel FID Navigator	28
4.4.2	FID Navigator Signal Stability	29
4.4.3	Advantages and Limitations of the FID Navigator Approach	29
4.4.4	Future Work	31
4.5	Acknowledgement	32
5	FID-based Motion Sensitive Quality Metric and Retrospective Motion Correction for Clinical Magnetic Resonance Images	33
5.1	Introduction	33
5.2	Methods	35
5.2.1	Data Acquisition	35
5.2.2	Retrospective Motion Correction	35
5.2.3	Qualitative Image Quality Assessment	36
5.2.4	FID-Based Motion Detection	37
5.3	Results	39
5.3.1	Prevalence and Nature of Motion Artifacts in the Collected Data	39
5.3.2	Image Quality Before and After Correction	39
5.3.3	FIDnav Based Quality Metric Design	40
5.3.4	FIDnav Based Motion Classification Based on k-space Location	44
5.4	Discussion	45
5.4.1	Advantages and Limitations of the Utilized Motion Correction	45
5.4.2	Advantages and Limitations of FIDnav-Based Motion Detection	46
5.4.3	Future Work	47
5.5	Acknowledgement	47
6	Prospective Head Motion Correction with FID-Triggered Image Navigators	49
6.1	Introduction	49
6.2	Methods	51
6.2.1	FIDnav Acquisition and Calculation	51
6.2.2	MP-RAGE Data Acquisition and Experimental Design	53
6.2.3	IMGnav Acquisition and Image Registration Accuracy	54
6.2.4	Quantitative Image Quality Assessment	56
6.3	Results	57
6.3.1	IMGnav and Its Registration Accuracy	57
6.3.2	FIDnav, Triggering Events, and Detected Motion	58
6.3.3	Quantitative Assessment of Image Quality Improvements after Motion Correction	63
6.3.4	Effect of Reacquisition on Image Quality	64

6.4	Discussion	65
6.4.1	Registration Accuracy of IMGnav	65
6.4.2	FIDnav Triggered Motion Detection and Correction	66
6.4.3	Advantages and Limitation of the Proposed Motion Correction Method	67
6.4.4	Future Work	68
6.5	Acknowledgement	68
7	Host Sequence Influence on FID Signal	69
8	Outlook and Conclusion	73
8.1	Direction for Future Research	75
8.2	Conclusion	77
	Bibliography	85
	Curriculum Vitae	87
	Publications	89

List of Figures

2.1	FID navigator signal formation	4
2.2	Multi-channel head coil and symbolic depiction of FID signal reacting to motion	4
2.3	Effect of motion on image quality	5
3.1	Publication trend over the past years	8
3.2	Overview of external hardware based correction methods	9
3.3	Overview of MR based correction methods	9
3.4	Overview of retrospective correction methods based on dedicated sampling strategies	10
4.1	FID signal steady-state	20
4.2	Translational and rotational motion parameters as captured by the camera system from a subject scan	21
4.3	Accuracy and precision of FID based motion prediction	22
4.4	Correlation plot of FID predicted vs. true motion parameters	22
4.5	Motion prediction error for all subjects and scans individually	23
4.6	FID navigator signal from a subject at rest and a phantom	24
4.7	Closed up depiction of FID predicted breathing motion	25
4.8	Training and validation blocks	26
4.9	Prediction error for different motions patterns for training	26
4.10	Prediction reliability for different training data (number of samples, motion magnitudes)	27
5.1	Motion artifact prevalence in clinical data	39
5.2	Expert rating results of clinical data	40
5.3	Retrospective motion correction results of clinical data	41
5.4	FID signal change for different motion severity	42
5.5	ROC curves for different FID based motion detectors	42
5.6	ROC curves for FID signal standard deviation when used as motion detector	43
5.7	ROC curves for different modifications of and FID based detector	44
5.8	ROC curves for FID-based motion detectors with different k-space location weightings	45
5.9	Logistic regression for FIDI	45
5.10	FIDI and QI with their respective thresholds	46

List of Figures

6.1	Symbolic depiction of the proposed prospective motion correction strategy . .	54
6.2	IMGnav acquisition pattern	55
6.3	IMGnav and its registration reliability	57
6.4	Different FID navigators with detected motion events	59
6.5	Prospective motion correction results from experiment A	61
6.6	Prospective motion correction results from experiment B	62
6.7	Quantitative evaluation of motion correction results	63
6.8	Image correction results with and without reacquisition	64
6.9	Quantitative motion correction results with and without reacquisition	64
7.1	FID navigator signal change influenced by the host sequence	70
7.2	FIDnav signal magnitude change in a single coil element for a phantom and human scan	71

List of Tables

4.1	Model input variants with and without the temporal component that have been tested.	16
4.2	Acquisition parameters.	17
4.3	SNR and prediction power of the FIDnav.	19
5.1	Data overview	36
6.1	Data set acquisition variants	55
6.2	Summary of all acquired data	60
7.1	Acquisition parameters.	70

1 Preface

1.1 Objectives and Overview of this Thesis

Magnetic resonance imaging (MRI) is widely used in clinics to visualize the human body noninvasively. Although, this imaging modality has many advantages in comparison to other techniques as X-ray, computed tomography or ultrasound it poses some challenges to the clinical routine as well. One of the major limitation of the technique is its acquisition time and with it the high susceptibility to subject motion. Motion during an MRI examination leads to artifacts and may degrade the image quality to a non-diagnostic level. In this thesis it was investigated how the problem of motion can be tackled for head scans with the use of a very simple MR signal - the free induction decay (FID) when acquired with a multi-channel head coil array. The structure of the thesis is as follows.

Chapter 1 provides an overview of the thesis and summarizes its main contributions.

Chapter 2 gives a general introduction. First, the FID signal is explained and how it can be used as the so called multi-channel FID navigator. Second, the effect of motion in MRI is described and lastly the problem of motion in clinical MRI is presented.

Chapter 3 reviews the literature in the field of head motion correction in MRI and states the current problems in the field, which motivates the use of the FID navigator.

Chapter 4 describes the relationship between head motion and a multi-channel FID signal. Here, the results of a study are presented where the multi-channel FID signals are correlated with motion parameters from a highly accurate optical motion tracking system.

Chapter 5 presents a use of the FID signal as means for detection of motion corrupted images. An FID based image quality metric is proposed and its performance is validated on a clinical data set where the images were rated by expert radiologist. Further, the results of a retrospective motion correction method based on autofocusing combined with the FID signal information are shown.

Chapter 6 describes a technique for prospective motion correction utilizing the FID signal for motion detection. The FID signal is used here to trigger the acquisition of a low resolution imaging navigator for obtaining the motion parameters through image registration. Brain volume segmentation results as well as an automated quality index were used as a quality metric for images before and after correction.

Chapter 7 presents a study on how the host sequence influences the FID-signal and what implications it might have on FID based motion detection methods.

Chapter 8 summarizes the thesis and provides a conclusion and an outlook on future work and investigations.

1.2 Main Contributions

The main contributions of this thesis are:

- Implementation of the FID navigator acquisition module in a gradient-echo and in an MP-RAGE sequence.
- Demonstration of the relationship between head motion and a multi-channel FID signal. Results were published in Babayeva et al. (2013) and Babayeva et al. (2015b).
- Investigation of the potential of the FID signal to be used for a retrospective motion correction method based on autofocusing. Results were published in Babayeva et al. (2014b) and Loktyushin et al. (2015a).
- Presentation of a novel use of the FID signal to derive a quality index for motion artifacts.
- Presentation and implementation of an FID-based prospective motion correction technique for MP-RAGE sequences. Results were published in Babayeva et al. (2014a) and Babayeva et al. (2015a).

2 Introduction

In this chapter the necessary basics of magnetic resonance signal and image formation are described. The focus is put on the topics which are considered relevant for understanding the problem of motion in magnetic resonance imaging (MRI) as well as the free induction decay (FID) signal as a tool to tackle it. For further reference and for a detailed description of physical phenomena and notation behind MR physics the reference to the books by Haacke et al. (1999) and McRobbie et al. (2006) is proposed.

2.1 Free Induction Decay and Motion

The free induction decay (FID) signal is the basic signal in MRI (Haacke et al., 1999). It is created by flipping the magnetization towards the transverse plane and is measured by a receive coil which is sensitive to magnetization perpendicular to the main magnetic field B_0 of the scanner. The strong B_0 field aligns the magnetic moment of the protons in the body of a subject. To generate an MR signal, a pulse is generated by a radio frequency (RF) field and tuned to the resonance frequency of a proton. The RF pulse is briefly applied forcing the nuclei to flip their spins. After the RF field is turned off, the magnetization of the protons returns to its initial state, where it aligns again with the B_0 field. This process is called relaxation and is called the free induction decay. This signal can be measured again with an RF receive coil. This transverse magnetization oscillates at the Larmor frequency and its magnitude decays rapidly in form of an exponential as shown in Fig. 2.1.

In accordance with the Biot-Savart law the relationship between the magnetic field B generated by an electric current I in a thin wire is proportional to the position \mathbf{r} as shown in Eq. 2.1 (taken from Haacke et al. (1999)) with $d\mathbf{l}$ being the vector differential along the wire and μ_0 being the magnetic permeability constant. Or according to the principle of reciprocity

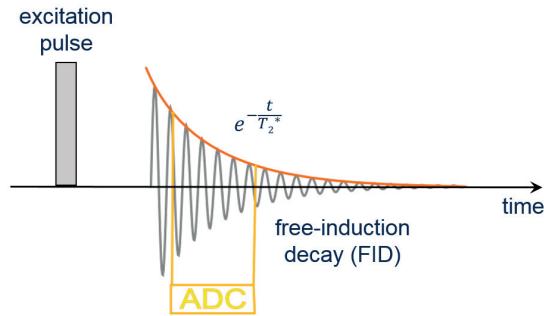


Figure 2.1: The FID signal can be picked up by an analog digital converter (ADC) which measures the voltage in a receiver coil. The measured voltage magnitude decays with a T_2^* damping. The FID signal is induced by an excitation pulse also called radio frequency (RF) pulse.

the current in a wire is proportional to the magnetic field.

$$B(\mathbf{r}) = \frac{\mu_0}{4\pi} \int_{wire} \frac{I d\mathbf{l} \times \mathbf{r}}{|\mathbf{r}|^3} \tag{2.1}$$

When we apply the law of Biot-Savart to MR that means that the signal magnitude of the FID depends on the distance of the measured object from the receiver coil element. Nowadays, so called multi-channel coil arrays are used for MR imaging and with sufficiently many coil elements positioned around the object of interest it should be theoretically possible to determine the displacement of this object within the coil array.

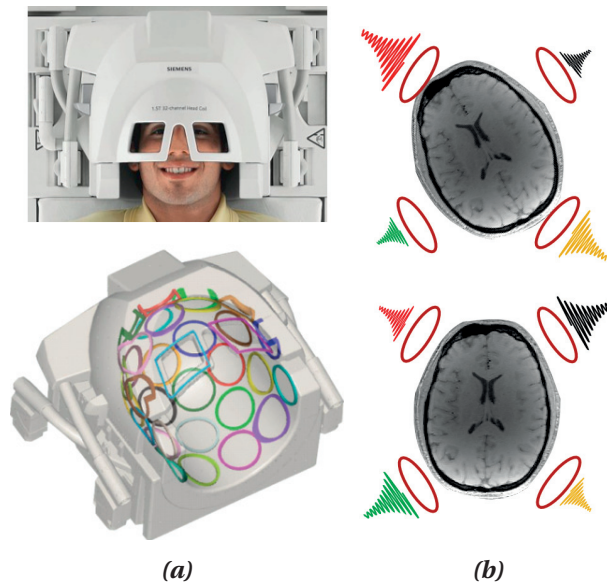


Figure 2.2: a: A multi-channel head coil with 32 coil elements (courtesy of Siemens). b: FID signal changes with respect to its position within a multi-channel coil array.

2.2 Motion Effects in Magnetic Resonance Imaging

To obtain a spatially encoded MR image, one of the orthogonally oriented gradients alters the static magnetic field, such that the resonance frequency of the protons varies with position and only protons in one layer (slice) are in resonance and can be flipped by the RF field. Shortly after the RF excitation, another gradient is turned on. This induces a controlled dephasing of the spins in a way that the precession phase of the proton spins is different at each line of the slice. This gradient is the phase encoding gradient. A third gradient is responsible for frequency encoding and makes the spins precess with different frequencies, such that again only the signal from the ones in resonance can be detected by the RF coils. From here, the origin of the MR signal can be recovered mathematically by means of its phase-frequency relationship and transformed into image space by applying an inverse Fourier transform to the acquired signal.

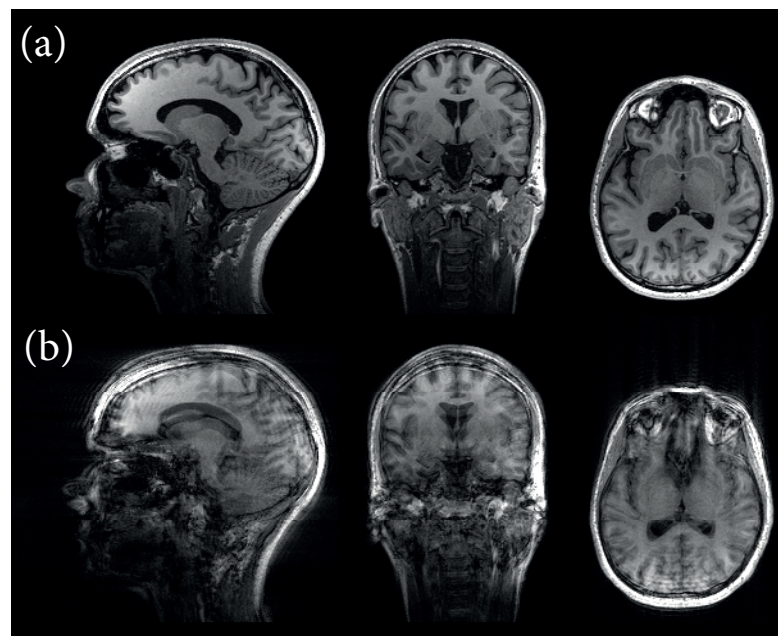


Figure 2.3: The effect of translational motion in the frequency encoding head-feet direction on image quality of an MP-RAGE sequence. *a*: motion free image *b*: translational motion causing blurring and ghosting artifacts in the image

The described principle relies on the assumption that the imaged object is rigid and its position does not change significantly during the acquisition. However, an MR scan can last from seconds to minutes, making this modality highly vulnerable to subject motion (Malamateniou et al., 2013). Especially elderly patients and children have difficulties to remain still throughout the procedure. Therefore, motion is the most common artifact cause in MRI (Erasmus et al., 2004) leading to increased diagnosis costs and patient stress, due to necessary repetition of the scan or even patient sedation.

As the final image is created by an inverse Fourier transform of the raw data, where a data point in image space corresponds to a weighted sum of all points in Fourier or k-space, motion causes data inconsistencies. This means that alteration of one data point in k-space results in changes of the whole image, manifesting themselves as image blurring, ghosting or contrast changes (Wood and Henkelman, 1985) (Fig. 2.3). Consequently, many motion correction strategies have been developed to minimize or eliminate motion artifacts. Besides of bulk subject motion, physiologic motion (cardiac and respiratory motion, peristalsis etc.) is another source of motion artifacts in MR imaging. However, the focus here is on correction of bulk motion of the patient's head.

2.3 Clinical Impact of Motion in MRI

Several extensive studies have been conducted to investigate the effect of motion in clinical MRI. Especially elderly and pediatric patient cohorts often experience an elevated level of distress and discomfort during the scan due to claustrophobia, anxiety and simply long scan times. This might lead to agitation and patient motion during the data acquisition procedure and affect the image quality such that a rescan or even patient sedation might be necessary.

In a study by (Maréchal et al., 2015) 764 clinical images have been reviewed by clinical experts and 1.7% have been identified to be unusable. Another large multicenter study reported that motion occurs in 40% of the medical examinations, in 10% being caused by motoric unrest of the patient leading to severely impaired image quality (Oberstein et al., 1990). Similar values of artifact occurrence in clinical MR scans were found in (Dantendorfer et al., 1997) where 12.8% of the images were motion corrupted and 6.4% had a non-diagnostic image quality. Thus, motion during MR examinations can be well considered to be the major source of image artifacts with substantial financial implications (Andre et al., 2015).

3 State of the Art and Problem Statement

Here, recently proposed motion correction techniques are reviewed based on published literature and its advantages and disadvantages are discussed in order to reveal the motivation behind the use of the FID signal to address the problem arising from bulk subject motion during an MRI acquisition.

In the past decades the number of publications addressing or discussing the problem of motion increased each year (see Fig. 3.1). The methods to mitigate motion artifacts range from MR signal based techniques to scanner independent (external sensor-based) tracking systems.

MR Signal Based Methods: Some sequence or acquisition-based methods sample the center of k-space in a redundant fashion to reduce the effects of motion. Other sequence dependent methods use so-called navigators, where additional MR signal, apart from imaging data, is acquired and subsequently utilized to obtain positional information. This information is used either prospectively to tie the scanner coordinate system to the subject during the measurement in order to make the sequence robust against motion artifacts or retrospectively, where the motion artifacts are corrected after acquisition. Most sequence-based techniques have in common that they increase the already long acquisition time, which is undesirable in a clinical context.

External Sensor-Based Techniques: External tracking systems are largely independent of the imaging sequence, thus the acquisition time is not affected. However, the use of additional hardware is needed, whose system components must be designed in an MR-compatible way, making it an expensive method. Also, calibration and set-up of the system, i.e., positioning of external markers, in the beginning of the scan may be an obstacle for the use in clinical applications.

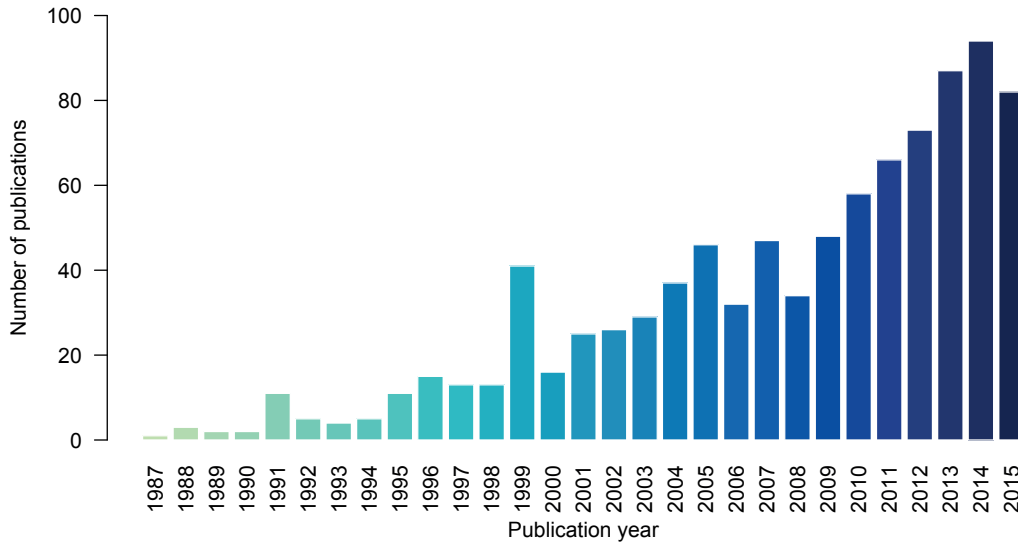


Figure 3.1: Number of publications by year as appeared on <http://www.ncbi.nlm.nih.gov/pubmed> (search was performed with the keywords 'motion correction mri' on Aug. 6th 2015). This list includes publications discussing rigid and non-rigid motion correction methods.

In the context of this thesis, we focus on structural brain imaging and for the purpose of this thesis work the motion will be approximated as rigid and described with three translational and three rotational parameters. Depending on the type of motion, **prospective** or **retrospective** correction strategies may be applied to reduce or to eliminate the artifacts. Through-plane motion is more difficult to compensate for and causes severe image distortions, whereas in-plane motion is less demanding and can be even corrected with image post-processing methods. The most adequate way to correct for through-plane motion is by means of prospective motion correction techniques, where the gradient coordinate system follows the moving subject during the whole acquisition.

3.1 Prospective Motion Correction

Prospective motion correction schemes are traditionally based on navigators (Tisdall et al., 2012), inter-volume (Thesen et al., 2000) or inter-slice (Kim et al., 1999) image registration or external tracking systems (Ooi et al., 2009; Peshkovsky et al., 2003; Qin et al., 2013). External optical tracking devices, where a marker is attached to the patient's head and is tracked by a camera (Aksoy et al., 2011; Herbst et al., 2012; Zaitsev et al., 2006), have a good tracking accuracy and can correct for motion in real-time (Fig. 3.2a and Fig. 3.2b). An external system, based on miniature RF coils, was also proposed recently (Ooi et al., 2013). Here, active markers in form of little coils are placed on the head of a patient and can be tracked with the scanner receive coils and gradients (Fig. 3.2c). Another, recently proposed motion

3.1. Prospective Motion Correction

correction technology is using field probes which are attached to subject's head to track its motion (Haeberlin et al., 2014) (Fig. 3.2d). Such systems provide sub millimeter accuracy and very good tracking speed.

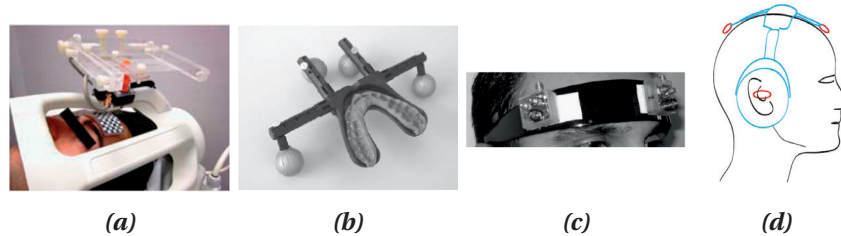


Figure 3.2: External motion correction tracking systems. *a:* In-bore camera and self-encoded marker (Aksoy et al., 2011) *b:* Retro-reflective markers with mouth piece (Zaitsev et al., 2006) *c:* Active markers (Ooi et al., 2009) *d:* Field probes (Haeberlin et al., 2014)

MR-signal based i.e., navigator techniques for prospective motion correction are also becoming increasingly popular and sophisticated. Numerous strategies with various complexity of the navigator have been proposed during the past years (Alhamud et al., 2012; Tisdall et al., 2012; White et al., 2010). Depending on its design, the navigator can provide different information about the occurred motion. The simplest one is the FID navigator (Kober et al., 2011), which monitors the center of k-space and is not spatially encoded. Nevertheless, this signal contains motion information and can be used to identify motion corrupted images and trigger a correction mechanism (Kober et al., 2012). The FID navigator was first proposed to reduce respiration- and system-induced B_0 shifts (Hu and Kim, 1994; Pfeuffer et al., 2002) and it was also used to correct for chest motion in abdominal acquisitions (Brau and Brittain, 2006). Spherical (Welch et al., 2002), Cloverleaf (van der Kouwe et al., 2006) or volumetric navigators (Tisdall et al., 2012) are able to provide exact motion parameters for translation and rotation and correct the coordinate system of the gradients for subsequent scans (Fig. 3.3). Such navigators are acquired during the scan and can detect and quantify motion in real-time.

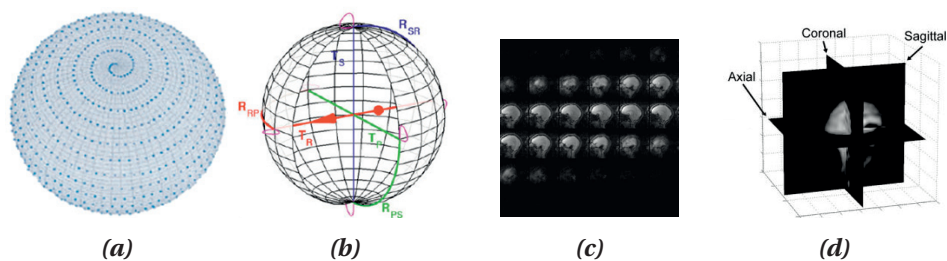


Figure 3.3: Navigator based motion tracking techniques. *a:* Spherical (Welch et al., 2002) *b:* Cloverleaf (van der Kouwe et al., 2006) *c:* vNAV (Tisdall et al., 2012) *d:* PROMO (White et al., 2010)

3.2 Retrospective Motion Correction

Retrospective methods are applied after raw data acquisition during image reconstruction. These correction schemes require information on the occurred motion, which is usually delivered by the images themselves or based on some motion tracking mechanism during the scan (e.g., navigators).

PROPELLER (Pipe, 1999) is a well-known self-navigating method and is routinely used in clinical scans. It collects data in k-space on concentrically rotated strips ('blades') of parallel lines (Fig. 3.4a). The redundant k-space information from the center, holding most of the image information, is exploited to conclude on the underlying motion to be able to correct for it. Another technique uses spiral-shaped sampling of the k-space to offer robustness against motion (Liao et al., 1997) (Fig. 3.4b). TRELIS (Maclaren et al., 2008) uses a similar approach as PROPELLER but it samples the k-space uniformly and uses the redundant parts of the 'blades' to correct for motion before image reconstruction (Fig. 3.4c).

A different class of retrospective correction is based on autofocusing where chunks of k-space data are adjusted such that an image based quality criterion i.e., cost-function is optimized (Atkinson et al., 1999; Loktyushin et al., 2013). Such methods have the advantage of not to require addition data and report adequate correction results for small motions. However, their capability of correction for small motions is limited and the computation times are still beyond clinical requirements.

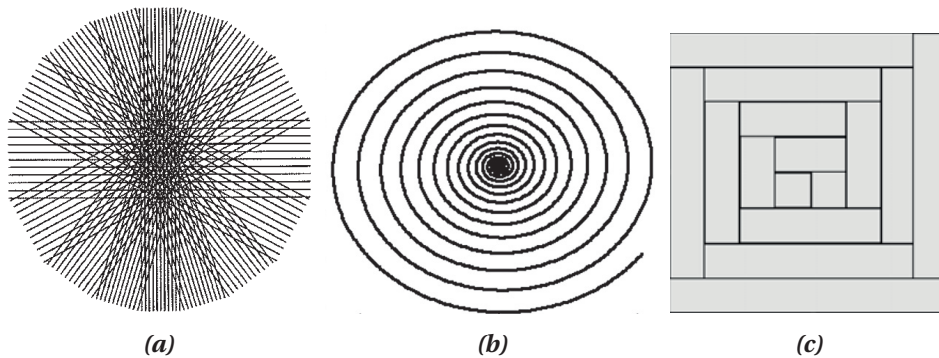


Figure 3.4: Retrospective motion correction strategies using different k-space sampling trajectories to make the acquisition more robust towards motion. a: PROPELLER (Pipe, 1999) b: SPIRAL (Liao et al., 1997) c: TRELIS (Maclaren et al., 2008)

3.3 Problem Statement and Motivation

Reducing motion sensitivity of MR imaging would be a great asset for clinical and research applications, increasing the efficacy of clinical studies as well as the patient throughput by avoiding rescans of motion corrupted data sets. Even though many motion correction strategies have been proposed and some of them are already used in clinical applications, fundamental limitations remain and no 'one-size-fits-all' solution could yet be found (Zaitsev et al., 2015).

Retrospective techniques as for example PROPELLER or TRELLIS approaches require long scan times due to redundant data acquisition, which is undesirable for clinical use. Also, retrospective correction techniques don't allow for thru-plane motion correction, thus the need for prospective strategies as MR sequence independent external tracking devices. They require, however, additional hardware, which is usually expensive, as it has to meet clinical standards and be able to operate at high magnetic field strengths. In addition to that, when a fiducial marker is used for tracking and placed on subject's skin, skin slippage can be an issue. Moreover, these approaches add to the complexity of an already elaborate MR scanner. Navigators, on the other hand, do not rely on additional hardware, and with their use it is possible to correct for motion prospectively. But still, additional scan time has to be sacrificed, as more data needs to be acquired only for motion tracking.

In the context of structural brain MRI, little successful work has been done to comprehensively detect and correct for subject motion using the MR signal. This is despite the fact that many of clinical scans are neuroimaging exams, most of them being structural MRI exams. The reason for this mismatch is based on two aspects: *a*) structural brain scans are performed with high spatial resolution (around 1 mm in-plane resolution or higher) and motion characterization needs to provide a precision greater or equal to half of the voxel dimension (Maclaren et al., 2013); *b*) the scan times are in the range of several minutes and the object is not repetitively imaged as in other methods such as EPI. Hence, due to already long acquisition times, additional scans for motion characterization are prohibitive in clinical scenarios.

To meet the stringent MR sequence and imaging requirements on timing and accuracy, the subject of this thesis is to explore in detail and to optimize a method for motion detection and correction, which utilizes a multi-channel FID signal. An FID acquisition is unpretentious in terms of timing requirements and can be easily added to any MR sequence, making it an attractive solution for the motion problem. It has been recently shown that motion can be reliably detected with an FID signal (Kober et al., 2011), however, no positional information can be provided by this method without relying on other means to extract the underlying motion parameters. Therefore, we propose to exploit the information of the FID signal when acquired by a spatially distributed multi-channel coil array and also to explore other means of obtaining the exact motion parameters.

4 Accuracy and Precision of Head Motion Information in Multi-Channel Free Induction Decay Navigators for Magnetic Resonance Imaging

This chapter was published in Babayeva et al. (2015b).

Abstract Free-induction-decay (FID) navigators were found to qualitatively detect rigid-body head movements, yet it is unknown to what extent they can provide quantitative motion estimates. Here, we acquired FID navigators at different sampling rates and measured simultaneously head movements using a highly accurate optical motion tracking system. This strategy allowed us to estimate the accuracy of FID navigators for quantification of rigid-body head movements. Five subjects were scanned with a 32-channel head coil array on a clinical 3T MR scanner during several resting and guided head movement periods. For each subject we trained a linear regression model based on FID navigator and optical motion tracking signals. FID-based motion model accuracy and precision was evaluated using cross-validation. FID-based prediction of rigid-body head motion was found to be with a mean translational and rotational error of 0.14 ± 0.21 mm and $0.08 \pm 0.13^\circ$, respectively. Robust model training with sub-millimeter and sub-degree accuracy could be achieved with 100 data points. The obtained linear models appeared to be subject-specific as inter-subject application of a 'universal' FID-based motion model resulted in weak prediction accuracy. The results show that substantial rigid-body motion information is encoded in FID navigator signal time courses. Although the applied method currently requires the simultaneous acquisition of FID signals and optical tracking data, the findings suggest that multi-channel FID navigators have a potential to complement existing MR and camera based tracking technology for accurate rigid-body motion detection and correction in MRI.

4.1 Introduction

Motion artifacts degrade the quality of MR images and may render them unsuitable for diagnostic purposes or automated post-processing methods as in, for example, automated brain segmentation (Maréchal et al., 2012). The implications of subject motion during an MR examination have been extensively studied ((Ehman and Felmlee, 1989; Erasmus et al., 2004; Gedamu and Gedamu, 2012; Malamateniou et al., 2013; Mortamet et al., 2009; Smith and Nayak, 2010), among others). Intuitively, shortened acquisition times will reduce the likelihood that motion occurs. However, despite substantial developments on faster acquisition methods, sequence design and new reconstruction techniques during the past decades, scan times still reach several minutes in clinical routine brain MRI protocols, leaving images susceptible to motion artifacts. To address this problem, numerous methods have been proposed to track subject motion and to reduce its consequential impact on image quality. These methods are applied either retrospectively or prospectively.

One class of retrospective correction methods mitigates motion artifacts through dedicated acquisition schemes (for example by oversampling the k-space center). These additional data allow an estimation of motion parameters as performed in the PROPELLER method and its variants (Johnson et al., 2011; Pipe, 1999). Such self-navigating techniques, however, reduce scanning efficiency due to inherent oversampling. Other, image-based correction strategies optimize a cost function which evaluates a specific image quality parameter (*e.g.*, sharpness) (Atkinson et al., 1997; Loktyushin et al., 2013; Manduca et al., 2000). Although these methods do not require redundant sampling and report good correction results for small motion, they have been shown to be of limited utility at greater motion amplitudes, have a high dependency on the employed cost function (McGee et al., 2000) and require computation times which are at present still beyond clinical requirements. Prospective motion correction schemes present a more challenging task from an engineering viewpoint; however, these schemes are of increasing popularity and have several advantages over retrospective techniques. They allow for real-time adjustments of the scanner gradients and RF system, thus enabling consistent sampling of the k-space in the presence of motion and suppress spin-history effects or signal dropouts. Such correction strategies are either based on MR navigators (Alhamud et al., 2012; Hess et al., 2011; Ordidge et al., 1994; Sachs et al., 1994; Thesen et al., 2000; Tisdall et al., 2012; van der Kouwe et al., 2006; Welch et al., 2002; White et al., 2010) or external tracking systems (Aksoy et al., 2011; Maclaren et al., 2012; Ooi et al., 2009; Peshkovsky et al., 2003; Qin et al., 2013, 2009; Zaitsev et al., 2006).

Current optical tracking systems have been demonstrated to provide excellent precision in the order of $10\mu\text{m}$ and 0.01° at high sampling rates (Qin et al., 2013), allowing for real-time and sequence-independent motion correction of rigid-body motion. It is noteworthy that all external tracking systems, however, require the integration of additional MR-compatible hardware and need to perform reliably in clinical routine, especially when used for prospective motion correction. Moreover, most of the currently existing MR-compatible optical tracking systems are based on tracking a fiducial marker which must be physically attached to the

body. This may compromise the clinical workflow and pose problems with patients who do not tolerate the markers. Additionally, any marker motion which is not correlated to the head motion for example due to face mimics will lead to motion artifacts.

MR-based navigator techniques, on the other hand, do not require dedicated hardware but use portions of the image data or acquire supplementary data to derive positional information of the examined body part during the MR acquisition. Numerous navigator strategies have been proposed during the past years that allow for the adjustment of the coordinate system of the gradients and excitation pulses in real-time (Brau and Brittain, 2006; Hu and Kim, 1994; Kober et al., 2012, 2011; Pfeuffer et al., 2002).

The simplest possible navigator acquisition is the free induction decay navigator (FIDnav), which monitors the MR signal without any spatial encoding. It was originally proposed to reduce B0-field fluctuations (Hu and Kim, 1994; Pfeuffer et al., 2002). It also proved useful for shimming (Splitthoff and Zaitsev, 2009) and for improvements in abdominal acquisitions (Brau and Brittain, 2006). Recently, the FID signals have been explored in more detail to qualitatively detect motion events and trigger correction mechanisms if the observed FIDnav signal exceeds an empirical threshold value (Babayeva et al., 2014a; Kober et al., 2012, 2011). In this work, we investigate the accuracy and precision of positional information contained in multi-channel FID navigators beyond the previously reported simple qualitative detection schemes.

4.2 Methods

4.2.1 Motion and FID Signals

Today, multi-channel coil arrays are routinely used in clinical MR imaging. These coils offer good coverage of the imaged object, enable the employment of parallel imaging strategies, and provide increased signal-to-noise ratio due to the close proximity of the coil elements to the object. We hypothesize that complex FID navigators (FIDnav) signal-time courses acquired with a receive coil array with a large number of channels can be used for motion tracking of a rigid body under the assumption of a sufficient spatial coverage of the imaged object. In the following experiments, we restrict our investigation to head imaging where the motion can be assumed to be rigid. We postulate that head motion is systematically related to changes in the multi-channel FIDnav signals. The position of the head in a three-dimensional space is denoted as a response variable $Y(t) \equiv (Y_1(t); Y_2(t); \dots; Y_6(t))$ for three translational and three rotational coordinates and different time points $t = 1, 2, \dots, T$. The position can be then expressed by a combination of FIDnav signals from different coil elements, *i.e.*, the explanatory variables with intercept as the first entry $X(t) \equiv (X_1(t); X_2(t); \dots; X_N(t))$ where N is the number of coil elements and X_c is the FIDnav signal as detected by a single coil element $c = 1, 2, \dots, N$. Hereby, the FIDnav signal at time t is a scalar value calculated from samples in a single read-out.

Chapter 4. Accuracy and Precision of Head Motion Information in Multi-Channel Free Induction Decay Navigators for Magnetic Resonance Imaging

$X \equiv (m_1^*, m_2^*, \dots, m_N^*)$
$X \equiv (m_1^*, m_2^*, \dots, m_N^*)$ and $\gamma t = 0$
$X \equiv (\phi_1^*, \phi_2^*, \dots, \phi_N^*)$
$X \equiv (\phi_1^*, \phi_2^*, \dots, \phi_N^*)$ and $\gamma t = 0$
$X \equiv (m_1^*, m_2^*, \dots, m_N^*, \phi_1^*, \phi_2^*, \dots, \phi_N^*)$
$X \equiv (m_1^*, m_2^*, \dots, m_N^*, \phi_1^*, \phi_2^*, \dots, \phi_N^*)$ and $\gamma t = 0$
$X \equiv (r_1^*, r_2^*, \dots, r_N^*)$
$X \equiv (r_1^*, r_2^*, \dots, r_N^*)$ and $\gamma t = 0$
$X \equiv (z_1^*, z_2^*, \dots, z_N^*)$
$X \equiv (z_1^*, z_2^*, \dots, z_N^*)$ and $\gamma t = 0$
$X \equiv (r_1^*, r_2^*, \dots, r_N^*, z_1^*, z_2^*, \dots, z_N^*)$
$X \equiv (r_1^*, r_2^*, \dots, r_N^*, z_1^*, z_2^*, \dots, z_N^*)$ and $\gamma t = 0$
$X \equiv (r_1^*, r_2^*, \dots, r_N^*, z_1^*, z_2^*, \dots, z_N^*, m_1^*, m_2^*, \dots, m_N^*, \phi_1^*, \phi_2^*, \dots, \phi_N^*)$
$X \equiv (r_1^*, r_2^*, \dots, r_N^*, z_1^*, z_2^*, \dots, z_N^*, m_1^*, m_2^*, \dots, m_N^*, \phi_1^*, \phi_2^*, \dots, \phi_N^*)$ and $\gamma t = 0$

Table 4.1: Model input variants with and without the temporal component that have been tested.

Different selections of points are considered and are described in detail in the Results section 4.3.1. The general form of the model is then $Y_j = f_j(X) + \epsilon_j$, where f_j is a regression function with a residual error ϵ_j in the j^{th} motion direction (translational and rotational motion parameters). We will investigate a linear model of the form $f(t)_j = \alpha_j + B_j X(t) + \gamma_j t$ for the estimation of the motion parameters Y . The time component t is added as an explanatory variable to account for possible linear, time-dependent signal changes of the FIDnav or the camera data with γ being its estimated contribution to the model. Furthermore, α is the intercept estimate and $B_j = (\beta_1^j, \beta_2^j, \dots, \beta_N^j)$ is a vector with β_c^j as the unknown model parameters for each of the channels c and motion directions j . The head position in the j^{th} dimension $Y_j(t)$ is then related to the FID signal $X(t)$ from N channels as follows:

$$\begin{pmatrix} Y_j(t_1) \\ \vdots \\ Y_j(t_T) \end{pmatrix} = \begin{pmatrix} 1 & X_1(t_1) & \cdots & X_N(t_1) & t_1 \\ \vdots & \vdots & \ddots & \vdots & \vdots \\ 1 & X_1(t_T) & \cdots & X_N(t_T) & t_T \end{pmatrix} \begin{pmatrix} \alpha_j \\ \beta_1^j \\ \vdots \\ \beta_N^j \\ \gamma_j \end{pmatrix} + \begin{pmatrix} \epsilon_j(t_1) \\ \vdots \\ \epsilon_j(t_T) \end{pmatrix}$$

We will evaluate the residual error ϵ_j for different model inputs X . To achieve this, FIDnav will be calculated from the complex FID signal as shown in Table 4.1 with

$$r_c^*(t) = \frac{(r_c(t) - r_{ref,c})}{r_{ref,c}}, z_c^* = \frac{(z_c(t) - z_{ref,c})}{z_{ref,c}},$$

$$m_c^*(t) = \frac{(m_c(t) - m_{ref,c})}{m_{ref,c}}, \phi_c^* = \frac{(\phi_c(t) - \phi_{ref,c})}{\phi_{ref,c}}$$

Parameter	3D GRE + FIDnav	FIDnav only
TR	25.0 ms	12.5 ms
TE	3.0 ms	3.0 ms
α	12°	8°
TA	6:07 min	6:11 min
Band width	240 Hz/Px	240 Hz/Px
Matrix (RO×PE×PAR)	256×256×144	n.a.
Voxel size	1.0×1.0×1.2 mm ³	n.a.
GRAPPA	×2, 24 ref. lines	n.a.
Field of view in phase	87.5%	n.a.
Slice partial Fourier	6/8	n.a.
Total number of FIDnav samples during the scan	1328	29568

Table 4.2: Acquisition parameters.

where the real and imaginary components or the magnitude and the phase of the complex FID signal s_c from a coil element c at any time point are given by $s_c = r_c + iz_c = m_c e^{i\phi_c}$ and were normalized using a complex reference signal from the beginning of the scan $s_{ref,c} = r_{ref,c} + iz_{ref,c} = m_{ref,c} e^{i\phi_{ref,c}}$. Note that only normalized signal changes, *i.e.*, relative to the reference position, were used for motion estimation. Both camera data and FIDnavs used the same point in time as reference. The exact time point will be defined in the section 4.3 ‘Results’.

Provided that X and Y are known, the model parameters α , β , and γ will be estimated through least-squares optimization. In the following investigations, we assume a linear relationship between the multi-channel FIDnav signal changes and the underlying rigid-body head movements as expressed in the definition of f_j . To assess the quality of the estimates we evaluate the mean absolute error (accuracy) and the standard deviation (precision) of the error ϵ_j . All calculations are performed using MATLAB (MathWorks, Natick, MA, USA).

4.2.2 Experimental Set-Up and Data Acquisition

To determine the model parameters α , β , and γ a sequence of experiments were conducted in which the subjects were instructed to perform different head movements inside the scanner. The FIDnavs were acquired and the motion was tracked simultaneously by an optical system comprising a spatially encoded retro-reflective marker and an in-bore camera (Maclaren et al., 2012). The tracking marker was placed on a customized mouth piece for rigid-coupling to the skull.

After obtaining written consent, five healthy volunteers were scanned at 3T (Magnetom Tim Trio, Siemens, Germany) using a 32-channel head coil array. Each subject underwent the acquisition of six scans per session of which four involved voluntary head motion. The

Chapter 4. Accuracy and Precision of Head Motion Information in Multi-Channel Free Induction Decay Navigators for Magnetic Resonance Imaging

subjects were instructed to perform a sequence of head movements consisting of four different motion patterns: nodding ('nod'), translation in the scanner z-direction ('z-tra'), head-shaking ('shake'), and drawing a virtual eight with the nose tip ('fig 8'). Motion periods of 20 s in duration were interleaved with 10 s periods without motion and were guided by commands using the intercom system of the scanner. This sequence of motion patterns was repeated three times during one scan. For two series with motion, a non-selective 3D gradient-echo sequence was modified such that one FIDnav was acquired after ten imaging excitations (3D GRE + FIDnav), *i.e.*, every eleventh TR or every 275 ms, corresponding to a sampling rate of 3.6 Hz. During each FID readout, 512 complex data points were sampled. Another two datasets were acquired with a protocol where solely the FID signal was sampled every TR without any additional gradients for image formation (FIDnav only), matching the sampling frequency of the optical system of 80 Hz in order to exploit the sampling capability of the FIDnav signal (see Table 4.2 for an overview). Also, in addition to RF-spoiling a spoiling gradient has been incorporated after each FID read-out to guarantee signal dephasing prior to the next RF-pulse. Finally, each of the subjects underwent an additional scan with both sequences where they were asked not to move. For this study the shimming condition was set only once in the beginning of the scanning session for each subject.

In addition, phantom scans were performed to observe the stability of the FID navigator signal in absence of physiological influences. Here, a spherical water phantom from Siemens (175 mm diameter; 1.25g NiSO₄ + 6H₂O per 1000g H₂O) was used and stabilized by padded head cushions inside the coil. The optical marker was attached to the phantom and tracked by the camera as in the human scans.

4.3 Results

4.3.1 FID Navigator Signal-to-Noise Ratio and Steady-State

One data point of the FIDnav signal intensity time course series from each coil element was calculated by taking the average of all 512 data samples from a single, spatially non-encoded read-out, to increase the signal-to-noise ratio of the FIDnav without any substantial loss in temporal resolution of the FIDnav data. The decision of averaging over the whole FID read-out was motivated by an initial evaluation where we compared the signal-to-noise ratio (SNR) of the FIDnav time course depending on the utilized read-out samples *i.e.*, samples from the beginning, the middle, the end of the read-out and the average over all points. SNR is hereby defined as the ratio between the mean of the signal over the whole time course and its standard deviation. This evaluation was based on the data from the phantom experiments. It was evident that taking the average over all points as well as taking only a single point from the beginning of the read-out samples provided the highest SNR value (see Table 4.3). A further evaluation of the volunteer motion prediction performance based on the used read-out samples showed that using the average over the whole ADC provided the best accuracy and precision and therefore motivated taking this setting for the FIDnav calculation.

read-out samples used for the FIDnav	SNR**	translation error [mm]***	rotation error [deg]***
	averaged over all coil elements r: real component z: imaginary component		
middle (215)	r: 206; z: 102	0.16±0.14	0.14±0.16
average over points 4 to 509	r: 268; z: 142	0.15±0.12	0.12±0.13
4 th sample point*	r: 257; z: 286	0.24±0.17	0.15±0.17
509 th sample point*	r: 106; z: 71	0.16±0.14	0.15±0.15

* The three first and last points of the read-out do not contain any valid information due to digital filter adjustments in the beginning and the end of the acquisition window

** Evaluation was done on phantom data from a single 3D GRE + FIDnav scan

*** Results from cross validation on data from a single 3D GRE + FIDnav scan from a moving subject

Table 4.3: SNR and prediction power of the FIDnav.

The FID read-out in our experiment takes approximately 4 ms and it can be assumed that during this time no significant positional changes of the head occur; therefore the reduction of all read-out samples to a single data point is justified. Furthermore, we assumed that no signal cancellation occurred, as could be caused by off-resonance, due to appropriate shimming.

The real and imaginary components as well as the magnitude and the phase of the complex FIDnav signal from a coil element were normalized using a reference signal from the beginning of the scan. The reference signal was calculated as the mean of all FIDnavs acquired during a 3 seconds time window starting after the steady-state was reached. Fig. 4.1 shows the magnitude of the FIDnav signal for one coil element and for two different acquisitions, where the FIDnav signal was acquired during a '3D GRE + FIDnav' sequence and where only the FIDnav signal was acquired during the scan.

Steady-state was considered as achieved when the signal changes *i.e.*, the partial derivative over time was less than 1%, which, according to Bloch simulations, occurs after approximately 4.1 seconds or 165 excitations in the modified gradient-echo case and after approximately 3.7 seconds or 296 excitations in the FID only acquisition. For matters of consistency, the first 5 seconds of all data sets were discarded from the evaluations.

4.3.2 Accuracy and Precision of Motion Prediction Based on FID Navigator Data

One third of the measurement was used to compute the model parameters α , β , and γ by performing a linear regression through least-squares optimization of FIDnav signals and camera data ('training'). The training period corresponds to 442 and 9856 data points for '3D GRE+FIDnav' and 'FIDnav only' acquisition, respectively. Subsequently, the model was validated by predicting the head motion parameters during the remaining 2/3 (4 minutes) of the measurement using the previously obtained model parameters ('validation', see Fig. 4.2). The training and validation was performed within each six-minute scan of the same subject.

Chapter 4. Accuracy and Precision of Head Motion Information in Multi-Channel Free Induction Decay Navigators for Magnetic Resonance Imaging

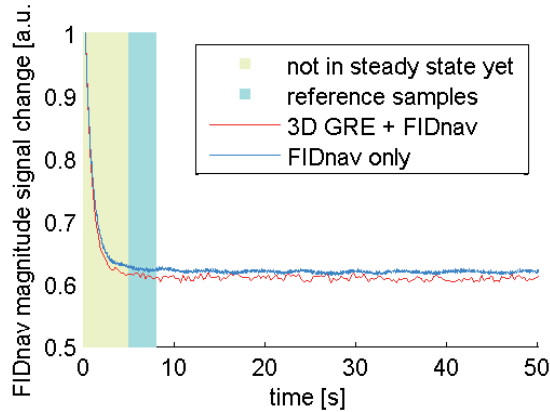


Figure 4.1: Normalized FIDnav signal magnitude time course from one subject acquired without voluntary motion for the first 50 sec of the scan. The first 5 seconds of the FIDnav prior to steady-state are discarded. The following 3 seconds of the signal in steady-state are taken as reference. The difference in the magnitudes can be explained by the different acquisition parameters with respect to repetition time and excitation angle in the 3D GRE+FIDnav acquisition and the FIDnav only acquisition.

The prediction accuracy and precision of the model was evaluated using 4-fold-cross-validation within one single scan (intra-scan) by shifting the training block to the beginning, middle, and the end of the same scan (I-III) as well as by choosing the training and validation data points at random (IV). Also, an inter-scan cross validation was performed by training the model with data from one scan and performing the validation on motion data from another scan but the same subject. The motion trajectories of one exemplary series with head motion as obtained from the camera system and the FIDnav time course of a single coil element are shown in Fig. 4.2. For the presented experiment, motion quantification with the camera system revealed translational and rotational motion up to 24 mm and 11° , respectively.

The validation over all subjects and scans showed that the linear model performs best when using the real/imaginary parts or the magnitude/phase of the FIDnav as model input among all tested input variants (Fig. 4.2). Such a model predicts the camera measurements for all six motion parameters with an overall translational and rotational mean accuracy and precision of 0.14 ± 0.21 mm and $0.08 \pm 0.13^\circ$ (Fig. 4.4). Notably, also for larger motion, the assumption of linearity between the FIDnav signal changes and the motion parameters appears to be valid (cf. Fig. 4.4).

Systematic differences in the prediction accuracy are visible for different motion directions and scans ('3D GRE+FIDnav' compared to 'FIDnav only' sequence set-up) as can be seen in Fig. 4.5. For some subjects and experiments (e.g., subject 5, 2nd scan, translation in x; subject 4, 1st scan, translation in z), the error variance is higher than for other experiments. The differences in the prediction error for different scans and motion directions are significant, however, on the order of magnitude of 10^{-2} mm or degrees for translational and rotational motions respectively. Rotational motion in z direction and translational motion in y direction can be predicted with lower errors as compared to the remaining directions.

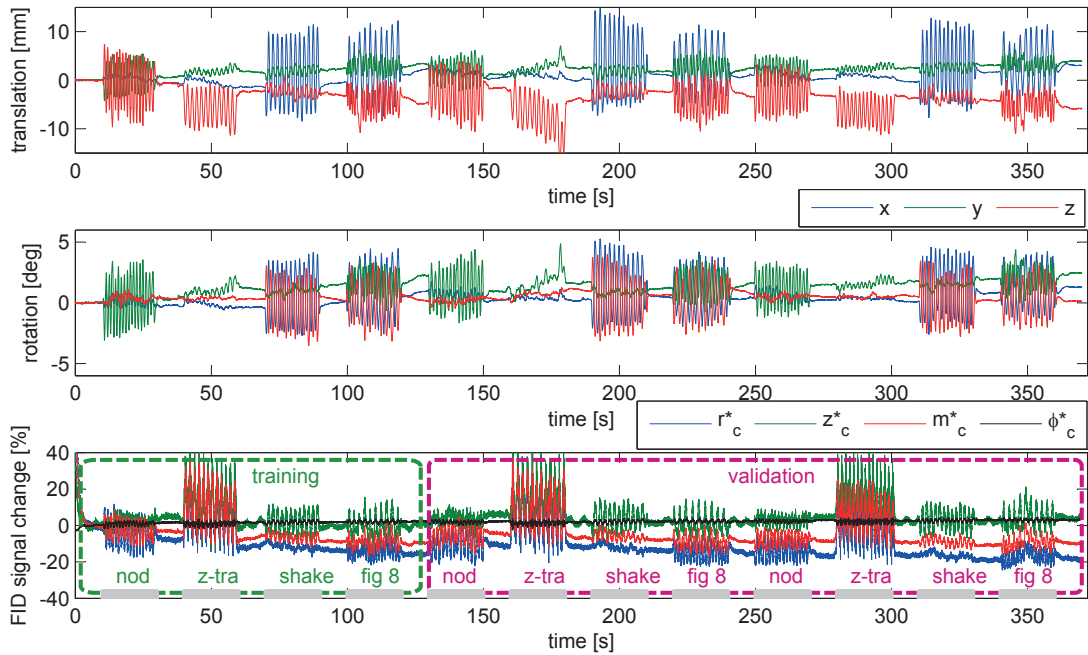


Figure 4.2: Translational and rotational motion parameters as captured by the camera system from a subject scan. Real r^* and imaginary parts z^* as well as the magnitude m^* and the phase ϕ^* of the FIDnav time course for one single coil elements; The subject was instructed to perform the 4 motion patterns nodding, z-translation, head shaking and drawing a virtual eight with the nose during the training (green box) and the validation parts (red box). Grey bars at the bottom mark the motion periods. During intermediate periods the subjects were asked to rest in one position.

Further, the data from the '3D GRE+FIDnav' scans reveal a lower prediction power than from the 'FIDnav only' scans. This can be explained by the much denser sampling rate of the 'FIDnav only' experiments and more robust regression results due to a bigger sample size. Prediction errors larger than three times the standard deviation of the error were considered as outliers and account for of the total data points. We observed maximal translational and rotational errors of up to ~ 3 mm and $\sim 3^\circ$.

4.3.3 FID Navigator Signal Stability

As described in (Babayeva et al., 2014a), an FID navigator signal may also be subject to changes due to scanner-related signal fluctuations. Indeed, time-dependent FIDnav signal drifts were observed, especially for the phase and the imaginary part of the FIDnav signal, as can be seen in Fig. 4.6. However, these drifts are slow compared to FIDnav signal changes caused by motion, which was confirmed by phantom scans. The differences in the slopes of the drifts in different experiments could have been caused by the different warm-up times of the scanner due to previous experiments and its temperature induced shim changes.

Chapter 4. Accuracy and Precision of Head Motion Information in Multi-Channel Free Induction Decay Navigators for Magnetic Resonance Imaging

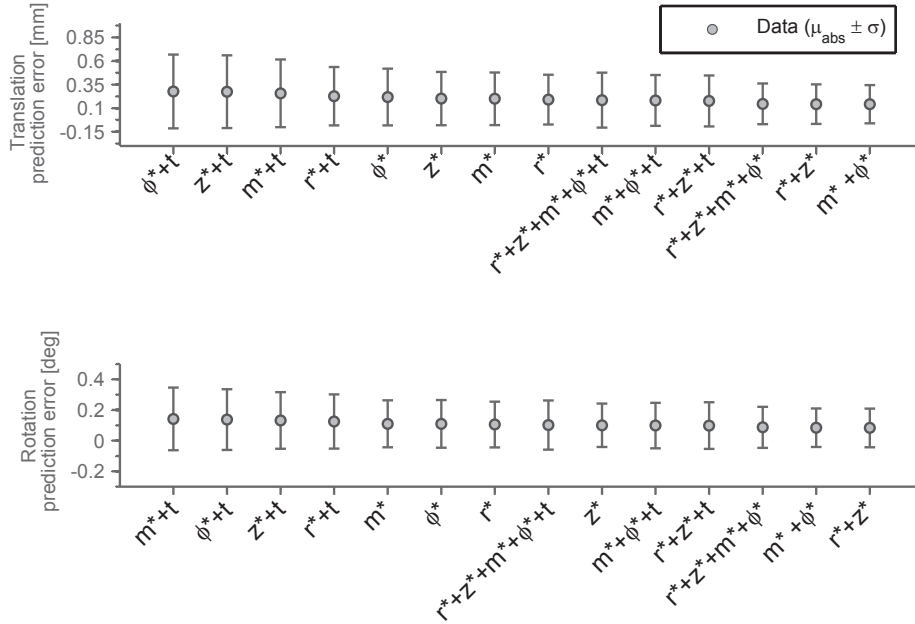


Figure 4.3: Accuracy (μ_{abs}) and precision (σ) for all subjects after cross-validation and different model inputs with and without the temporal component. The output is sorted according to the absolute mean prediction error. Using the magnitude and the phase or the real and the imaginary parts of the FIDnav provides the best performance of the linear model.

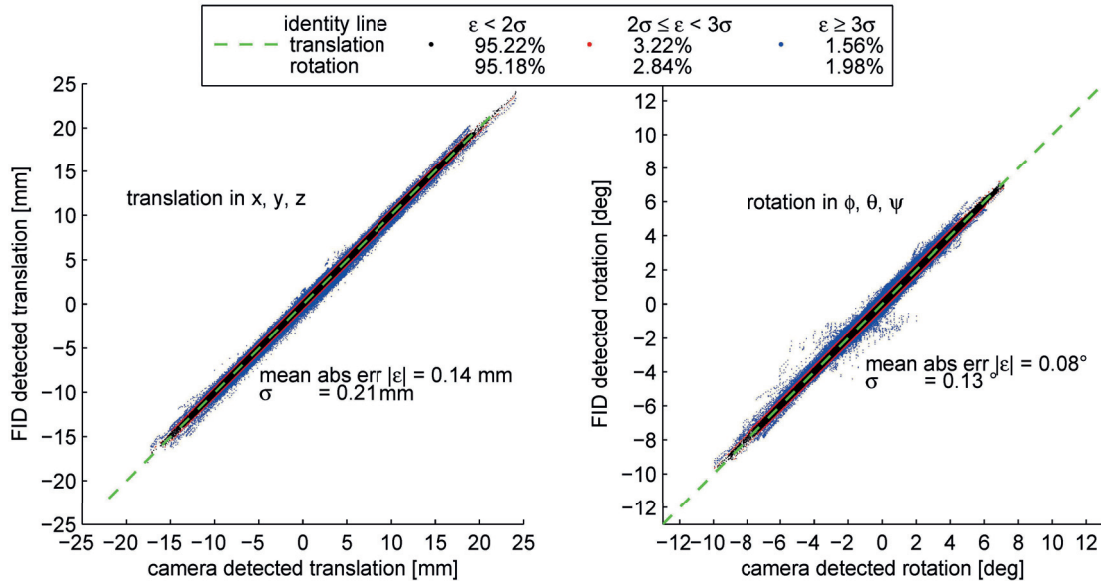


Figure 4.4: Predicted FID-based translational (left) and rotational (right) motion versus camera-detected motion from 20 scans of 5 volunteers (4 scans with motion per volunteer). As model input the real and the imaginary component of the FIDnav signal was taken. The extent of the motion parameter error ϵ is coded with different colors corresponding to multiples of the standard deviation σ (black $\epsilon < 2\sigma$, red $2\sigma \leq \epsilon < 3\sigma$, and blue $\epsilon \geq 3\sigma$) together with their proportion relative to the data set. Line-of-identity is indicated in green.

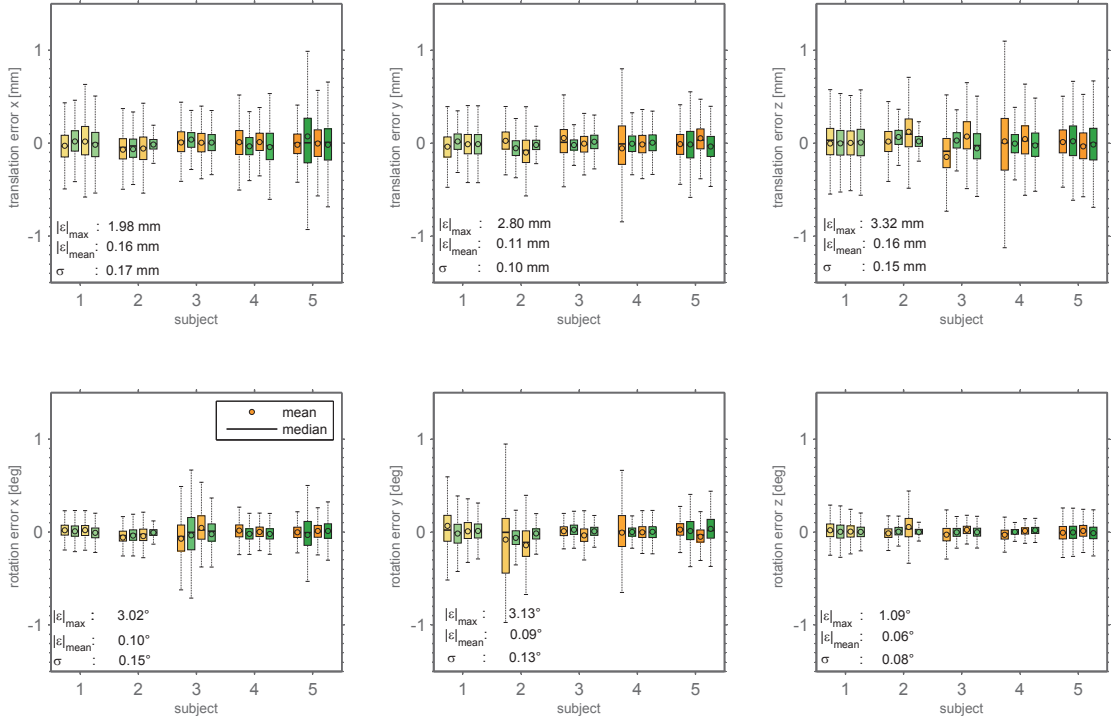


Figure 4.5: Prediction error for all 5 subjects and experiments (3D GRE+FID in green and FID only in orange) where the subject was moving and motion directions with the respective maximal absolute error, absolute error mean and the error standard deviation. The boxplot visualizes the distribution of the error with the mean and the median where the box encapsulates the data between the 25th (Q1) and 75th (Q3) percentiles, the whiskers extend to the most extreme data points not considered outliers. As outliers were considered data points further away from the mean than $1.5(IQR)$ with $IQR = Q3 - Q1$ being the inter quartile range.

Motivated by these time dependent FIDnav signal changes, an additional time component was added to the model. However, as shown in Fig. 4.3, this does not contribute to a better motion prediction in terms of accuracy and precision. Physiological effects from respiration and cardiac cycles may introduce spurious signal fluctuations. The FIDnav signal exhibited modulations due to breathing, which correlate with small head movements caused by respiratory motion, also detected by the camera system. A linear model can be trained with these data without voluntary motion; the resulting model is able to predict also the small periodic head displacements in the sub-millimeter range (Fig. 4.7). Cross-validation only for data without voluntary motion revealed an accuracy and precision of 0.12 ± 0.18 mm for translational and $0.06 \pm 0.09^\circ$ for rotational motion and r_c^* and z_c^* as model inputs.

4.3.4 The Ability of the Linear Model to Extrapolate Between Different Motion Types

We propose the use of a linear model to show the correlation between subject head motion and the multi-channel FIDnav signal. The employed subject head motion consisted of four

Chapter 4. Accuracy and Precision of Head Motion Information in Multi-Channel Free Induction Decay Navigators for Magnetic Resonance Imaging

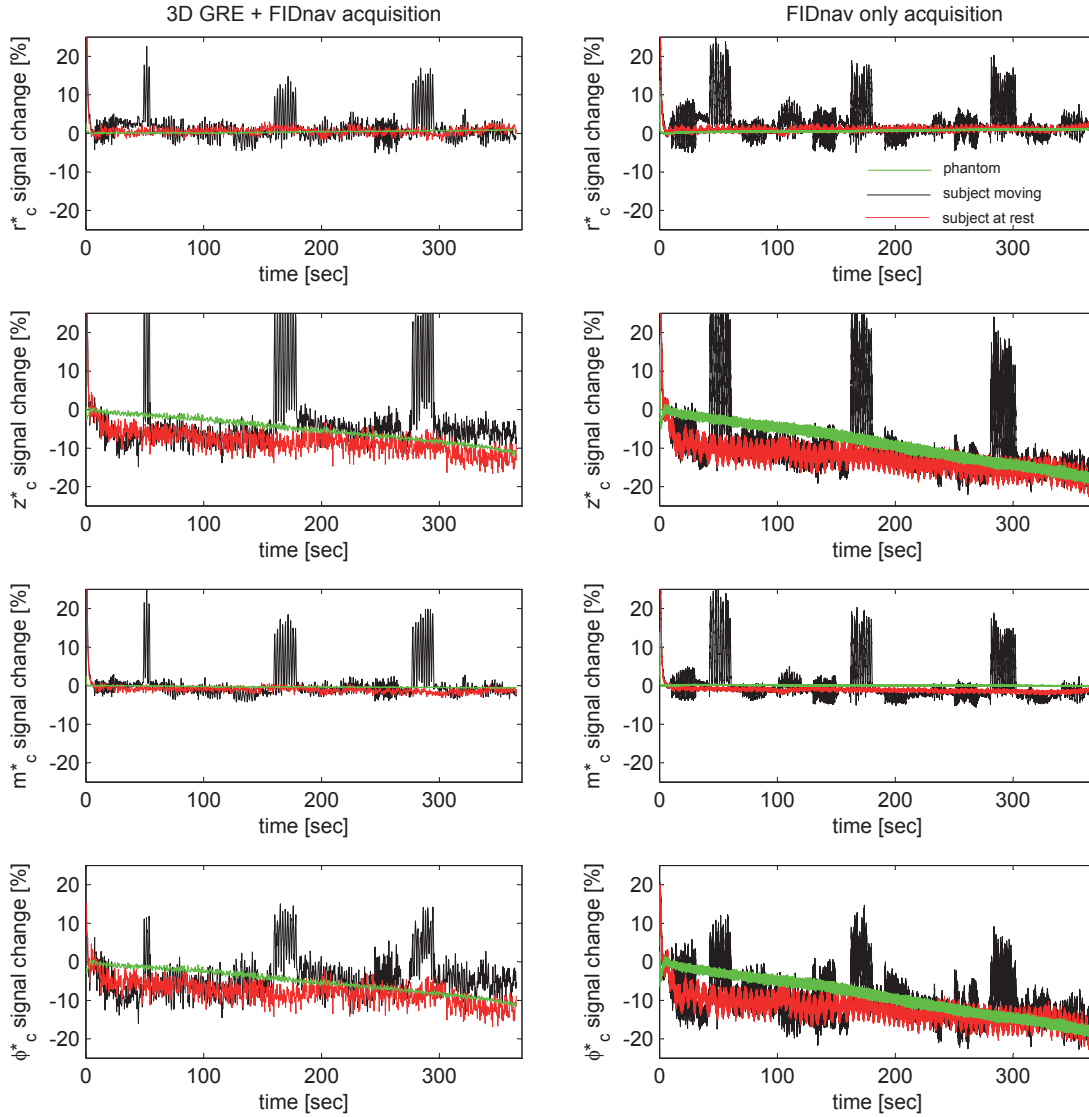


Figure 4.6: Real and imaginary parts as well as the magnitude and the phase of the FIDnav signal time course from a subject that performed motion (black) and at rest (red) as well as from a phantom scan (green). A time dependent signal trend is visible in both human and phantom scans.

different motion patterns raising the question whether such a linear model is capable of extrapolating to motion types which are different from the training data set. To evaluate this ability, the model was trained with one motion type *e.g.*, 'z-tra' and validated on data from a different motion type *e.g.*, 'fig 8' (Fig. 4.8) for all scans with motion. We evaluated the accuracy and precision for all motion type combinations used for the training and validation procedure (Fig. 4.9). Using head shaking and translational motion in the z-direction of the scanner for training produces best prediction results. It is possible to predict translational and rotational motion with an overall accuracy and precision of 0.21 ± 0.31 mm and $0.12 \pm 0.18^\circ$ ('shake') and 0.24 ± 0.39 mm and $0.14 \pm 0.28^\circ$ ('z-tra').

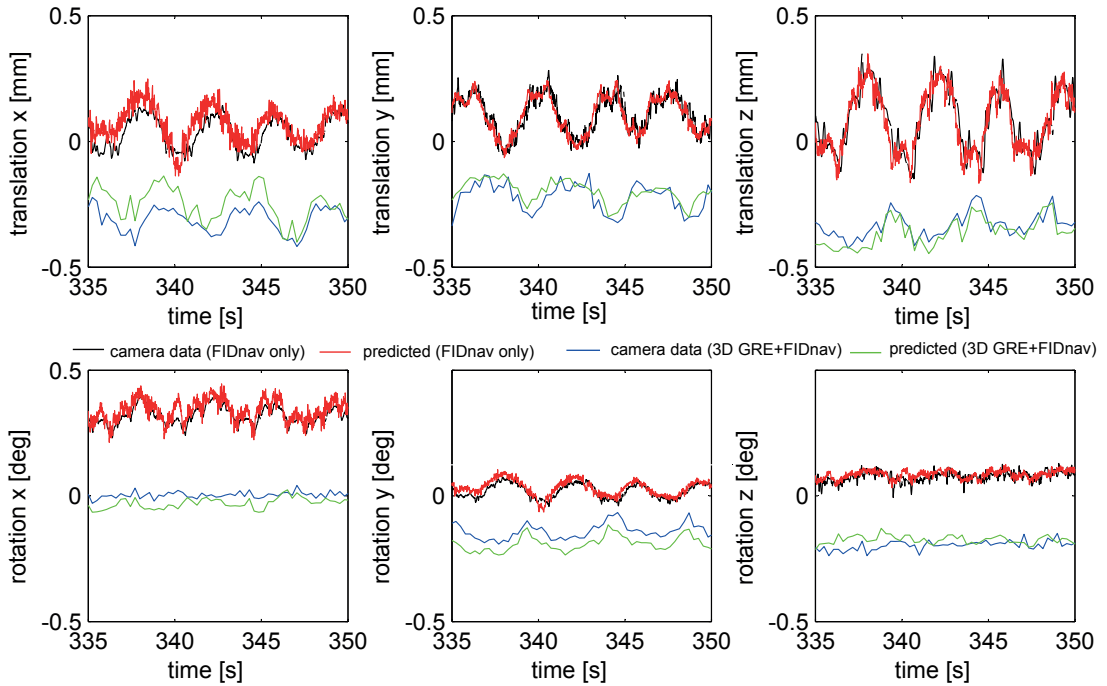


Figure 4.7: Ground-truth motion trajectory as provided by the camera system as well as FIDnav-based predicted motion trajectories from acquisitions with the modified gradient-echo acquisition as well as FID only scans. Only 15 seconds of the total time course are shown. The subject was asked not to move. Breathing motion is clearly visible in both predicted and ground-truth trajectories.

Furthermore, the analysis showed that prediction errors are comparably higher (0.41 ± 0.84 mm and $0.19 \pm 0.39^\circ$ for translations and rotations) when training the model with nodding motion and validating it on data from the 'z-tra' motion type.

Also, a model trained with data from 'fig 8' motion performs with a lower accuracy and precision when validated with the 'z-tra' motion type (0.41 ± 0.75 mm and $0.17 \pm 0.31^\circ$). By utilizing two different motion types such as nodding and shaking at the same time for training, the prediction accuracy can be improved to and when performing the validation on 'z-tra' and 'fig 8' motion data.

4.3.5 Minimal Training Data Requirements

To assess the minimal data requirements in terms of the number of data points that are needed to reliably train the linear model, the following analysis was performed. The training data were randomly chosen from a single time series for all scans and subjects and varied between 5 and 250 data points. The validation data set was also chosen at random and consisted of 1000 data points that were different from the training data set but from the same scan. As input the real/imaginary components of the FIDnav were taken. The described training and validation procedure was repeated 400 times to ensure statistical significance based on the

Chapter 4. Accuracy and Precision of Head Motion Information in Multi-Channel Free Induction Decay Navigators for Magnetic Resonance Imaging

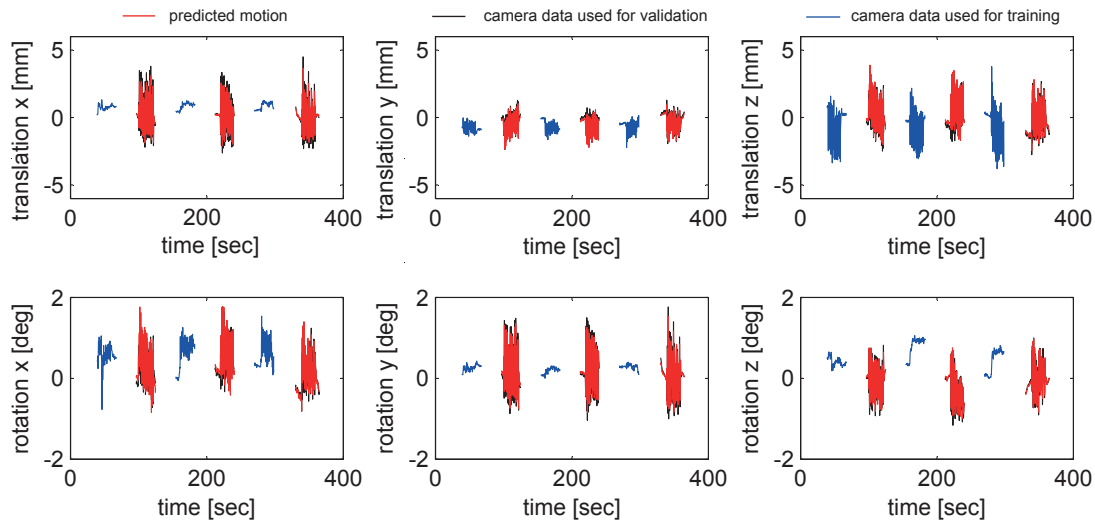


Figure 4.8: Ground truth motion trajectories as provided by the camera system together the FIDnav based predicted data. The training (blue) was performed with translation in the scanner z-direction ('z-tra') whereas validation (red, black) was done with data where the subject was drawing a virtual eight with the nose tip ('fig 8'). The data shown here is from a 3D GRE + FID nav acquisition.

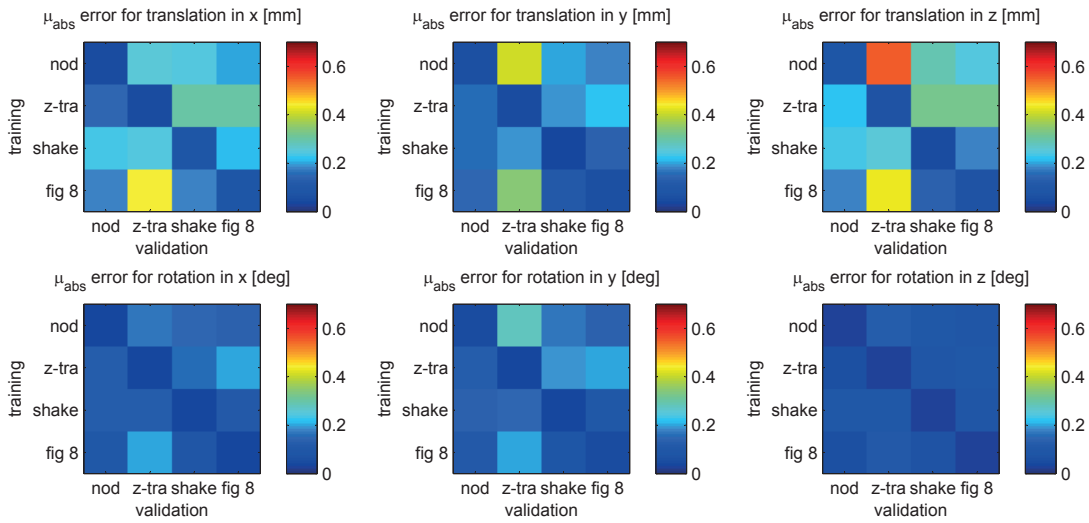


Figure 4.9: Mean absolute prediction error for all scans and different combinations of motion types used for model training and validation. The color code represents the value of the prediction error.

Wilcoxon rank sum test. The test showed that the mean of the prediction error is the same as with 1000 repetitions for a single data set. The accuracy and precision was evaluated to assess the reliability of the predicted motion parameters. Fig. 4.10 shows that approximately 100 points are sufficient to train a model which is able to predict head movements with an accuracy and precision of 0.21 ± 0.31 mm and $0.12 \pm 0.18^\circ$. Using 240 samples as applied here the accuracy can be improved by another 40% to and 0.13 ± 0.17 mm and $0.07 \pm 0.10^\circ$.

Another analysis has been performed with regard to required motion shape or magnitude, complementing the analysis performed in the previous section. We evaluated the prediction power of models trained with 100 data samples of motions with different magnitudes. These samples were selected to have a uniform distribution over a fixed range (*i.e.*, uniform distribution of motion samples in the interval $[-2 + 2]$ mm). A 4-fold cross-validation was used to assess the accuracy and the precision of the model by shifting the training and validation blocks to the beginning, the middle and the end of the data set while randomly choosing the samples. The training set was chosen from 1/3 of the data and the validation was done on the remaining 2/3 of the data points.

The results from all experiments showed that already motion magnitudes of ± 2 mm and $\pm 1^\circ$ for translations and rotations, respectively, allow the model to be trained and to predict previously 'unseen' motion of bigger amplitudes with an absolute error of 0.30 ± 0.30 mm and $0.14 \pm 0.14^\circ$ (see Fig. 4.10). Also, motion magnitudes > 2 mm and $> 1^\circ$ do not seem to improve the model and only the number of samples has a significant effect on the prediction quality in terms of prediction error.

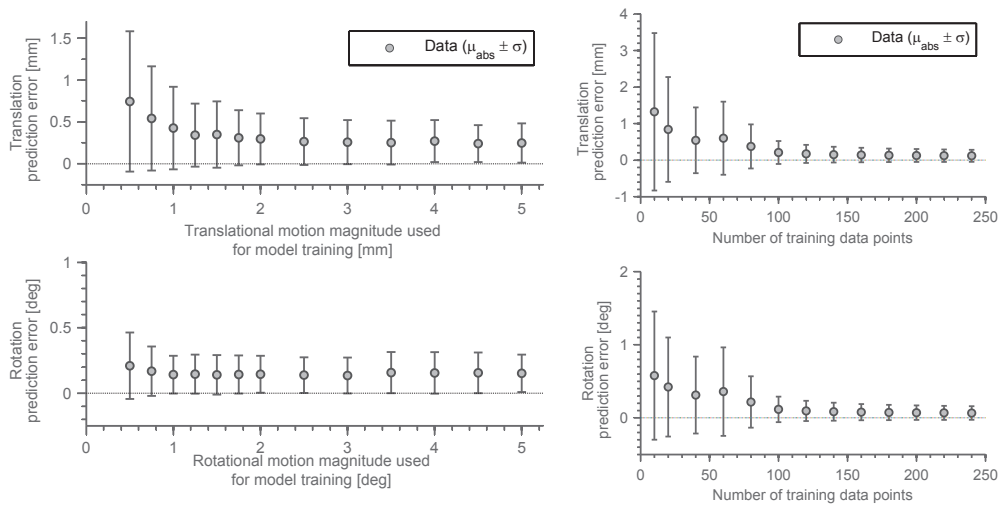


Figure 4.10: The mean prediction accuracy μ_{abs} and precision σ for linear models which have been trained with different amount of sample points and motion magnitudes. The data is shown for translational and rotational motion.

4.3.6 Inter-Scan and Inter-Subject Model Differences

Ideally, the motion model could be universally applied, *i.e.*, would be applicable to all subjects in a given head coil, which would enable the use of FIDnavs for motion correction without using ground-truth motion parameter data (as obtained by the camera system here). With this goal in mind, we investigated the prediction ability of the motion model between different subjects and scans. However, a model which is trained on data from a different subject was not able to provide good prediction results. In this case, a prediction error larger than the motion

Chapter 4. Accuracy and Precision of Head Motion Information in Multi-Channel Free Induction Decay Navigators for Magnetic Resonance Imaging

magnitude was observed. Consequently, we state that FIDnav signal changes are to a great extent subject- and coil-specific due to different head and coil geometries, positioning, as well as different coil loading and shimming conditions. This is currently the limiting factor for extending this motion quantification technique to inter-subject use, *i.e.*, for finding a generic FIDnav-motion model. However, once a model has been trained for a certain subject and session, it can be reused for different scans within this session as long as the subject remains in the scanner and the FIDnav is acquired in the same manner. The prediction accuracy and precision of inter-scan cross-validation was found to be 0.75 ± 1.3 mm and $0.40 \pm 0.67^\circ$ for translational and rotational motion in comparison to 0.14 ± 0.21 mm and $0.08 \pm 0.13^\circ$ when the training and validation was done within the data from the same scan. We found that the scenario where training and validation is done with data from different scans is only possible using the magnitude signal m_c^* as model input. This suggests that the phase is more sensitive to changes between scans.

4.4 Discussion

4.4.1 Prediction Accuracy of the Multi-Channel FID Navigator

According to theory the tracking accuracy of a motion detection device has to be several times higher than the image resolution in order to ensure successful motion correction with low artifact-to-noise ratio (Maclaren et al., 2013, 2010). It was recently shown that translations and rotations in the range of 0.5-1.5 mm or 0.5-1.5 degrees cause a loss of information in MRI data with a voxel size of $1 \times 1 \times 3$ mm³ of 23.7% and 11.8% respectively, leading to errors in quantitative evaluations of brain lesions (Gedamu and Gedamu, 2012). However, another study showed that slow, predominantly through-slice motion of 0.1 mm as caused by breathing does not cause significant artifacts for high resolution RARE images with a voxel size of $0.27 \times 0.27 \times 2$ mm³ (Herbst et al., 2014). Taking into account the aforementioned studies and the result of our experimental work, we state that a multi-channel FID navigator technology with the presented accuracy and precision of 0.14 ± 0.21 mm and $0.08 \pm 0.13^\circ$ for translation and rotation could be considered sufficient for rigid-body motion correction in MR acquisitions with a voxel size of up to ~ 1 mm³. Despite the sufficient mean accuracy, the detected outliers of up to 3 mm and degrees could potentially cause artifacts. Hence, it is important to understand the exact source of such outliers in order to eliminate them. It is further to mention that for the prediction performance the use of the real/imaginary signal representation is advantageous to the magnitude/phase representation due to phase wraps occurring in the latter case.

However, even though with bigger prediction errors, the use of only the magnitude of the FIDnav enables the model to be reusable for several scans within one session and the same subject. In order to assess the real impact of the FIDnav prediction errors on the image reconstruction, a strategy is needed where the FIDnav predicted trajectory is used to correct for the occurred motion which is subject to future investigation. It was evident that the prediction performance was better in certain motion directions as well as outliers (up to 3 mm and

degrees for translations and rotations respectively) were detected. These rare outliers might be caused by several effects: non-rigid motion as jaw or tongue movements, marker shifts of the optical system, and the non-symmetrical geometry of the utilized head coil. The non-rigid motion as well as the marker shifts lead to discrepancies in the FIDnav signal and optical data. Missing coils in one specific direction of possible head movements might reduce the performance of the proposed FIDnav based motion prediction approach.

4.4.2 FID Navigator Signal Stability

The phantom scans as well as human scans at rest were analyzed with respect to the effect of gradient activity near the FIDnav sampling in the 3D GRE acquisition. We suspected that thermal effects may have an influence on the FIDnav stability and possibly manifest themselves in higher temporal dependency of FIDnav signal in the '3D GRE+FIDnav' acquisition. However, our data did not exhibit such effects. One might speculate that the eddy currents were sufficiently canceled in the applied protocols or that a steady-state was reached; the picture may however change in gradient-demanding acquisitions such as diffusion scans. Nevertheless, the observed temporal dependency of the FIDnav signal motivated us to include the time as an additional input parameter into the model. The evaluation of the residual motion prediction error revealed, however, that the temporal component reduces the performance of the model in terms of accuracy and precision. We thus assume that the model is intrinsically capable of compensating for potential drifts by combining FIDnav signal from channels with opposed temporal dependency. Another explanation might be that the model is not able to find a correct relationship between the temporal component and the time-varying motion trajectory, especially in experiments with intended subject movements.

The FIDnav-based model was also able to predict small head movements as caused by respiration. This result indicates that the multi-channel FIDnav is very sensitive not only for substantial head movements, but is also able to detect small signal changes originating from involuntary physiological movements of the subject.

4.4.3 Advantages and Limitations of the FID Navigator Approach

The accuracy and precision assessments performed in this work were assuming that the accuracy of the available camera system (reported precision: $10 \mu\text{m} / 0.01^\circ$ (Maclaren et al., 2012)) is to date the best possible measurement of head motion within an MR scanner. Relying on the positional information as provided by the camera system, this work demonstrates that substantial rigid-body motion information is encoded in multi-channel FIDnavs and can be decoded with mean errors in the sub-millimeter and sub-degree range. The FIDnav uses hereby the simplest form of MR-signal acquisition by rapidly measuring the FID and can be added to practically any sequence without influencing the magnetization (*e.g.*, by placing a read-out after an excitation of the host-sequence) and thus does not affect the overall image quality.

Chapter 4. Accuracy and Precision of Head Motion Information in Multi-Channel Free Induction Decay Navigators for Magnetic Resonance Imaging

As described previously, the first five seconds of the FIDnav are ignored since the magnetization is not yet in a steady-state in the employed gradient-echo sequence and additional three seconds are used for normalization. This has to be taken into account as no motion information is available during this time. Methods to accelerate the stabilization of the signal as for example suggested in (Busse and Riederer, 2001) by introducing a saturation pulse can be considered to reduce this dead time. In the performed experiments, we assume a simple linear relationship between the FIDnav signal and the motion data provided by an in-bore camera. With this in mind, it should be theoretically possible to extract the parameters of such a linear model with only few data points of the ground-truth motion and the corresponding FIDnav signal. We have shown that 100 data points of low motion magnitudes are sufficient to train a linear model and still be able to obtain prediction results with an accuracy and precision below 1 mm/1°.

Furthermore, although the proposed linear model is capable of extrapolating between different motion types when different motion patterns were used for training and validation, the best performance was obtained when using nodding and shaking motion together for model training. Using only one motion type to predict before 'unseen' motion types showed considerably lower performance. Predicting translational motion along the scanner bore proved to be most difficult if only one motion type was used for model training. We assume that this is caused by the physiological shape of the head and the coil geometry (*i.e.*, the positioning of the different coil elements with respect to 'z-tra' motion).

This raises the question of the practicability of the method as a 'standalone' motion management approach. One strategy is to use the knowledge about the ability of the multi-channel FIDnavs to provide accurate quantitative motion information for its applicability in robust motion detection applications as proposed in (Kober et al., 2011). These techniques, where the FIDnav is used to classify segments of acquired data as corrupted by motion and to trigger a reacquisition, heavily rely on the sensitivity and specificity of the employed threshold of the FIDnav evaluation. Such technologies could be improved by including the quantitative knowledge about the motion magnitude in such a classifier.

Another way of using this information could be to establish a model training step without the need of a camera system. From a theoretical point of view, such training ideally would take place before an examination scan and should be significantly shorter than the imaging sequence itself, as a re-scan might be otherwise more appealing than a long pre-scan. The subject would be asked to change the head position during the prescan to acquire a training data set specifically designed for the sequence targeted for motion correction. The motion parameters for the model training would be obtained by co-registration of the image navigators.

It can also be considered to collect a sufficient amount of data to train a universal motion model, which takes into account the subject-specific model features such as head geometry, initial head position inside the coil-array, and shim settings. However, as of now, we do not

consider this approach promising, due to the vast parameter space which would have to be covered. We could show that by considering only the magnitude of the FIDnav signal, it is possible to train a subject-specific model that is able to provide prediction results in a subsequent scan (inter-scan validation) with a mean accuracy below 1mm/1°. Although, the prediction errors are larger compared to intra-scan validation and the different acquisitions are within the same 3D GRE sequence, it is a promising result towards a model training strategy which could yield a model for the entire scan session comprising different acquisitions. This, however, would be compromised even further by different sequences with possible artefactual effects on the incorporated FIDnav signal (*e.g.*, diffusion weighting, turbo-spin-echo etc.) and would require an appropriate strategy to render the FIDnav signal inter comparable throughout the whole scan session.

Another limitation to the FIDnav technique concerns slice-selective imaging. Motion detection relies on signal changes arising from different head positions relative to the receive coil. With respect to slice-selective sequences the FIDnav signal is subject to changes as caused by differences in the selected anatomy of the head in case the 2D pulse is used for the FIDnav acquisition. Hence, the FIDnav will detect possibly counter balancing signal changes arising not only from the head motion but also from the differences in the slice positions. Therefore, additional investigations are needed in this regard to propose another FIDnav acquisition strategy and to draw further conclusions.

Different coil geometries might present another challenge to the FIDnav ability to track motion reliably. It might be expected that missing coils in certain directions *e.g.*, open cage coils without an antennae in the z-direction of the scanner would lead to difficulties in predicting motion in this specific direction based on the FIDnav signal.

Furthermore, non-rigid motion which is not necessary related to displacements in the brain regions but would cause signal changes in the FIDnav is a limitation of the presented technology. Certain coil elements which are located close to the jaw and neck region could be excluded to reduce this effect.

4.4.4 Future Work

Future work should aim at extracting the subject-specific mapping from the FIDnav signal changes to rigid head movements without relying on the optical tracking system.

One possible direction towards enabling the back-calculation of the motion parameters from the FIDnav signals is to train a linear model by measuring the coil sensitivities of the employed head coil and the subject-specific head geometry (*e.g.*, low resolution head and body coil images) as proposed in (Kober et al., 2010). This data could be used to simulate the FIDnav signal by 'moving' the MR image of the head in silico *i.e.*, applying a mathematical matrix transformation and weighting the 'moved' image by the estimated coil sensitivity profiles to subsequently translate FID signal changes during image acquisition in quantitative motion

Chapter 4. Accuracy and Precision of Head Motion Information in Multi-Channel Free Induction Decay Navigators for Magnetic Resonance Imaging

parameters for motion correction.

An alternative approach is to use the FIDnav for motion detection and to trigger a subsequent motion quantification mechanism (*e.g.*, imaging navigator) during the scan, if the FIDnav exceeds a certain threshold indicating subject head movement as already proposed in (Babayeva et al., 2014a; Kober et al., 2012). After several (≥ 100 data points as shown in this work) triggering events, there should be enough data (positional information and the corresponding FIDnav data from individual coil elements) to train a model and with it be able to quantify the head movements based on the FIDnav signal alone.

Also, models of higher complexity than linear additive ones could be considered. However, an initial investigation in employing quadratic and interaction terms or other machine learning paradigms as neural networks, did not indicate improvements in the motion assessment and a detailed investigation would go beyond the scope of this work.

Due to the simplicity of the FIDnav, it could be also used to complement existing motion tracking methodologies by providing a means of validation or guiding mechanism through additional information *e.g.*, additional regularization of retrospective correction methods based on autofocusing (Babayeva et al., 2014b) or validation of optical tracking technology which is heavily relying on rigid coupling of the tracking marker with the skull and could be perturbed by marker shifts.

4.5 Acknowledgement

We would like to thank Sebastian M. Waszak, Kieran O'Brien, Alexis Roche, Matthias Seeger, Bénédicte Maréchal, Rolf Gruetter, and Pavel Falkovskiy for valuable discussions and suggestions.

5 FID-based Motion Sensitive Quality Metric and Retrospective Motion Correction for Clinical Magnetic Resonance Images

This chapter is based on published work from Babayeva et al. (2014b) and Loktyushin et al. (2013).

Abstract Motion is a major source of artifacts in clinical magnetic resonance imaging. We have collected a representative data set of 109 clinical MP-RAGE images where the acquisition sequence was equipped with FID navigators and applied a recently proposed retrospective motion correction technique to all data. An expert radiologist then rated the images before and after correction to assess the image quality improvement. It was shown that severely motion corrupted images of non-diagnostic quality were improved to an extent that they were rated as clinically useful after motion correction. The image quality of data with less severe artifacts was also improved according to the rating. Additionally, we propose a novel image quality index based on the FID signal, which can detect images according to the strength and extent of its motion artifacts. The higher the FID-based quality index the higher is the probability for the corresponding data to be motion corrupted. This study shows that substantial image quality improvement can be achieved using the retrospective motion correction method and indicates that the technique bears the potential to improve the way the problem of motion is handled in the clinical context by providing automated means of motion artifact detection.

5.1 Introduction

Motion is prevalent in clinical magnetic resonance (MR) acquisitions especially with elderly and pediatric cohorts. Patients often experience a high level of distress and discomfort due to claustrophobia, anxiety and long scan times. This may lead to agitation and increased patient motion during an MR examination and degrade the quality of acquired images to

Chapter 5. FID-based Motion Sensitive Quality Metric and Retrospective Motion Correction for Clinical Magnetic Resonance Images

a non-diagnostic level such that a rescan and even patient sedation might be necessary (Munn and Jordan, 2013). A large multicenter study reported that motion occurs in 40% of the medical examinations, in 10% being caused by motoric unrest of the patient leading to severely impaired image quality (Oberstein et al., 1990). Another study reported similar values of artifact occurrence in clinical MR scans where 12.8% of the images were motion corrupted and 6.4% had a non-diagnostic image quality (Dantendorfer et al., 1997). Thus, not surprisingly, motion during MR examinations is considered to be the major source of image artifacts with substantial financial implications (Andre et al., 2015).

Advances in quantitative interpretation of MR-based data using morphological brain segmentation (Schmitter et al., 2014) require high-resolution and artifact free images. It was recently shown that motion-related artifacts cause a significant bias in the estimates of the cortical gray matter volume with an average apparent volume loss of roughly 0.7%/mm/min of subject motion (Reuter et al., 2015). The high-resolution imaging is associated with prolonged scan times, which again increases the risk of motion artifacts to be present.

Numerous motion detection and correction strategies have been proposed during the past decades, however, no universal solution that fits all imaging paradigms could be identified so far (Zaitsev et al., 2015). Most correction techniques are sequence specific or can only correct for special types of motion as in-plane motion. The existing motion correction methodologies can be split into two broad classes: prospective and retrospective motion correction techniques. Prospective motion correction is applied during the scan time, whereas retrospective correction is performed after the image is acquired. Most prospective correction techniques require either equipping the imaging sequence with navigators (Tisdall et al., 2012; White et al., 2010) or additional hard-ware to track the subject's motion, for example, optical cameras (Zaitsev et al., 2006). Both, prospective and retrospective motion correction techniques have their advantages and limitations. Prospective methods can correct for spin-history effects and prevent Nyquist violations due to inadequately sampled k-space. They require, however, sequence modifications to include the acquisition of the navigator, and depending on the navigator complexity these are not always easy to implement in all sequences. Prospective methods also often rely on external motion tracking hardware, which might not be compatible with the scanner setup i.e., because of an obstructed camera view due to a closed coil design. Retrospective correction techniques, on the other hand, can be applied to the data acquired with most of the sequences as the methods based on autofocusing (Atkinson et al., 1997; Loktyushin et al., 2013) but they fail in cases with severe motion degradation, which causes unrecoverable k-space data loss or can only be applied to in-plane motion as in case of the PROPELLER method (Pipe, 1999).

Further, the high sensitivity of computer-based quantitative image evaluations to motion artifacts motivates the development of automatic detection of even benign image degradations. Thus the possibility to assess the image quality quantitatively has an increased value in determination of the validity of morphological segmentation results. Such an automated quality assessment methodology, which is capable of identifying images of non-diagnostic

quality, can be based on background noise evaluation (Mortamet et al., 2009).

We have developed a novel motion artifact detection technique based on the recently proposed free-induction-decay navigator (FIDnav) (Kober et al., 2011). The manifestations of the motion artifacts depend on the affected k-space position (Maréchal et al., 2012; Zaitsev et al., 2015). FIDnav-based motion detection provides a means of determining at what time i.e., k-space position during the acquisition, subject motion occurred. We utilize this information to perform the FID-guided retrospective motion correction based on autofocusing (Babayeva et al., 2014b; Loktyushin et al., 2013). Further, we evaluate the performance of the proposed techniques with the use of the expert’s ratings and rankings of the corrected and uncorrected clinical MP-RAGE images and also assess the rating correlation with FIDnav-based motion artifact detection.

5.2 Methods

5.2.1 Data Acquisition

We have collected a data set of 109 MP-RAGE images (α /TI/TR/TA = 9° /900ms/2300ms/5:12 min, GRAPPA $2\times$ with 32 reference lines, different matrix and voxel sizes in the range of 1 mm) acquired for clinical purposes at our site (CHUV, Lausanne, Switzerland) over a time period of roughly 1 year. The images were acquired with five different scanners (Verio, Skyra, Aera, Trio, Prisma from Siemens Healthcare, Erlangen, Germany) and different head-coils (see Table 5.1 for a detailed overview). The data was anonymized in correspondence with local ethics regulations, hence, no information on demographics or disease diagnosis can be provided here. The prototype MP-RAGE sequence was modified in such a way that at the end of the read-out train in every TR an FIDnav acquisition was inserted ($\alpha = 5^\circ$, 512 samples in 2 ms).

5.2.2 Retrospective Motion Correction

All images were retrospectively motion corrected using two different motion correction techniques. First method used for correction was the recently proposed blind retrospective motion correction based on autofocusing (Loktyushin et al., 2013). This method relies on an optimization-based search of unknown motion parameters, where the cost function involves the image quality metric evaluated on intermediary motion corrected images. We call this method ‘blind’ due to the fact that the only source of information needed for optimization is the k-space data itself. The second method was a modification of the blind correction technique, where the information from FIDnav is used to constrain the optimization by restricting the set of explored motion trajectories (Babayeva et al., 2014b; Loktyushin et al., 2013). In this study, we are going to call it FID-guided correction. Additionally, we also reconstruct our data ‘as is’ (no motion correction) resulting in a total of three different image sets: without motion correction, with blind motion correction, and FID-guided motion correction. All computations were performed in MATLAB (Mathworks, USA).

Chapter 5. FID-based Motion Sensitive Quality Metric and Retrospective Motion Correction for Clinical Magnetic Resonance Images

Scanner type, field strength, soft ware version	Utilized coils	Number of channels used for acquisition	2014												2015		Total
			Mar	Apr	May	Jun	Jul	Aug	Sep	Oct	Nov	Dec	Jan	Feb			
Verio, 3T, VB17A	Head_32	32															38
	HeadMatrix_12+NeckMatrix+SpineMatrix	19															5
	HeadMatrix_12+NeckMatrix	16	1	0	3	4	4	3	5	4	1	0	13	17		8	
	HeadMatrix_12+NeckMatrix	10														1	
	HeadMatrix_12	12														2	
Skyra, 3T, VD13A	HeadNeck_64	64															7
	Head_32	32															1
	Head_32+Spine_32	36	0	0	2	1	0	0	0	0	0	0	2	5		1	
	HeadNeck_20	20														1	
Aera, 1.5T, VD13A	HeadNeck_20	20															20
	HeadNeck_20	16	2	1	0	0	7	0	2	3	1	2	6	8		1	
	HeadNeck_20+Spine_32	24														12	
Trio, 3T, VB17A	Head_32	32	0	1	1	0	0	0	0	0	0	0	0	0		2	
Prisma, 3T, VE11A	HeadNeck_64	64	0	0	0	0	2	0	0	4	2	0	1	1		10	
Total			3	2	6	5	13	3	7	11	4	2	22	31		109	

Table 5.1: Overview of the clinical MPRAGE datasets collected for this study. The 'Utilized coils' column shows a description of the head coil as well as additional coils used for data acquisition. The number after the underscore indicates how many coil elements in the selected coil matrix are available.

5.2.3 Qualitative Image Quality Assessment

Two different evaluations were performed to assess the image quality before and after correction. During both quality assessment procedures the rater was blinded to the respective reconstruction method. First, the image quality was rated in terms of blurring, ringing and ghosting artifacts inside (BGR inside) and outside (BGR outside) the brain region to be none, mild, moderate, or severe in accordance with the image quality criteria within the Alzheimer's Disease Neuroimaging Initiative (ADNI) study (Jack et al., 2008). Further, the images were rated to be either useful for clinical analysis or to be non-diagnostic when extensively motion corrupted. Second, the uncorrected images and those corrected with blind and with FID-guided method were ranked against each other according to their perceived image quality characterized in terms of blurring, ghosting, and ringing. The image with the best image quality was ranked first and the one with the worst quality was ranked third. If the images were perceived to be of the same quality they were assigned the same rank, i.e., if blind and FID-guided corrections were perceived to be similar but better than the uncorrected image then they both would be ranked first and the uncorrected image second.

One rater, a radiologist with 6 years of MR brain imaging experience, reviewed the images. These qualitative results were used as the 'gold-standard' for further FIDnav-based motion detection assessments.

5.2.4 FID-Based Motion Detection

It was shown that the FIDnav is able to detect motion events reliably (Kober et al., 2011) and even allow prediction of the underlying rigid head motion with a submillimeter and sub-degree precision (Babayeva et al., 2015b), when acquired with a multi-channel coil array. However, so far it is not possible to extract the motion trajectory from the FID-signal without the knowledge on its correlation with the underlying motion parameters.

Here, we would like to make use of the multi-channel FIDnav signal as means of quality index estimation for motion artifact detection of the our data set. The FID signal from a read-out is reduced to a single point for every channel by taking the complex average of all read-out samples and consider just the magnitude $m_c(t)$ of the complex signal as proposed in (Babayeva et al., 2015b).

For motion detection we will consider several FIDnav-based metrics and evaluate their performance with respect to their sensitivity and specificity to identify the images with none, mild, moderate, and severe motion artifacts inside the brain region using the radiologist's ratings as 'gold-standard'. We will further consider images having no visible motion artifacts as 'no motion' scans and all the others as 'motion' scans. Hereby, we excluded the FID signal from the neck and spine region coils, as only bulk rigid head movements were of interest for this study. Please note that for this classification problem it would be also possible to make use of classical machine learning tools such as support vector machines. However, we decided to show the differences between the artifact groups based only on selected FIDnav features to avoid the 'black box' problem caused by such tools making it difficult to draw a direct link between the classifier and the data. Also the relatively small sample size restricts us to the use of simple statistical methods.

We will call the first detector $FIDnav_{AICC}$, where 'AICC' stands for all channels. For this metric we evaluate the relative finite difference FIDnav signal magnitude $(m_c(t) - m_c(t - 1)) / m_c(t_{ref})$. First two samples from the FID time series were omitted to ensure that the signal is in a steady-state meaning that $t_{ref} = 3^{rd}$ repetition. Also the mean μ_{AICC} and standard deviation σ_{AICC} over the whole time course of the acquisition for every channel is calculated separately. If a relative signal change higher than $3\sigma_{AICC}$ in more than N channels then the part of k-space acquired during this TR is considered to contain a motion event i.e., outlier. We sought to find the optimal number of relevant channels N by correlating the FIDnav-based artifact detection to the 'gold-standard' visual evaluation of the image quality with respect to best sensitivity and specificity. We will also consider another threshold mechanism that we will call moving standard deviation $\sigma_{AICCmov}$, which is calculated based on the moving average over the whole FIDnav time course and does not take the FIDnav values of the identified motion events into consideration i.e., standard deviation for t is calculated from all data points acquired up to $t - 1$, if FID signal at t is higher than 3 times the standard deviation then it is considered as a motion event and not taken into the calculation for the reference standard deviation at the next time point. This detector will be referred to as $FIDnav_{AICCmov}$.

Chapter 5. FID-based Motion Sensitive Quality Metric and Retrospective Motion Correction for Clinical Magnetic Resonance Images

We pose that the FID signal changes if motion is present during the acquisition this would mean that the temporal variation of the signal would become higher and would be reflected by the standard deviation of the signal. We propose to calculate the standard deviation over the normalized finite difference of the FID signal $(m_c(t) - m_c(t-1))/m_c(t_{ref})$ over all channels σ_{FIDnav} and will investigate its performance as a potential motion detector.

Another FIDnav-based detector will be referred to as $FIDnav_{NCmax}$, where 'NCmax' stands for N number of channels with maximal signal change among the channels at every time point. Here, we use the mean of the FIDnav finite difference signal $(m_c(t) - m_c(t-1))/m_c(t_{ref})$ from N_{NCmax} channels where the absolute signal change was maximal as the metric for each time point. The optimal number of the channels N_{NCmax} is estimated through specificity and sensitivity measures of the proposed metric. If the obtained $FIDnav_{NCmax}$ value exceeds the empirical threshold τ_{NCmax} then the corresponding time point is considered to be a motion event as described in (Babayeva et al., 2015a). In contrast to $FIDnav_{AUC}$ where the threshold is calculated for each scan individually, here, the empirical threshold τ_{NCmax} is obtained from the three times the standard deviation $3\sigma_{NCmax}$ of the 'no motion' scans over the whole scan time. Hence, it is also important to investigate which influence does the field strength, scanner or coil type used for data acquisition has on this threshold, otherwise τ_{NCmax} needs to be calculated separately for each group (i.e., field strength, scanner or coil type).

It is known that motion artifacts manifest themselves differently depending on the location in k-space affected by motion (Maréchal et al., 2012; Zaitsev et al., 2015). If motion is present during the acquisition of high frequencies then the artifacts are less visible and the image quality may be less deteriorated than in cases where the central low-frequency parts of k-space are affected by motion. We exploit this information in our FID-based motion detection by applying larger weights to the FIDnav corresponding to the center of k-space. Again, the optimal weighting curve parameters are found by correlating the FID-based detection and qualitative ratings. Here, we evaluate a parabolic

$$w_{Parabola}(t) = 1 - \left(\frac{t - \mu_{k-space}}{\mu_{k-space}/a} \right)^2 \quad (5.1)$$

and a Gaussian weight curve

$$w_{Gauss}(t) = e^{-\frac{(t - \mu_{k-space})^2}{2\sigma_{k-space}^2}} \quad (5.2)$$

Both weight curves are centered at k-space center $\mu_{k-space}$ (i.e., corresponding to t where the data from the center of k-space are acquired). The curves have also a 'width' $\sigma_{k-space} =$

N_{lin}/a and N_{lin} being the total number of k-space lines. The variable a is set based on sensitivity and specificity evaluations of the specific weighted FID-based motion detector. We introduce the optimal FID-based quality index, which is calculated as a weighted sum over all FIDnav values and which we call **FIDI** (Eq. 5.3). Finally, we propose FIDI bounds for different artifact classes based on a logistic regression fit of the data.

$$FIDI = \sum_t w(t)FIDnav(t) \quad (5.3)$$

Additionally, we have calculated the quality index (QI) proposed by (Mortamet et al., 2009) for all uncorrected images in order to compare the results to the FIDnav-based quality metrics.

5.3 Results

5.3.1 Prevalence and Nature of Motion Artifacts in the Collected Data

The expert ratings revealed that 4% (4 cases) of the original (uncorrected) images had severe, 13% (14 cases) moderate, and 15% (17 cases) mild artifacts inside the brain region and 9% (10 cases) severe, 14% (15 cases) moderate, and 43% (47 cases) mild artifacts in the background. 6% (6 cases) of images were rated to be of non-diagnostic quality (Fig. 5.1).

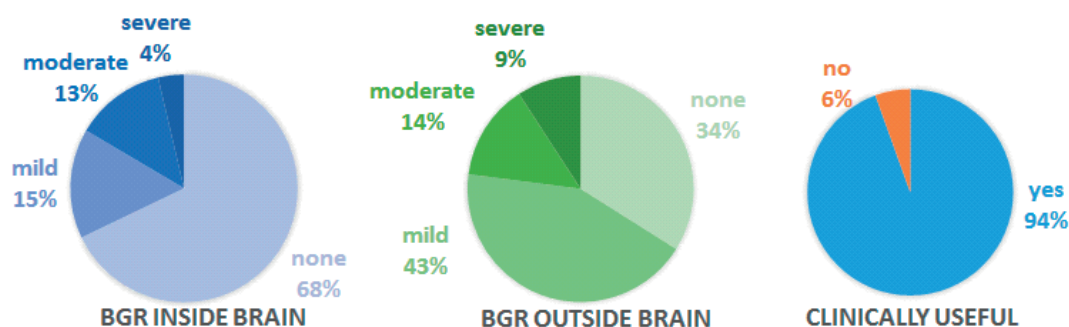


Figure 5.1: Blurring, ghosting, and ringing (BGR) artifact prevalence inside and outside the brain region in the images according to qualitative ratings as well as their clinical utility.

5.3.2 Image Quality Before and After Correction

Retrospective motion correction was found to improve the overall image quality (Fig. 5.2 and Fig. 5.3) as assessed by the expert's ratings. When considering BGR artifacts inside the brain the number of severely corrupted images was reduced with blind correction from 4 to 2 cases and eliminated in the FID-guided correction. Moderate artifacts inside the brain region could be reduced through both correction algorithms from 14 to 8 cases and the number of

Chapter 5. FID-based Motion Sensitive Quality Metric and Retrospective Motion Correction for Clinical Magnetic Resonance Images

cases with mild motion artifacts was changed from 17 to 26 by blind and to 21 by FID-guided correction. Mild background artifacts (mainly N/2 GRAPPA related ghosts) were however increased after applying the correction from 47 to 75 cases after blind and 68 cases after FID-guided correction. Moderate background artifacts increased from 15 to 17 cases after blind and decreased to 12 after FID-guided correction. Severe artifacts were reduced after both corrections from 10 to 3 and to 2 cases for blind and FID-guided correction respectively. After blind correction only 2 images were flagged as having no clinical utility, however after FID-guided correction all images were found clinically useful.

FID-guided motion corrected images were ranked first in 83 cases compared to blind correction (58 cases) and without any correction (60 cases). In a single case, the image quality was found to deteriorate after FID-guided correction. In this case, moderate ringing artifacts appeared inside the brain region, which were rated as mild in the original image before correction, however were removed by blind correction (Fig. 5.3c). The images were assigned the second rank in 51 cases after blind and in 25 cases after FID-guided correction compared to 20 without correction.

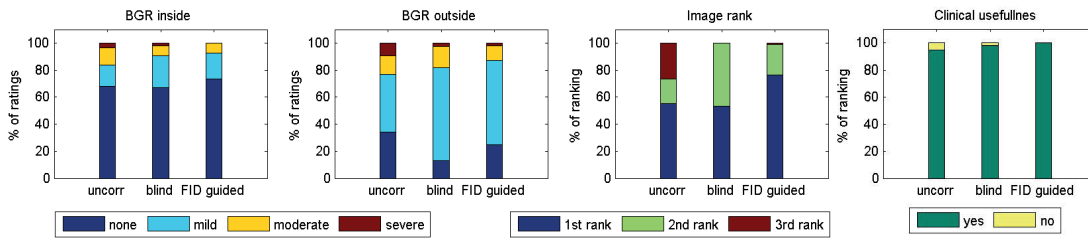


Figure 5.2: Qualitative expert ratings results for blurring, ghosting, and ringing artifacts inside and outside of the brain region as well as clinical utility before and after blind and FID-guided retrospective motion correction.

5.3.3 FIDnav Based Quality Metric Design

The FID signal is a multi-dimensional time series signal and it was prepared as described in the Methods section in order to eventually be able to identify motion corrupted images based on a single index derived from the FID data. In Fig. 5.4 it is shown how the FID signal and the respective detector change depending on the underlying motion.

When using the motion detectors $FIDnav_{AIC}$ and $FIDnav_{AICmov}$ several variables have to be set. It was to determine what number of relevant coil elements N , as well as the amount of detected motion events provide the best results to distinguish images with different artifact severity. We have investigated the mentioned variables with respect to its influence on the receiver operating characteristics (ROC) of the related $FIDnav_{AIC}$ and $FIDnav_{AICmov}$. The specificity and sensitivity for different number of coil elements as well as detected motion events are shown in Fig. 5.5.

The results show a low performance of the proposed detectors ($FIDnav_{AIC}$ and $FIDnav_{AICmov}$) due to the dependency of the FIDnav temporal variance on motion leading

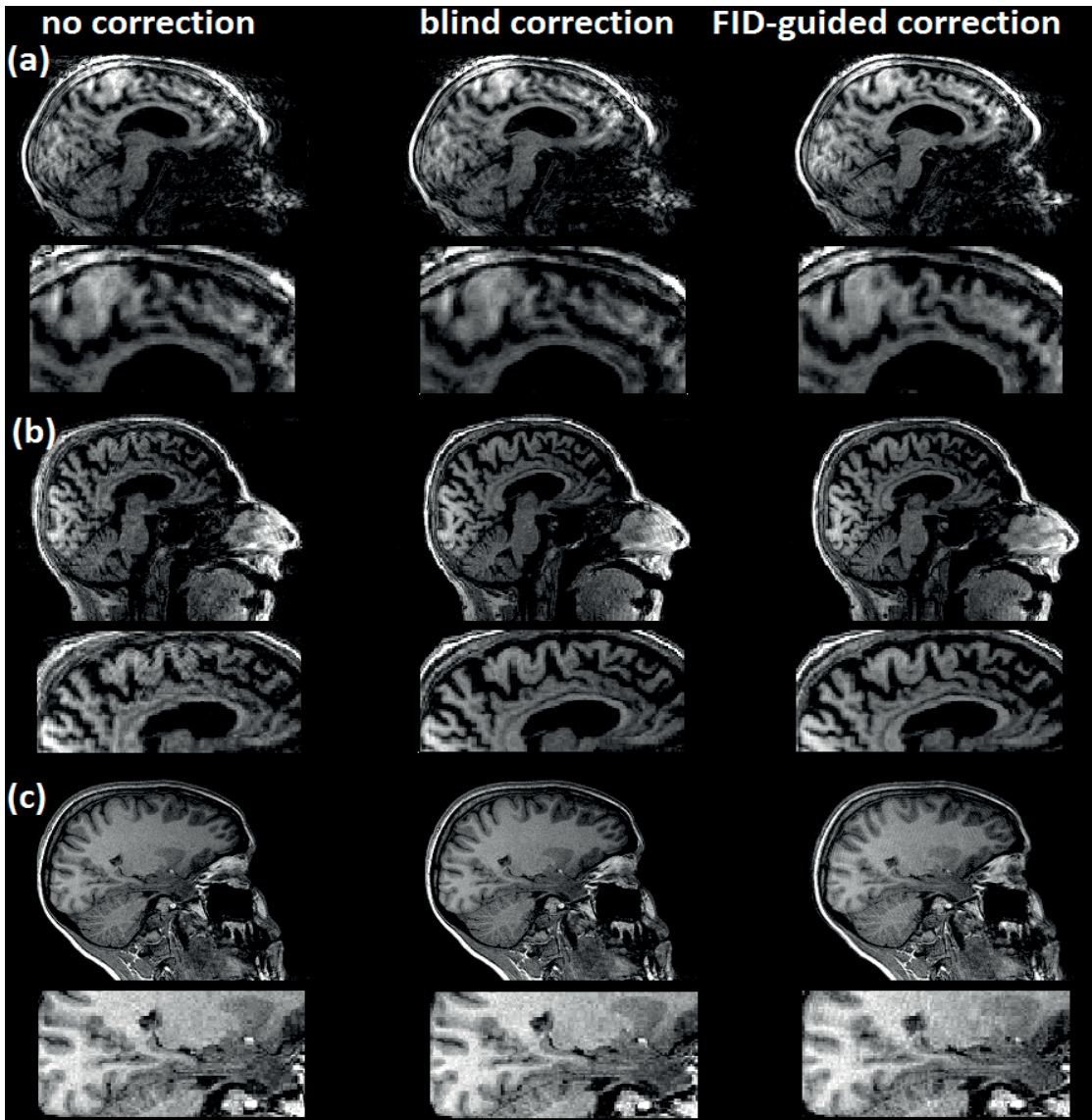


Figure 5.3: Images before and after blind and FID-guided retrospective motion correction from different subjects with a zoom on a part of the brain and different severity of blurring, ghosting, ringing artifacts inside the brain before correction: (a) severe; (b) moderate; (c) mild. Blind correction: (a) severe; (b) moderate; (c) none. FID-guided correction: (a) moderate; (b) mild; (c) moderate;

to an increased number of false positives with a specificity close to 50%. Only when detecting images with moderate artifacts among images with none artifacts a specificity of 87% and sensitivity of 78% for $N=2$ and 4 motion events can be reached (see Fig. 5.5c). However, setting the threshold empirically e.g., to the multiple of standard deviation of 'no motion' FIDnav data in the case of $FIDnav_{AICmov}$, does not provide a compelling improvement in the ROC. Hence, this finding leads us to investigate the temporal variability of the FIDnav from all coil elements as a detector σ_{FIDnav} . We noticed that only the field strength of the scanner has a significant influence on the standard deviation of the FIDnav. Number of utilized coil

Chapter 5. FID-based Motion Sensitive Quality Metric and Retrospective Motion Correction for Clinical Magnetic Resonance Images

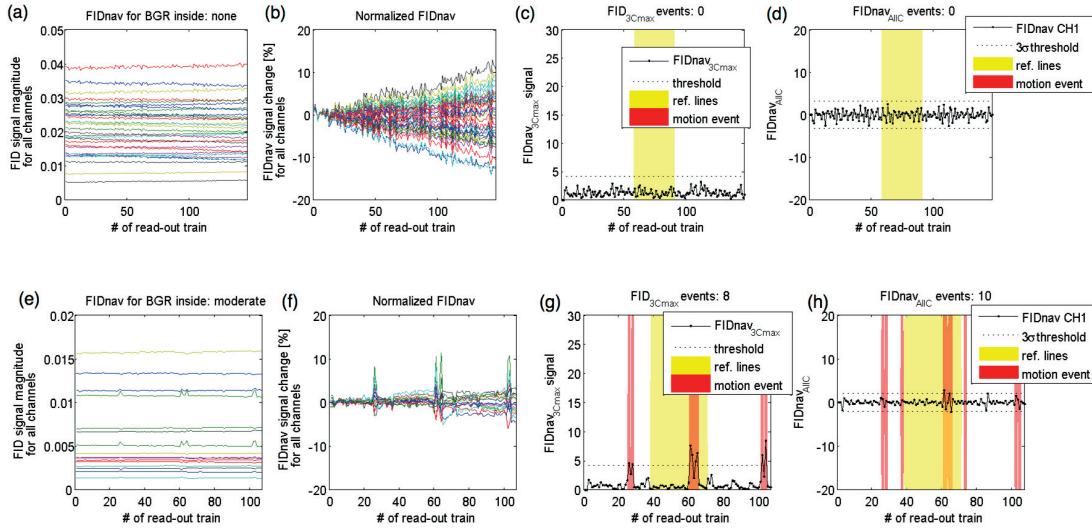


Figure 5.4: FID signal in its raw form (a, e) after normalization $m_c(t)/m_c(t_{ref})$ (b, f) and after modification for motion detection as $FIDnav_{3Cmax}$ (c, g) and $FIDnav_{AIIC}$ (d, h) for data sets without any motion artifacts and moderate motion.

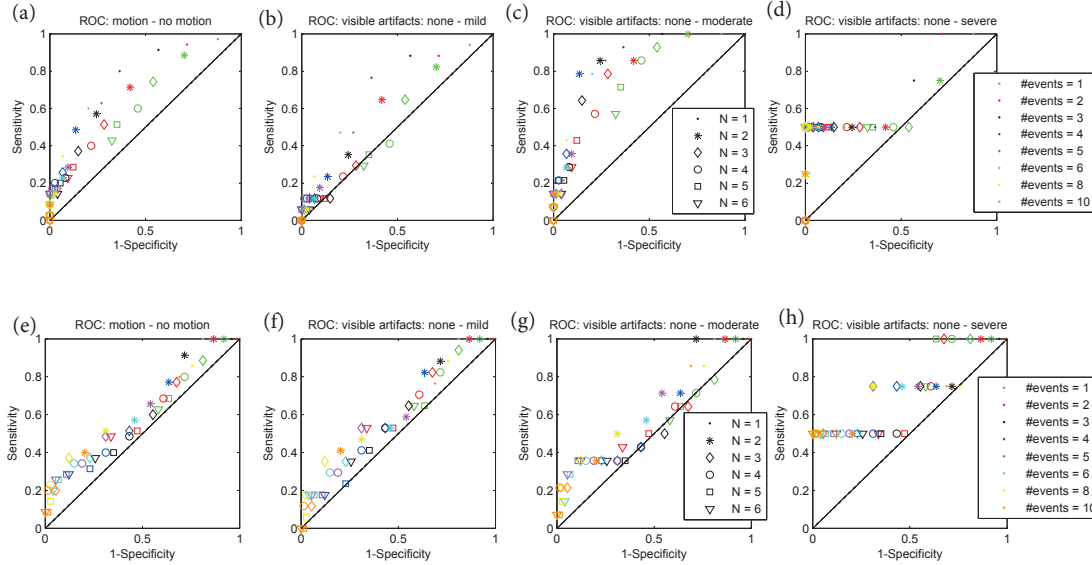


Figure 5.5: For $FIDnav_{AIIC}$ (a-d) and for $FIDnav_{AIICmov}$ (e-h): show receiver operating characteristic (ROC) curves for different settings of relevant channels N (N) and the number of detected motion events ($\#events$) during the scan and its respective specificity and sensitivity for identifying the level of motion corruption.

elements as well as the scanner type does not have a significant effect on the FIDnav variability. Therefore, all following FIDnav evaluations will be performed separately for the 1.5 and 3T data.

Going back to the FIDnav signal standard deviation σ_{FIDnav} among all channels the

motion detection capabilities were as following. Data from 1.5T scanners are detected to be motion corrupted or not with a sensitivity of 82% and a specificity of 87% (Fig. 5.6a). Images with mild motion corruption are identified with a sensitivity of 83% and a specificity of 80%. Sensitivity and specificity of 89% and 87% respectively is observed for moderate motion. Severely corrupted images can be detected with a 100% reliability. For 3T data according to Fig. 5.6b images with mild artifacts can be identified with a sensitivity and specificity of 73% and 81% respectively. Images with moderate artifacts can be detected with a sensitivity and specificity of 80% and 90%. Images corrupted by severe motion are detected with 100% sensitivity and specificity. Images with and without motion cluster at a sensitivity and specificity rate of 78% and 81% respectively.

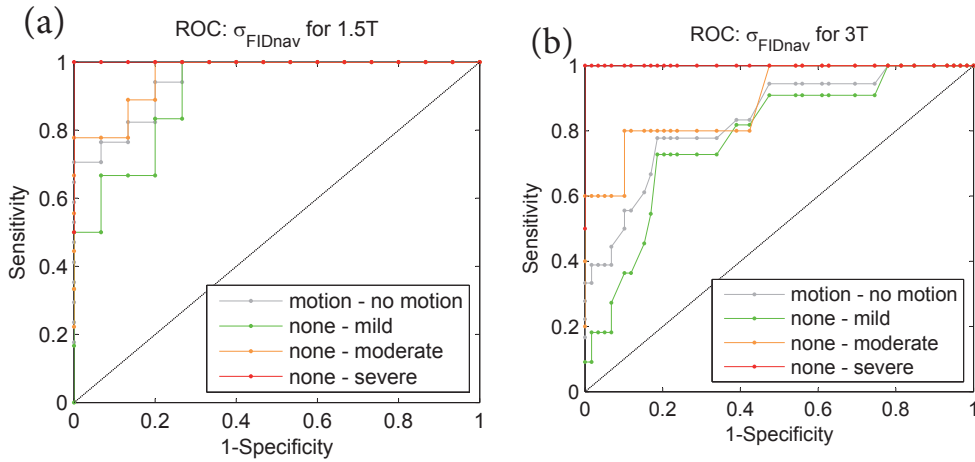


Figure 5.6: Shows the receiver operating characteristic (ROC) curves for a range of the standard deviation chosen as a detection limit [0.5 2.3] and its respective specificity and sensitivity for distinguishing groups of different artifact severity for the scanners of 1.5T and 3T field strength.

A similar evaluation was performed to find an optimal design for a detector based on $FIDnav_{NCmax}$ with respect to the number of relevant coil elements N_{NCmax} (Fig. 5.7). The results show that for $N_{NCmax} = 3$ and without any motion events the best sensitivity and specificity can be achieved to identify images without artifacts. Here, a sensitivity of 69% and a specificity of 92% were possible. Setting N_{NCmax} to 5 provided the best ROC for identifying images with mild artifacts of 53% and 85% sensitivity and specificity respectively. To detect images with moderate artifacts best results are achieved for $N_{NCmax} = 3$ with sensitivity at 93% and specificity at 92%. For identifying images with severe artifacts N_{NCmax} seems to be irrelevant. Data with ≥ 20 motion events correspond to severe image degradations with sensitivity and specificity equal to 100%. We could also observe that taking more than 6 coil elements for the calculation of the $FIDnav_{NCmax}$ did not improve the motion detection results. Hence, for further analysis we will set the number of relevant coil elements to $N = 3$ and refer to this $FIDnav$ based detector as $FIDnav_{3Cmax}$ i.e., a mean of the maximal signal change from three channels is taken for all further analysis.

Chapter 5. FID-based Motion Sensitive Quality Metric and Retrospective Motion Correction for Clinical Magnetic Resonance Images

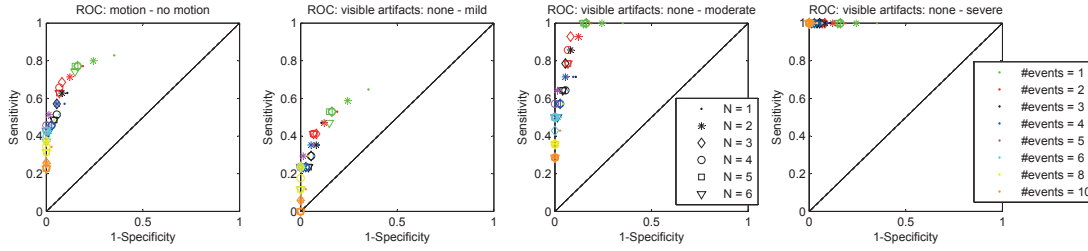


Figure 5.7: Receiver operating characteristic (ROC) curves for $FID_{nav_{NCmax}}$ as motion detector with different settings of relevant channels N_{NCmax} (N) and number of detected motion events ($\#events$) during the scan and its respective specificity and sensitivity for distinguishing groups of different artifact severity.

5.3.4 FIDnav Based Motion Classification Based on k-space Location

To make use of the additional information in the FIDnav on the time where motion was present during the acquisition we apply a weight to every motion event depending on its location in k-space. We will investigate a parabolic as well as a Gaussian weight curve and will aim at finding the optimal parameters for the respective curves. For the parabola we aim at finding the optimal crossing with the horizontal axis and for the Gaussian at the optimal σ . For both weight curves the vertex is fixed to be 1 for a motion event occurring at k-space center. The final FIDnav motion score FIDI is then calculated as a sum of weighted $FID_{nav_{3Cmax}}$ values at the k-space location, where a motion event was identified. We investigated different weight curves again with respect to sensitivity and specificity of the resulting weighted $FID_{nav_{3Cmax}}$ for its ability to detect motion in the underlying data set. Both, Gaussian and parabolic weight curves present near to identical results (Fig. 5.8). For the Gauss weight curve the best setting was identified to be $\sigma = N_{lin}/2.3$ and the parabola to cross the horizontal axis at $N_{lin}/1.5$ with N_{lin} being the total number of k-space lines. The Gauss weighting performs by 1% better than the parabolic weighing in identifying the data with mild artifacts with a sensitivity of 53% and a specificity of 86%. For other groups the performance is identical. Images with moderate artifacts can be identified with a specificity of 100% and sensitivity of 92%. Severely motion corrupted images can be detected with a 100% sensitivity and specificity rate.

Due to better performance of the Gaussian weight curve we continue our evaluation with it. Now we aim at finding the optimal thresholds for the FIDnav based motion index FIDI which divides the given data into the four artifact groups (none, mild, moderate, and severe) by performing a logistic regression (Fig. 5.9). Based on the regression results we identified the following FIDI thresholds for each of the groups: $FIDI_{motion} \geq 8$, $FIDI_{mild} \geq 13$, $FIDI_{moderate} \geq 40$, $FIDI_{severe} \geq 205$. These are the values of FIDI where the regression curve crosses the 0.5 probability value. The higher the FIDnav based index FIDI the higher the chance of the image to be motion corrupted e.g., a FIDI higher or equal 8 may correspond to a dataset with motion artifacts.

Also, a comparison with an existing quality metric QI as proposed by (Maréchal, 2011; Mortamet et al., 2009) was performed (Fig. 5.10). Both, QI and FIDI perform well on the

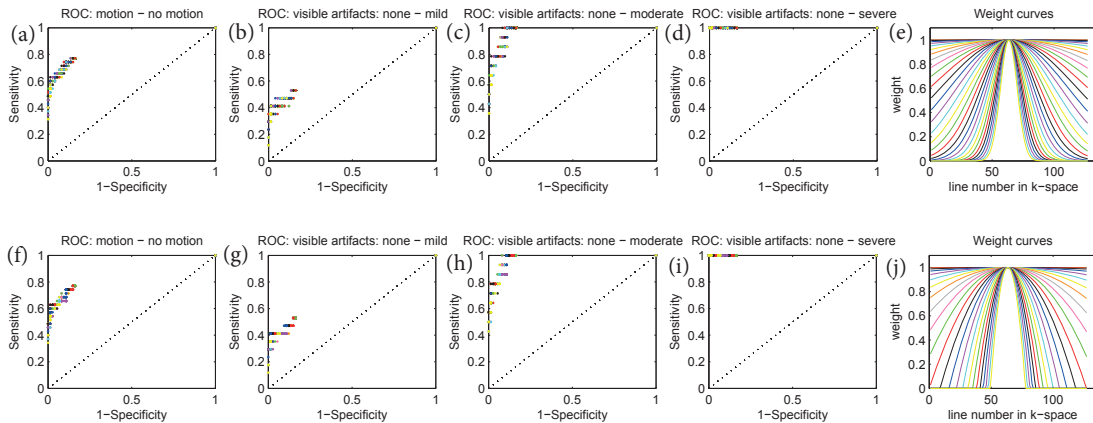


Figure 5.8: ROC curves for the weighted $FID_{nav3C_{max}}$ with different shapes of the weight functions and its ability to distinguish data sets of different artifacts groups: (a-d) Gaussian weights (f-i) parabolic weights. Color code corresponds to the respective shape of the weight function in (e) and (j).

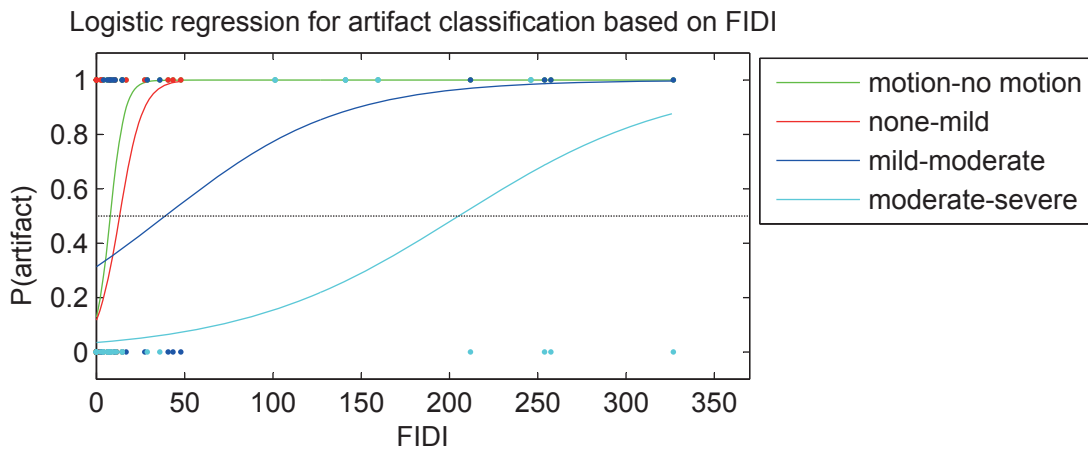


Figure 5.9: Logistic regression for FIDI and its probability to correspond to a different artifact groups.

detection of data sets with severe and no motion artifacts. For mild and moderate motion there is a discrepancy in both indexes.

5.4 Discussion

5.4.1 Advantages and Limitations of the Utilized Motion Correction

The recent studies have shown that motion in MRI examinations has a noticeable effect on the clinical workflow and presents a non-negligible financial impact due to rescans or patient sedation. In this study we further explore the problem of motion in a clinical setting by analyzing 109 clinical MP-RAGE images. Based on the expert radiologist ratings we report the estimates on the prevalence and severity of motion artifacts and find them similar to the

Chapter 5. FID-based Motion Sensitive Quality Metric and Retrospective Motion Correction for Clinical Magnetic Resonance Images

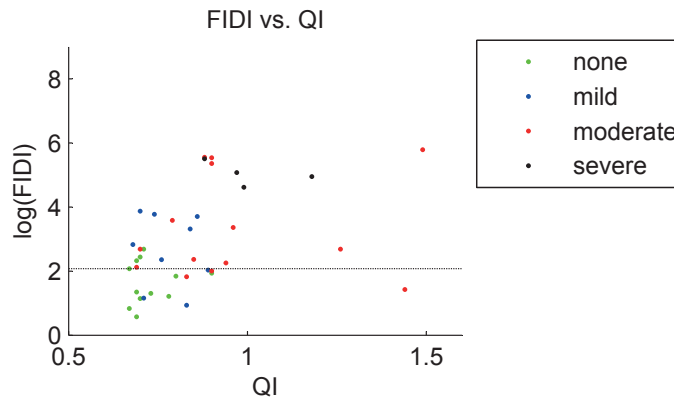


Figure 5.10: FIDI with its threshold indicated by a dashed line at 8 for FIDI for detection motion corrupted images. The lower the QI value the better the image quality.

previous studies. We also apply a retrospective motion correction technique to the collected data and based on the expert ratings confirm the ability of the method to improve the image quality.

We have evaluated blind and FID-guided motion correction methods in order to assess their ability to handle the clinical data. We observed that FID-guided motion correction approach performed better than blind correction except for a single case, where the correction introduced spurious ringing to the image. Since the original image is preserved, however, unlike after prospective motion correction, it would be still possible to use the uncorrected data for a final diagnosis.

Although, after FID-guided motion correction the images were all rated to be of a clinically useful quality, not all motion artifacts could be fully removed. This is due to a major limitation of retrospective correction techniques when it comes to severe head motion that leads to missing k-space data, which cannot be restored after the image has been acquired.

5.4.2 Advantages and Limitations of FIDnav-Based Motion Detection

Computer-aided disease prediction from quantitative image analysis requires high resolution MR data which should not have artifacts due to motion. This opens a new field of automated image quality calculations that assess the reliability of the quantitative results, for example in brain volume segmentations. A reliable image quality index might be able to eliminate the necessity to visually examine the image itself and for disease prediction just rely on the reported volume numbers instead. To our knowledge, only few automated and reference free motion sensitive quality criteria have been explored. Mortamet et al. (2009) rely on evaluations of the background noise in the image to assess the image quality quantitatively. Lin et al. (2007) and McGee et al. (2000) propose the use of a gradient entropy which evaluates the edges i.e., sharpness of an image. Another index for image quality is the signal-to-noise ratio (SNR) and

is traditionally used for MR images (Kaufman et al., 1989).

We present a novel methodology to quantitatively assess the image quality based on the recently proposed FID signal. Such FID signal or FIDnav can be added easily to a sequence with only minimal timing requirements and be used to observe the signal fluctuations during the scans. Since it is known that the FIDnav, as any MR signal, depends on the proximity of the examined object to the receive coil it is possible to relate fluctuations in the acquired signal directly to motion. By observing the FIDnav temporal behavior it is also possible to provide information on the time when motion occurred during the acquisition and stop the scanning if too many motion events are identified. We propose a novel formulation of an FID signal based quality index FIDI and suggest an empirical threshold to identify motion corrupted images for $FIDI \geq 8$. In this study we decided not to use any of the established classification techniques from the field of machine learning and rather design a classifier 'by hand' for better understanding of the chosen classifier features. This 'white box' approach, however, limits us to fully investigate the reliability of the classifier as well as potentially more features that could yield better performance. Further, the relatively low sample size of 109 cases might not be sufficient to show robust statistical behavior of the classifier. However, due to the high time effort for the rating and ranking of the images we consider the current data set adequate to derive first conclusions from this pilot study. Although, our data set exhibits similar numbers for prevalence of motion as in studies with higher sample size indicating representative results, we assume that higher classification robustness would be achieved with more data sets.

The FIDnav signal is not only sensitive to rigid head motion, it can be also influenced by any non-rigid motion as swallowing or other mouth movements. Such non-rigid motion might not have a severe impact on the resulting image quality, hence, this would lead to a discrepancy in the reported FIDI and the underlying, possibly nonexistent, motion artifacts in the region of interest, i.e., anatomies relevant for diagnosis.

5.4.3 Future Work

Future work will focus on the integration the retrospective motion correction techniques as well as the proposed quality index into the clinical workflow. This would make it possible to conduct large scale studies and to assess the direct impact on the diagnosis. Other FIDnav-based classifiers for the detection of motion corrupted images as well as classical data mining methods such as random forests or support vector machines could be investigated to identify motion relevant features of the FID signal and classify the data even more reliably.

5.5 Acknowledgement

We would like to thank Sebastian M. Waszak, Alexis Roche, Davide Piccini, Guillaume Bonnier, Tom Hilbert, Mario Fartaria De Oliveira, and last but not least Pavel Falkovskiy for valuable discussions and suggestions.

6 Prospective Head Motion Correction with FID-Triggered Image Navigators

This chapter is based on published work from Babayeva et al. (2014a) and Babayeva et al. (2015a).

Abstract Motion is still a major source of artifacts in clinical magnetic resonance imaging. To manage motion we explore the utilization of a multi-channel FID signal for subject's head movement monitoring in order to employ an MR image navigator based correction only when relevant motion occurred. The acquisition of the FID signal as well as the image navigator is integrated into a three-dimensional MP-RAGE sequence to correct for rigid head motion during the acquisition. We introduce two different methods to extract binary motion information from the FID signal, which is highly sensitive to positional changes of the head and is used to trigger the acquisition of the image navigator. The image navigator is then co-registered to a reference image to obtain the motion parameters and to adjust the scanning orientation respectively when needed. The image navigator is specifically designed to match the acoustic and magnetization characteristics of the MP-RAGE sequence targeted for correction. We perform brain volume segmentation and quality index calculations to quantitatively assess the motion correction performance of the proposed approach.

6.1 Introduction

Reducing motion impact on brain MR imaging would be a great asset to routine and clinical research applications, making studies more cost-efficient and leading to increased patient throughput. Despite of many advances in the field of rigid motion correction in MRI no general solution could yet be found (Zaitsev et al., 2015). All suggested correction techniques target specific sequences or can correct for only specific motion types as for example only in-plane motion.

Chapter 6. Prospective Head Motion Correction with FID-Triggered Image Navigators

Motion correction methods are categorized into prospective and retrospective ones. Prospective methods are applied during the sequence run time by periodically adapting the acquisition coordinate system to follow the imaged object and have the advantage to be able to compensate even for considerably big motion magnitudes and also to correct for spin history effects. The prospective motion correction strategies are traditionally based on MR-based navigators of various complexity (Tisdall et al., 2012; van der Kouwe et al., 2006; White et al., 2010), external tracking systems as an optical camera with a marker (Zaitsev et al., 2006), or active coils (Ooi et al., 2013). External tracking hardware can provide very accurate motion information, be integrated with various sequences, and correct for spin history effects. However it relies on fiducial markers that might not be well tolerated by the subject, and on an unobstructed field of view, which can be compromised by a closed coil design. MR-based navigators are potentially valuable complements for prospective motion correction as no additional hardware for external devices is required but a tradeoff between tracking accuracy and navigator complexity has to be considered. Higher navigator complexity provides better tracking and hence correction results but may cost more additional scan time or be incompatible with the target sequence design. Retrospective methods address the problem of motion after the image has been acquired and are ideally independent of the MR imaging modality. A famous retrospective correction method is called PROPELLER (Pipe, 1999) (also called BLADE at Siemens context (Fries et al., 2009)), where the center of k-space is oversampled to have redundant information that is then used to adjust k-space lines to achieve better image quality. Another class of retrospective correction techniques is based on autofocusing (Atkinson et al., 1997; Loktyushin et al., 2013). The advantage of these methods is that they can even correct for non-rigid motion (Loktyushin et al., 2015b), however they are limited by their inability to address large motion magnitudes, which lead to unrecoverable missing k-space data.

In this investigation, we explore the possibility of a new prospective motion correction strategy, which utilizes the recently proposed free-induction-decay navigator (FIDnav) (Kober et al., 2011) for motion monitoring and detection to drive the acquisition of a more complex image navigator (IMGnav) for motion tracking and correction when needed. This helps to reduce the scan time and/or gradient activity overhead as required for a repetitive acquisition of an IMGnav. Moreover, the scan time for FIDnav is almost negligible and the time costly IMGnav is triggered only if motion occurred.

In this study we focus on the MP-RAGE sequence and a dedicated, i.e., a specifically for this sequence designed IMGnav. It needs one TR for its acquisition and has the same number of RF-pulses in order to have minimum impact on the magnetization profile of the target MP-RAGE sequence, and has a similar acoustic noise pattern. The FID signal, however, is acquired every TR at the end of each read-out train during sequence runtime. Only if motion is detected according to the changes in the FIDnav signal, an IMGnav acquisition is triggered, followed by registering of the IMGnav to a reference IMGnav volume in order to obtain new positional information and to change the orientation of the gradients prospectively.

6.2 Methods

6.2.1 FIDnav Acquisition and Calculation

The purpose of this study was to

1. present different ways of combining the multi-channel FID signal from different coil elements into a single scalar FIDnav, which is then used for motion detection as already shown in Chapter 5 for retrospective labeling of motion events in clinical MP-RAGE images. In order to detect motion events based on the FIDnav a threshold is necessary. We propose two different ways of setting the threshold. One way is to set the value a priori to be the same for all subjects and scans (FID_{nav}^{fast} and FID_{nav}^{slow}). This approach is considered to be more sensitive to motion than the method proposed in (Kober et al., 2011) as only channels with maximal signal change are considered. The other way is to set the threshold according to statistical characteristics of the signal which are estimated during the scan based on few FIDnav samples from the beginning of the acquisition (FID_{nav}^{theo}) similar to the technique proposed in (Kober et al., 2011). Both threshold setting scenarios have their advantages and disadvantages and will be discussed later.
2. investigate how well the FIDnav reacts to different types of motion (head nodding, shaking, and head-feet translation)

The functionality was implemented in a prototype MP-RAGE sequence. An FID signal was sampled ($\alpha = 9^\circ$, 64 points in 0.2 ms, TI = 1532 ms) following an additional non-selective excitation pulse at the end of the GRE block of the MP-RAGE sequence. The FIDnav was evaluated in different ways to detect motion events. One modification of the FIDnav was meant to be able to detect slow motion (e.g., muscle relaxation) and fast head motion (e.g., rapid head turning). To distinguish signal changes due to motion an empirical threshold was chosen. These FID signal calculations we will refer to as FID_{nav}^{fast} and FID_{nav}^{slow} . The other way of the FIDnav calculation relies on an adaptive threshold which was calculated based on several FID signal values from the beginning of the scan to avoid the need for an empirical setting of threshold. These values were used to calculate expected statistical properties i.e., mean and variance of the signal to detect outliers. Outliers were then classified as motion events. We will refer to this FIDnav as FID_{nav}^{theo} .

For the detection of rapid and slow head movements with an empirical threshold, a scalar FIDnav value was calculated by combining the signals from coil elements where the signal change was maximal among all channels. Rapid motion at a time point t is observed by signal changes as compared to the preceding repetition at $(t - 1)$, whereas slow movements at time t are reflected by FIDnav changes as compared to the first repetition of the scan (see Eq. 6.1). An empirically derived threshold of 5% increase in FID signal for slow movements and 8% signal change for fast movements was chosen to trigger the acquisition of an IMGnav. During pre-scans these thresholds proved appropriate with respect to non-motion related FID

Chapter 6. Prospective Head Motion Correction with FID-Triggered Image Navigators

signal fluctuations, which cause higher scan run times due to unnecessary motion correction, and sensitivity to detect real motion events. Here, $|s(n)|$ is the absolute value of the complex average of all points from one single FID read-out acquired in the t^{th} repetition, and c denotes the coil element. The avg_{3Cmax} operator takes the FIDnav from those three coil elements where the signal change is maximal and averages them and the avg_{AIC} takes the average over all coil elements. We used the average of three coils to minimize the effect of random signal fluctuations. The first two signal time points (equals the first two TRs) were excluded from the FIDnav calculation due to the signal not being in steady-state yet i.e., $|s(3)|$ is used for signal normalization. Hence the motion detection starts at the third TR. If either FID_{nav}^{fast} or FID_{nav}^{slow} exceeded the empirical threshold then the respective TR was considered to contain a motion event.

$$FID_{nav}^{fast}(t) = avg_{3Cmax} \left| \frac{|s(t)| - |s(t-1)|}{|s(3)|} \right| \quad FID_{nav}^{slow}(t) = avg_{AIC} \left| \frac{|s(t)| - |s(3)|}{|s(3)|} \right| \quad (6.1)$$

The adaptive threshold for the FIDnav with a theoretical value was calculated based on statistical behavior of the signal. For this FIDnav we evaluated the FID signal by calculating its temporal standard deviation σ_{AIC} for every channel separately (see Eq. 6.2). If the FIDnav of any single time point t revealed a signal change higher than $3\sigma_{AIC}$ in comparison to the previous repetition $t-1$ in more than one channel then this TR was considered to contain a motion event similar to FID_{nav}^{fast} . If only one channel detects a signal change no action is taken as due the symmetry of the acquisition head coil it is considered not plausible that signal changes in only one channel can be caused by rigid body motion. We assume that if only one single channel detects FID signal changes, then these changes might be caused by other effects than motion. The detected motion events were excluded from the calculation of σ_{AIC} . The first two signal time points were again excluded from the evaluation as the signal was not considered to be in steady state yet. The next two time points were used to calculate the initial value of σ_{AIC} , such that motion detection could start only at the fifth signal point or TR after the start of the scan. Once, the fifth TR is reached motion detection is possible at any TR.

$$FID_{nav}^{theo}(t, c) = \left| \frac{|s(t, c)| - |s(t-1, c)|}{|s(3, c)|} \right| \quad (6.2)$$

6.2.2 MP-RAGE Data Acquisition and Experimental Design

The MP-RAGE images were acquired with the following parameters: TI/TR/TE/ α /TA = 900ms/2300ms/2.86ms/9°/5:21min, echo-spacing 7 ms, matrix $256 \times 256 \times 176$, 1.0 mm^3 isotropic, $2 \times \text{iPAT}$ with 32 ref. lines.

Two datasets were collected using different modifications of the FIDnav (FID_{nav}^{fast} , FID_{nav}^{slow} and FID_{nav}^{theo}) as described in the previous section and different motion patterns were investigated. After obtaining written consent, 10 healthy volunteers were scanned - five for each dataset. Based on the FIDnav, motion events were detected and the prospective acquisition of the IMGnav was triggered. The IMGnav was then co-registered to its reference from the beginning of the scan to derive new positional information of the head and to adjust the acquisition orientation accordingly (Fig. 6.1). The motion corrupted repetition was reacquired immediately after.

The first dataset A was acquired at 3T (MAGNETOM Verio, Siemens AG, Erlangen, Germany) operating under the VB17 software version and using a commercial 32-channel head coil. The subjects were instructed to change their head position three times during a scan upon verbal commands and to follow frequently observed motion patterns (Gedamu and Gedamu, 2012): translation in head-feet direction, head nodding, and shaking. The motion was performed as a one-time-event by repositioning the head accordingly and remaining in this position until the next verbal command. These scans were repeated by having the motion correction turned on and off to see the image quality changes from the correction technique. Two additional datasets (I, II) for scan – re scan comparison of images acquired without voluntary motion and with motion correction turned off but with the acquisition of the IMGnav were acquired for each subject, resulting in a total of 40 MP-RAGE volumes. To drive the motion correction FID_{nav}^{fast} and FID_{nav}^{slow} were utilized for motion detection. To assess the effect of reacquisition two sets of images were reconstructed. The first set by utilizing the reacquired repetition after a motion event and the second set without the reacquired data.

The second dataset B was as well acquired a 3T (MAGNETOM Skyra, Siemens AG, Erlangen, Germany) operating under the VD13 software version and using a commercial 32-channel head coil and the subjects were again asked to change their head position three times during the scan but now following a different motion pattern to save scan time due to an extended experimental design (data acquisition for the evaluation from Chapter 6.2.3). The first positional change is rotating the head to the left side, the second is moving the head back to center and down at the same time similar to nodding, and last is rotating the head to the right. Before the next scan the subject was instructed to return its head to the initial position looking straight up (left-down-right). Each subject was scanned by having the motion correction mechanism turned on and the motion parameters were stored in a file. This recorded motion trajectory was then used in order to recreate the motion artifacts that would appear if no motion correction was applied as described in (Herbst et al., 2014). This was accomplished by acquiring a dataset where the subject was instructed to remain still and the previously

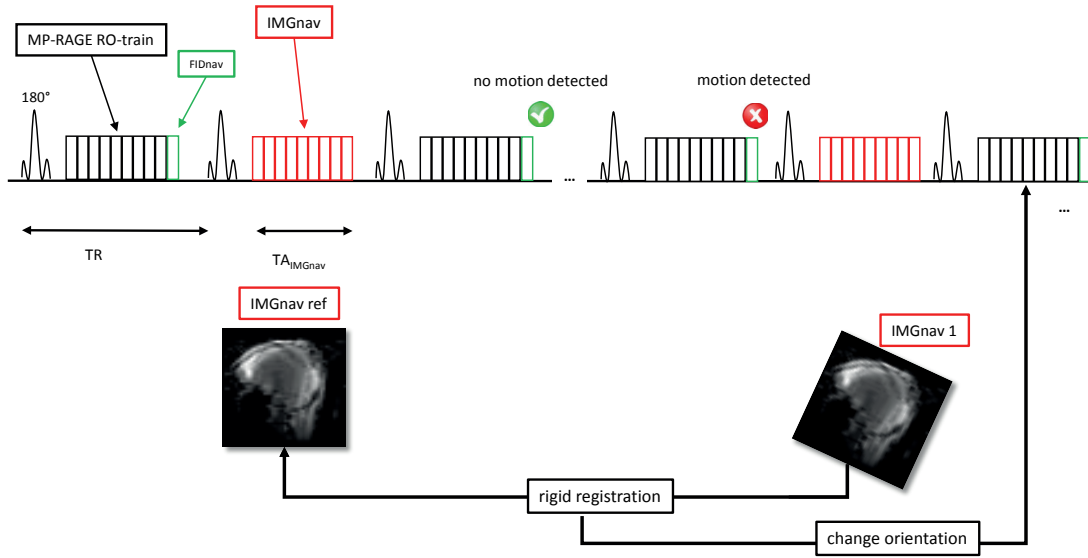


Figure 6.1: Symbolic depiction of the proposed MP-RAGE acquisition strategy with motion correction based on FIDnav triggered IMGnavs.

acquired motion trajectory was applied during the scan to change the coordinate system for each TR. Two additional datasets without voluntary motion and without motion correction were acquired for each subject for reference. For these datasets without motion no IMGnav were acquired. This resulted in a total of 20 MP-RAGE volumes. This dataset was used to explore the triggering reliability of FID_{nav}^{theo} . The images were reconstructed by utilizing the reacquired repetitions.

We would like to mention here that the data was acquired unintentionally from different scanners due to the unavailability of the Verio scanner during the study caused by a scanner software upgrade. Please, refer to Tab. 6.1 for an overview of the acquisition settings and utilized FIDnav calculation variants. Further, to reduce the scan time per subject due to an additional experiment that is described in 6.2.3 only one motion scan per subject was performed in the dataset B. Therefore, a heterogeneous motion pattern (left-down-right) was introduced to cover different motion directions in a single scan.

6.2.3 IMGnav Acquisition and Image Registration Accuracy

For the IMGnav we used a modification of a recently proposed multi-echo segmented 3D-GRE (Falkovskiy et al., 2016, 2013) but with a cylindrical k-space sampling pattern as shown in Fig. 6.2b ($\alpha/TA = 9^\circ/1.2\text{sec}$, echo-spacing 7 ms, 6 echoes, matrix size $64 \times 64 \times 32$, voxel size $4.1 \times 4.1 \times 6.0 \text{ mm}^3$). The standard MP-RAGE acquisition scheme was adapted to acquire multiple echoes using bipolar readout gradients. Phase-encoding gradients were inserted between the readout gradients to sample multiple portions of k-space per each excitation pulse. The reordering scheme was modified to group first echoes in the center of k-space to

dataset	MoCo setting	motion pattern	scanner type and software version	FID _{nav} and threshold variant
A.1-A.5	MoCo ON	nodding motion shaking motion z-translation	Verio, 3T, VB17	FID_{nav}^{slow} , FID_{nav}^{fast} , empirical threshold
	MoCo OFF	nodding motion shaking motion z-translation no motion $\times 2$		
B.1-B.5	MoCo ON	left-down-right	Skyra, 3T, VD13	FID_{nav}^{theo} , adaptive threshold
	MoCo OFF	inject motion no motion $\times 2$		

Table 6.1: An overview of the acquired datasets with its respective settings for FID_{nav} variants and motion patterns.

ensure the intended contrast (see Fig. 6.2a). A phase correction algorithm similar to the one used for EPI acquisitions was applied to remove phase inconsistencies between k-space lines acquired in the echoes with differing polarity. This correction was computed based on the lines acquired in the center of k-space.

The acquisition parameters of the IMG_{nav} were specifically designed to acquire a whole-brain volume with very similar properties as the GRE block of the host MP-RAGE with respect to the acoustic noise and impact on longitudinal magnetization. The unacquired k-space lines and partitions resulting from the cylindrical sampling pattern were zero filled for image reconstruction (see Fig. 6.2b).

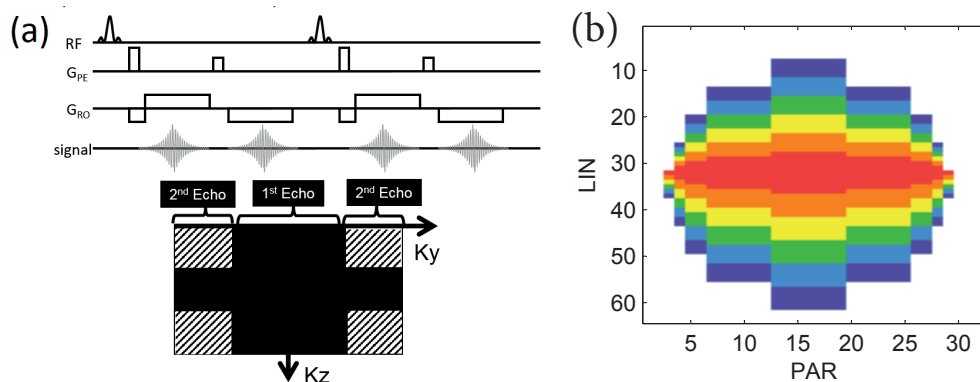


Figure 6.2: *a:* Acquisition sequence of the IMG_{nav} on an example with two echoes. *b:* Acquisition design of the IMG_{nav}; different colors label echo number (red 1st echo, orange 2nd echo, yellow 3rd echo, green 4th echo, blue 5th echo and purple 6th echo), whereas in white unacquired k-space locations are labeled and are filled with zeroes for reconstruction.

Chapter 6. Prospective Head Motion Correction with FID-Triggered Image Navigators

To derive the motion parameters from an IMGnav image registration was used. For that we utilized the 3D PACE registration algorithm used in the motion correction technique (Thesen et al., 2000). In order to assess the image registration accuracy we performed a simulated motion experiment. For that we acquired 100 IMGnavs volumes of a human subject in a row. Each IMGnav was preceded by an inversion pulse resembling the acquisition settings as it would be embedded into an MP-RAGE host sequence with a TR/TI of 2300/900 ms. For each of the volumes we changed the orientation or the acquisition according to a prescribed motion trajectory resembling frequently observed motion patterns (Gedamu and Gedamu, 2012) head nodding, shaking, and translation along the head-feet direction. This trajectory was recorded from a moving subject by an optical motion tracking system (Zaitsev et al., 2006) in an earlier study (Babayeva et al., 2015b) and was provided to the sequence in form of a text file.

After obtaining written consent five healthy volunteers were scanned with this sequence at 3T (MAGNETOM Skyra, Siemens AG, Erlangen, Germany) operating under the VD13 software and using a commercial 32-channel head coil. Subjects were instructed to remain motionless during the whole experiment. Additionally, 60 IMGnav volumes of a volunteer were acquired without changing the orientation, while the subject was again instructed to remain still during the scan in order to assess the registration variance when the subject is at rest.

6.2.4 Quantitative Image Quality Assessment

Motivated by a recent studies in Maréchal et al. (2012); Reuter et al. (2015) the performance of the proposed correction method was assessed by conducting brain volume segmentation in three regions using an automated morphometry package (Schmitter et al., 2014). The segmentation results of the scans with motion and correction, with motion but without correction or simulated motion respectively, and without motion and without correction were compared to the reference without motion and correction. We calculated the relative volume differences between the ‘no motion’ $V_{nomotion}$ and ‘motion’ V_{motion} cases for total intracranial volume (Δ_{TIV}), white matter (Δ_{WM}), and gray matter (Δ_{GM}).

$$\Delta = \left| \frac{V_{motion} - V_{nomotion}}{V_{nomotion}} \right| * 100$$

Further, a quantitative image quality assessment based on the background noise evaluation as described in (Maréchal, 2011; Mortamet et al., 2009) was performed on all MP-RAGE volumes to assess the change in the quality index (QI) with and without correction quantitatively as well with and without reacquisition on the dataset A.

6.3 Results

6.3.1 IMGnav and Its Registration Accuracy

The proposed motion correction can be only as good as the image registration reliability of the utilized IMGnav. Our experiments revealed that the employed registration framework was able to extract the motion parameters with a mean absolute error of 0.27 ± 0.38 mm and $0.19 \pm 0.24^\circ$ for translational and rotational motion, however with maximal registration errors of up to 2.0 mm and 1.3° (see Fig. 6.3c-d). The prescribed artificial trajectory was in the range of up to 17.9 mm and 5.5° for translations and rotations respectively (Fig. 6.3b). In Fig. 6.3a the IMGnav as acquired from one subject is shown and ghosting artifacts in the anterior-posterior direction on the sagittal and axial view are visible. This is also the phase encoding direction of the IMGnav acquisition. These artifacts are present in all IMGnav acquisitions from all subjects. In the experiment where 60 IMGnavs were acquired sequentially and the subject was asked to stay as still as possible the registration parameters showed motion around the zero line with the mean absolute translation and rotation of 0.02 ± 0.02 mm and $0.01 \pm 0.02^\circ$ respectively.

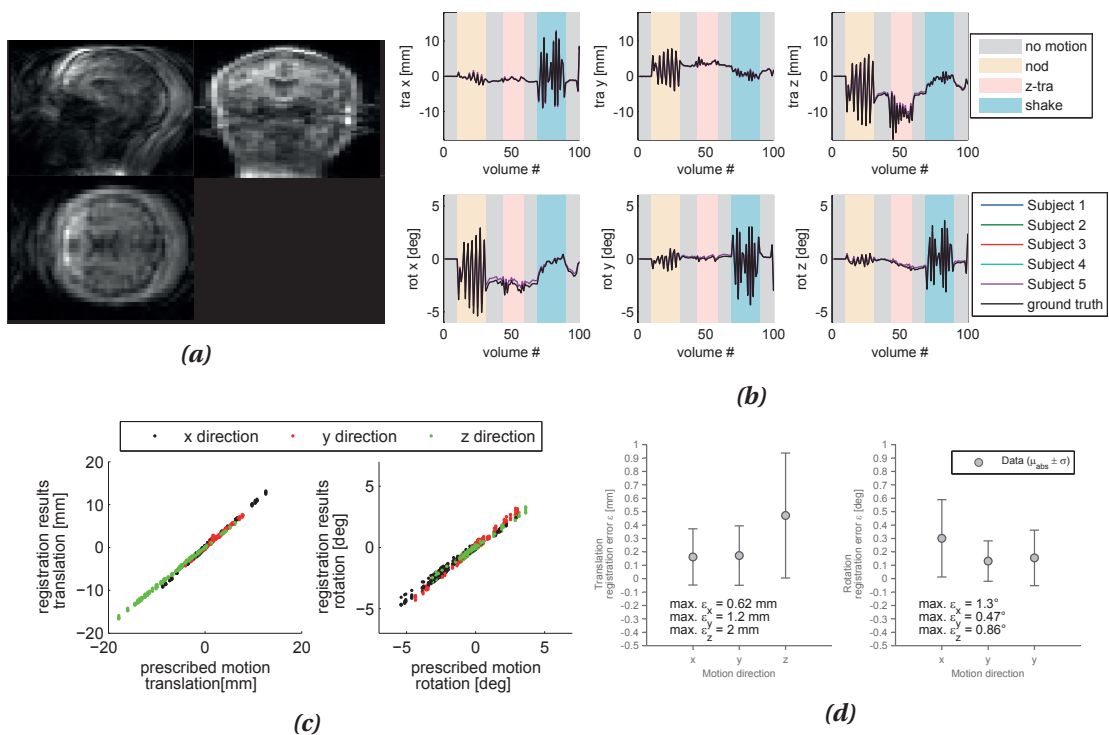


Figure 6.3: *a:* Sagittal, coronal and axial view of the IMGnav. *b:* Prescribed motion trajectory for the assessment of the registration reliability of the IMGnav. Artificial motion patterns for head nodding ‘nod’, head shaking ‘shake’, and moving the head in the head-foot direction ‘z-tra’, as well as periods without motion are depicted for rotation and translation in all six degrees of freedom. The resulting registration results for five different subjects are also shown. *c:* Registration results from all subjects versus the applied motion trajectory for translation and rotation in x, y, and z directions. *d:* Registration error for translations and rotations for all five subjects with its mean of the absolute error and standard deviation. Also, the maxima of the detected registration errors are shown.

6.3.2 FIDnav, Triggering Events, and Detected Motion

In our motion correction experiments we detected motion of up to 11 mm translation and 9° rotation as can be seen in Table 6.2. The motion correction took place only if the FIDnav reported a motion event in the corresponding repetition as described in Chapter 6.2.1 i.e., deliberate positional changes of the head after verbal commands. Verbal commands were given to the subjects three times during the acquisition of one MP-RAGE volume, however more motion events were detected by the FIDnav indicating its high sensitivity to motion or high amount of false positives (5%). During scans where the subject was asked to remain still few triggering events occurred. In the case of the dataset A, where FID_{nav}^{fast} and FID_{nav}^{slow} was used to detect motion, the acquisition of the IMGnav was sometimes (in 3 cases) initiated by the FID_{nav}^{slow} approximately after 2/3 of the total scan time as can be seen in Fig. 6.4a. Here, the registration parameters indicated very small positional changes of the head in the range of 1 mm and 1°.

In the case of subject A.1 for the ‘no motion’ scan a high number of triggering events was detected but the reported registration parameters did not indicate any significant positional changes of the head and also the image did not show any obvious motion artifacts. For the dataset B, where FID_{nav}^{theo} was driving the motion correction functionality, a higher amount of triggering events was detected at the beginning of the scan indicating that the dynamic threshold is inappropriate due to a low count of data points used for its calculation. True motion events, which we assume to take place only after verbal commands, were detected in all cases and the acquisition of the IMGnav was reliably triggered to provide the new positional parameters to the sequence and to reacquire the motion corrupted repetition.

In some cases several triggering events were detected after a verbal command was given to the subject to change its head position. In these cases the registration parameters showed that indeed the subject could not hold the new position immediately and moved its head even further or slightly back towards the original position (Fig. 6.4b, Fig. 6.5a, Fig. 6.6). This behavior was also confirmed by the subject in a discussion after the experiment. Overall a sensitivity of 100% and a specificity of 95% could be reported if the detected motion events are considered to be true only after a verbal command. In total there are 139 repetitions and 3 expected motion events per scan (60 scans in total) for acquisitions with intended head movements. Therefore, out of 8340 total repetitions there were 105 true positive and 395 false positive motion events.

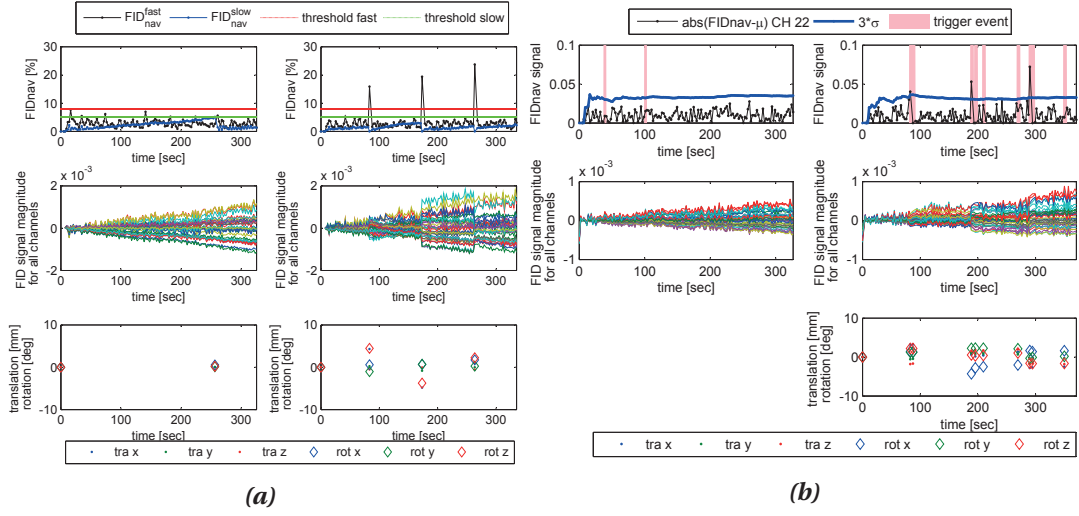


Figure 6.4: The triggering events and the corresponding motion trajectories as well as the normalized FID signal magnitude from all 32 coil elements are shown. The shown FID signal was shifted to zero for better visual representation. *a:* FID_{nav}^{slow} and FID_{nav}^{fast} for a subject at rest and performing shaking motion. *b:* FID_{nav}^{theo} for a subject at rest and changing head positions to the left, down, and right sides. The absolute FIDnav signal magnitude after normalization by the moving average μ is shown for one channel. The triggering events, where the dynamic threshold was exceeded in more than one channel, are also marked.

The proposed motion correction mechanism prolongs the scan time by two TRs after each triggering event: one TR (2300 msec) for the acquisition of the IMGnav and one TR for the reacquisition of presumably motion corrupted repetition. On average 8.3 motion events per volume scan were detected (see Tab. 6.2). The mean extra time, which is spent due to the enabled motion correction, was 41 seconds per volume scan if we consider all acquired data sets. In the scans where the subject was asked to stay still on average 4.9 motion events were detected by the FID_{nav}^{fast} and FID_{nav}^{slow} that correspond to 25 sec extra scan time per scan. The FID_{nav}^{theo} detected on average 7.5 motion events in no motion scans corresponding to 37 sec additional scan time per scan.

As shown in Fig. 6.5 and Fig. 6.6 artifacts are visible in images without motion correction. Although, visual improvement of motion corrected compared to uncorrected images is apparent, not all motion artifacts could be removed. In the motion corrected images residual ringing artifacts or even blurring or ghosting was visible (Fig. 6.5b).

Chapter 6. Prospective Head Motion Correction with FID-Triggered Image Navigators

subject	experiment	number of trigger events	extra time [sec]	maximal translation [mm]	maximal rotation [deg]	QI [a.u.]	TIV [ml]	WM [%]	GM [%]
A.1	MoCo ON, nodding motion	22	103.5	1.79	0.83	0.76	1420.1	27.70	52.67
	MoCo OFF, nodding motion	41	190.9	1.20	0.80	0.94	1419.7	27.82	51.42
	MoCo ON, shaking motion	18	85.1	2.42	3.50	0.83	1417.8	27.08	52.97
	MoCo OFF, shaking motion	20	94.3	2.96	3.38	1.29	1419.7	28.40	51.70
	MoCo ON, z-translation	32	149.5	2.87	1.81	0.78	1425.5	27.68	51.56
	MoCo OFF, z-translation	17	80.5	3.15	0.30	1.02	1372.7	24.87	54.49
	MoCo OFF, no motion I	16	75.9	0.68	0.43	0.69	1420.2	27.85	51.19
	MoCo OFF, no motion II	23	108.1	1.17	0.22	0.70	1422.2	28.23	51.19
A.2	MoCo ON, nodding motion	10	48.3	7.03	2.52	0.76	1209.5	28.23	49.61
	MoCo OFF, nodding motion	6	29.9	2.32	4.56	0.89	1183.3	27.34	51.72
	MoCo ON, shaking motion	4	20.7	7.19	6.40	0.95	1184.3	27.47	51.42
	MoCo OFF, shaking motion	5	25.3	10.97	9.26	1.34	1133.4	28.87	50.47
	MoCo ON, z-translation	13	62.1	7.15	1.74	0.74	1204.4	28.16	48.57
	MoCo OFF, z-translation	9	43.7	6.49	1.14	0.90	1145.5	27.09	51.07
	MoCo OFF, no motion I	5	25.3	0.89	0.11	0.72	1204.9	28.15	48.97
	MoCo OFF, no motion II	0	2.3	n.a.	n.a.	0.73	1207.9	27.94	48.51
A.3	MoCo ON, nodding motion	4	20.7	2.83	8.09	0.89	1411.9	27.39	53.83
	MoCo OFF, nodding motion	3	16.1	3.02	9.46	0.99	1385.8	26.63	52.89
	MoCo ON, shaking motion	3	16.1	4.82	4.47	0.89	1410.1	28.08	51.27
	MoCo OFF, shaking motion	3	16.1	4.52	4.07	1.11	1369.5	27.38	52.94
	MoCo ON, z-translation	13	62.1	10.51	1.90	1.03	1405.8	29.24	49.94
	MoCo OFF, z-translation	3	16.1	5.31	0.81	0.92	1373.1	26.04	53.16
	MoCo OFF, no motion I	1	6.9	0.58	0.53	0.7	1426.6	29.15	50.05
	MoCo OFF, no motion II	1	6.9	1.80	0.78	0.72	1426.4	29.16	49.71
A.4	MoCo ON, nodding motion	3	16.1	2.84	5.85	0.79	1447.9	27.49	55.94
	MoCo OFF, nodding motion	4	20.7	3.34	6.00	0.97	1425.8	26.55	54.78
	MoCo ON, shaking motion	5	25.3	3.78	6.46	0.92	1447.2	27.07	56.18
	MoCo OFF, shaking motion	3	16.1	3.70	3.80	1.13	1423.9	25.44	56.68
	MoCo ON, z-translation	4	20.7	2.25	0.16	1.08	1429.0	25.93	55.98
	MoCo OFF, z-translation	5	25.3	3.96	0.86	1.18	1440.4	27.54	55.68
	MoCo OFF, no motion I	2	11.5	0.83	0.07	0.80	1460.9	28.22	54.08
	MoCo OFF, no motion II	1	6.9	0.23	0.03	0.82	1466.4	28.22	53.94
A.5	MoCo ON, nodding motion	4	20.7	6.61	9.30	0.79	1506.4	30.15	49.79
	MoCo OFF, nodding motion	3	16.1	4.08	5.27	0.84	1454.2	29.03	50.47
	MoCo ON, shaking motion	3	16.1	5.92	6.83	0.76	1500.6	31.15	45.38
	MoCo OFF, shaking motion	3	16.1	6.28	7.51	0.79	1481.5	29.38	50.42
	MoCo ON, z-translation	6	29.9	7.60	6.09	0.79	1498.3	32.09	46.92
	MoCo OFF, z-translation	7	34.5	10.53	3.09	0.91	1476.8	31.88	48.01
	MoCo OFF, no motion I	0	2.3	n.a.	n.a.	0.75	1509.8	31.21	46.96
	MoCo OFF, no motion II	0	2.3	n.a.	n.a.	0.76	1510.5	31.65	47.40
B.1	MoCo ON, left-down-right motion	9	43.7	2.57	2.51	0.75	1647.0	27.11	54.22
	inject motion	5	25.3	n.a.	n.a.	0.81	1645.1	26.12	53.74
	no motion I	13	62.1	n.a.	n.a.	0.71	1650.2	27.83	53.57
	no motion II	11	52.9	n.a.	n.a.	0.73	1650.3	27.92	54.23
B.2	MoCo ON, left-down-right motion	13	62.1	2.60	3.05	0.68	1581.4	29.99	46.54
	inject motion	4	20.7	n.a.	n.a.	0.82	1579.5	28.30	49.95
	no motion I	7	34.5	n.a.	n.a.	0.63	1582.9	30.21	47.63
	no motion II	11	52.9	n.a.	n.a.	0.63	1584.5	30.10	47.90
B.3	MoCo ON, left-down-right motion	18	85.1	2.41	3.91	0.76	1738.3	27.57	55.28
	inject motion	6	29.9	n.a.	n.a.	0.76	1728.6	26.00	55.88
	no motion I	4	20.7	n.a.	n.a.	0.63	1753.4	33.00	50.70
	no motion II	3	16.1	n.a.	n.a.	0.64	1754.7	32.92	50.95
B.4	MoCo ON, left-down-right motion	9	43.7	3.23	4.31	0.69	1567.8	31.33	48.73
	inject motion	12	57.5	n.a.	n.a.	0.84	1553.1	29.08	52.99
	no motion I	2	52.9	n.a.	n.a.	0.71	1571.0	32.89	48.25
	no motion II	10	25.3	n.a.	n.a.	0.78	1570.4	29.32	52.15
B.5	MoCo ON, left-down-right motion	10	62.1	6.12	6.02	0.79	1855.3	29.98	51.64
	inject motion	6	48.3	n.a.	n.a.	0.88	1750.9	28.75	52.14
	no motion I	9	29.9	n.a.	n.a.	0.65	1744.9	33.65	48.77
	no motion II	13	43.7	n.a.	n.a.	0.64	1707.5	33.39	50.66

Table 6.2: An overview of all acquired data from all subjects with the corresponding number of detected motion events and the extra scan time which is needed for a the acquisition of the IMGnav and the rescan of the previous train-echo, which is considered motion corrupted. Also the maxima of the detected motion are shown together with the results from quantitative image quality assessment through the quality index (QI) and morphological brain segmentation results for total intracranial volume (TIV), relative white matter (WM), and gray matter (GM).

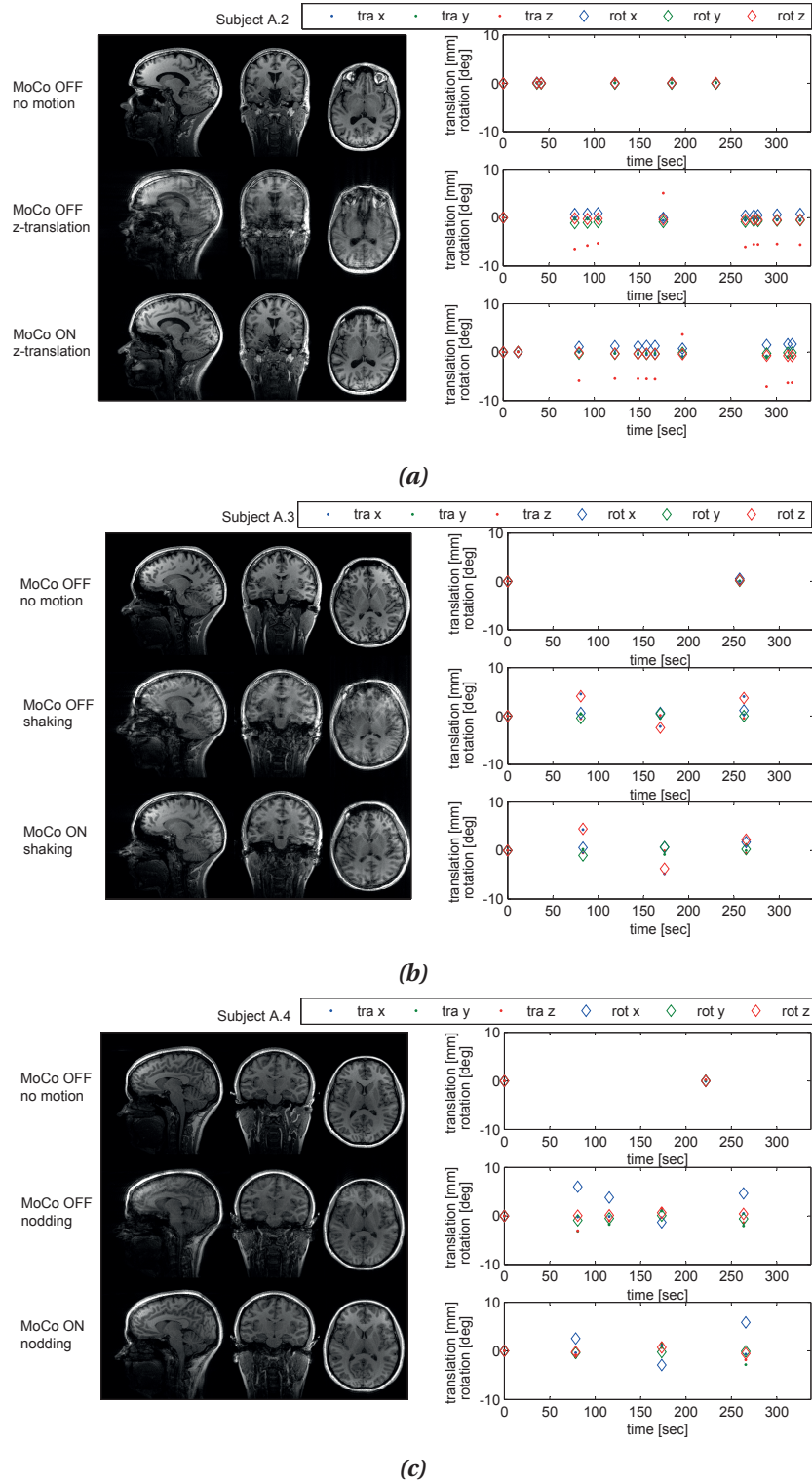
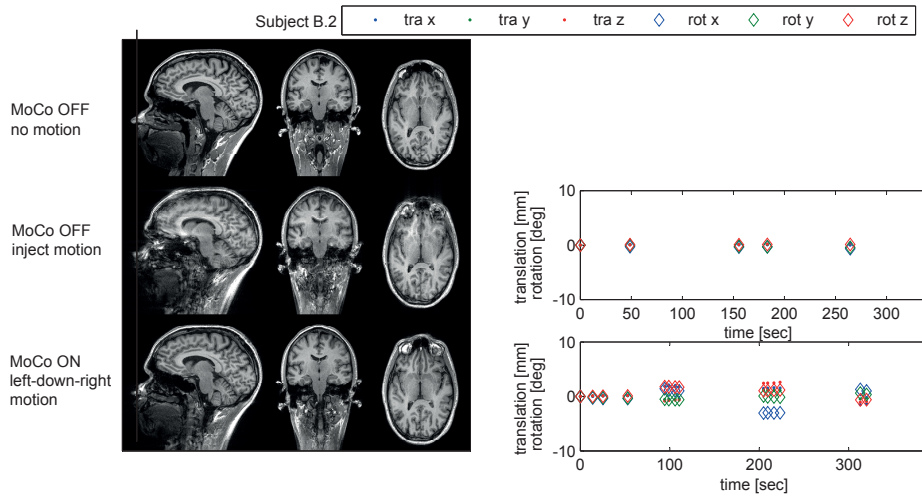
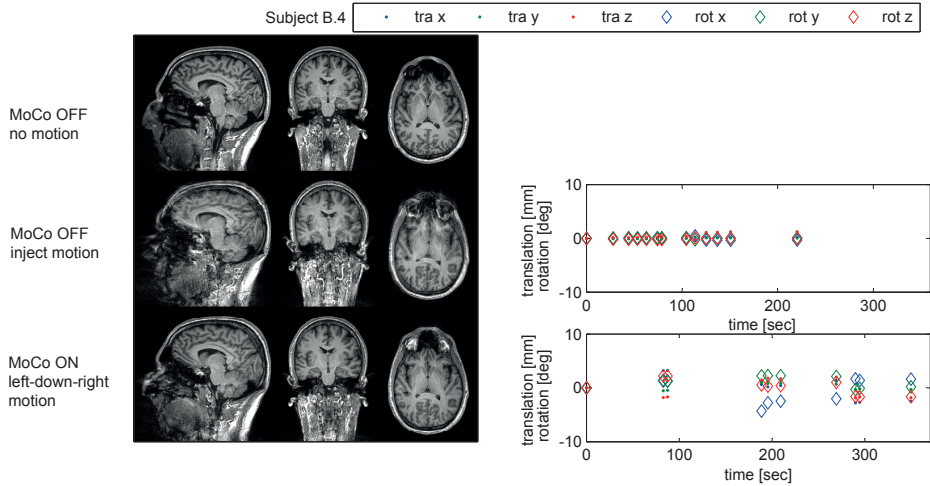


Figure 6.5: Motion correction results from the dataset A together with the detected motion trajectory for different subjects and motion patterns. An image acquired without any deliberate subject motion is shown for reference compared to the images with and without the motion correction mechanism in place. Here, the FID_{nav}^{low} and FID_{nav}^{fast} was used for the detection of motion events a: Subject A.2 with z-translation motion pattern b: Subject A.3 with shaking motion pattern c: Subject A.4 with nodding motion pattern.

Chapter 6. Prospective Head Motion Correction with FID-Triggered Image Navigators



(a)



(b)

Figure 6.6: Motion correction results from the dataset B together with the detected motion trajectory for different subjects and the left-down-right motion pattern. An image acquired without any deliberate subject motion is shown for reference compared to the images with and without the motion correction mechanism in place. Here, the FID_{nav}^{theo} was used for the detection of motion events for a: subject B.2 and b: subject B.4. No motion trajectory for the 'no motion' case is provided as no IMGnavs were acquired.

6.3.3 Quantitative Assessment of Image Quality Improvements after Motion Correction

Quantitative evaluation comparing segmentation results showed a mean absolute segmentation discrepancy of the data without motion to be at $\Delta_{TIV}=0.3\%$, $\Delta_{WM}=1.6\%$, and $\Delta_{GM}=1.7\%$ with a standard deviation at 0.7% for TIV, at 2.5% for gray matter, and at 3.3% for white matter. This is similar to values reported in (Falkovskiy et al., 2016). By applying the proposed motion correction methodology the mean absolute discrepancy in volumes to the 'no motion' measurements could be significantly reduced in our experiments from 2.2% to 0.9% for Δ_{TIV} and from 7.3% to 3.4% for Δ_{WM} (wrt. the volumes acquired without motion) (Fig. 6.7). The mean volume difference for gray matter Δ_{GM} was changed from 4.9% to 3.2% but above the significance level at $p=0.06$.

While, a visual image quality improvement was visible in all motion corrected data not in all cases a 'no motion' image quality could be achieved, which is also attested by the segmentation and QI evaluations. The mean segmentation discrepancy between scan and re-scan data ($\Delta_{TIV}=0.3\%$, $\Delta_{WM}=1.6\%$, and $\Delta_{GM}=1.7\%$) was less than in the images with motion correction ($\Delta_{TIV}=0.9\%$, $\Delta_{WM}=3.4\%$, and $\Delta_{GM}=3.2\%$).

The mean QI could be reduced from 0.82 to 0.73 for the dataset B and from 1.01 to 0.86 for the dataset A. The overall mean QI (datasets A and B) could be reduced significantly from 0.96 to 0.83. The lower the QI value the higher the image quality and a mean QI for 'no motion' data was calculated to be at 0.71. The odd ratio reveals that by using the motion correction mechanism it is seven times more likely to obtain high quality images according to QI (when setting the threshold for motion corrupted images to be at $QI \leq 0.82$) than without motion correction in place.

It could be observed that the method had increased difficulties with respect to the segmentation discrepancies and QI values in correction for nodding and shaking motion, whereas the correction of z-translation was providing better qualitative (visible artifacts) and quantitative results (see Table 6.2).

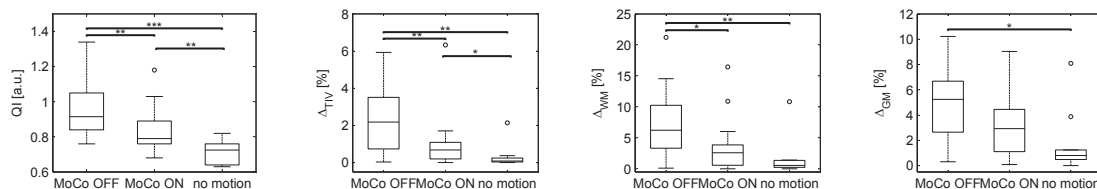


Figure 6.7: Quantitative evaluation of the image quality metric QI and the morphological brain volume segmentation results for data acquired with and without any motion correction (MoCo) compared to data acquired without motion (no motion) and without motion correction. Data from all subjects and experiments are shown. The stars indicate the significance level p of a rank-sum test (no star represents $p > 0.05$, * represents $p \leq 0.05$, ** represents $p \leq 10^{-2}$, *** represents $p \leq 10^{-3}$).

6.3.4 Effect of Reacquisition on Image Quality

We also investigated whether the reacquisition of presumably motion corrupted repetition adds value to the images in terms of image quality and segmentation results. For that two different reconstructions were compared for the dataset A where the reacquired k-space lines were utilized or discarded. It could be observed that less ringing in the brain region as well as in the background was visible for all inspected motion patterns in the reconstructions with reacquisition (Fig. 6.8). This observation was also confirmed by the quantitative evaluation of the quality index.

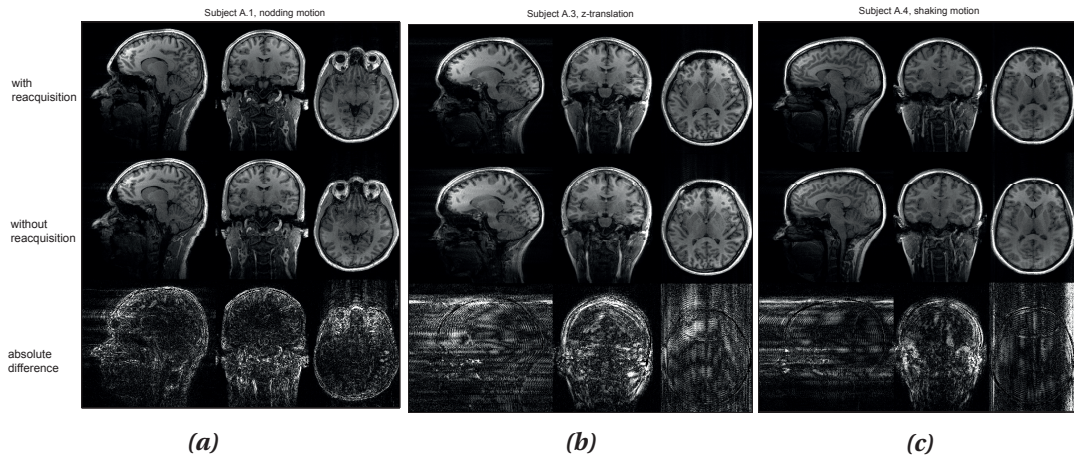


Figure 6.8: Reconstruction results from data with and without utilizing the reacquired repetitions as well as the absolute difference image from the two different reconstructions. *a:* Subject A.1 performing nodding motion. *b:* Subject A.3 performing motion in head-feet direction i.e., z-translation. *c:* Subject A.4 performing shaking motion.

As shown in Fig. 6.9 a mean QI of 1.07 was observed for images where no reacquisition was applied that is not significantly different from the QI of images without any motion correction (QI without correction: 1.01). This can be explained by QI's sensitivity to remaining background artifacts in images that were reconstructed without the use of reacquired lines. However, no significant differences in the brain volume segmentation discrepancies between motion corrected images with and without reacquisition was evident (Fig. 6.9).

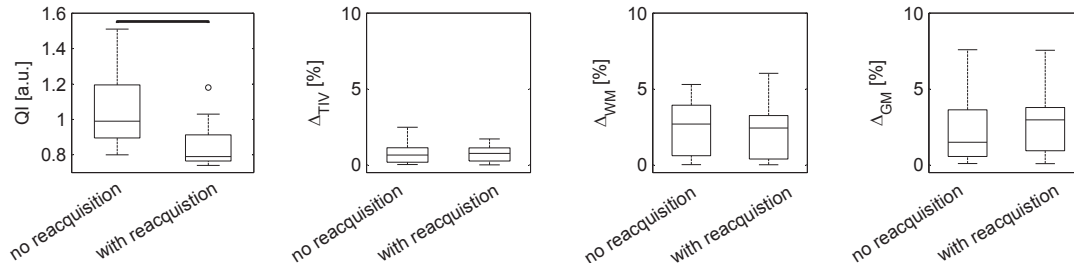


Figure 6.9: Quantitative evaluation of the image quality metric QI and the morphological brain volume segmentation results for data acquired with motion correction on but reconstructed with and without the use of the reacquired repetitions. Data from all subjects from set A are shown. The stars indicate the significance level p of a rank-sum test (no star represents $p > 0.05$, * represents $p \leq 0.05$, ** represents $p \leq 10^{-2}$, *** represents $p \leq 10^{-3}$).

6.4 Discussion

6.4.1 Registration Accuracy of IMGnav

To properly assess the motion estimation capabilities of the proposed method in the best possible way would be the use of a physically moving object e.g., a moving phantom where the motion coordinates are exactly known and can serve as ground truth. Such a device must be furthermore MR compatible and the applied motion should be synchronous to the sequence. Unfortunately, it is not trivial to create such a device. Hence, other ways of estimating the accuracy of the correction method have to be established. Several motion correction techniques utilizing an imaging navigator have been already proposed. For each of the methods also the motion prediction performance of the navigator was assessed. The registration parameters of the vNAV (Tisdall et al., 2012) were estimated through a stationary phantom resembling a pineapple. The authors report registration accuracies in the μm and 10^{-5}° range. Another study showed that the motion detected by the vNAV from a subject at rest was below 1 mm and 1° (Alhamud et al., 2012) and did not influence the sequence targeted for correction. PROMO (White et al., 2010) reports motion prediction errors below 10% of applied ground truth motion and tNAV is able to provide motion parameters with an accuracy of ± 0.5 mm and $\pm 0.5^\circ$ (Lin et al., 2014). In a study where the motion detection accuracy of PROMO was compared to a camera system for motion tracking (Gumus et al., 2015) the authors report a registration accuracy with a mean absolute error within 1 mm and 1 degree with maximal errors up to approximately 2.2 mm and 2.9 degrees.

We proposed a novel approach to estimate the accuracy of the IMGnav by changing the field of view position and orientation during the scanning process to simulate motion and hence having ground truth motion trajectory for the registration. This enabled us to assess the registration accuracy of our IMGnav and the reliability of the motion correction methodology. This approach, however, does not resemble the real effects of motion within a scanner and its implications on the image quality of the IMGnav. Positional changes during the acquisition process might not only invalidate the shimming settings but also change the appearance of the IMGnav or even introduce additional artifacts. These effects are not considered in this simulated motion case. Therefore we consider our reported accuracy, which also congruent with reviewed literature, to be the 'best case' accuracy without taking into account the possible unintentional movements of the subject during the artificial application of the motion trajectory.

The proposed IMGnav also shows ghosting artifacts in the anterior-posterior phase encoding direction. These artifacts might be the reason for the reduced registration accuracy for motion in this direction (translation in z, rotation in x).

6.4.2 FIDnav Triggered Motion Detection and Correction

We proposed several ways to calculate an FIDnav from the multi-channel FID signal magnitude. The FID signal can be added to practically any sequence without having an impact on scan time or the magnetization profile of the host sequence. The FID_{nav}^{slow} and FID_{nav}^{fast} allow to detect motion events reliably already after reaching a steady-state (after two repetitions in the MP-RAGE case). However, the main challenge is the setting of the triggering threshold. Our choice of the threshold was based on experience values (FID_{nav}^{slow} , FID_{nav}^{fast}), although, setting a fixed threshold for all subjects contradicts the reported finding from (Babayeva et al., 2015b). Here, it was shown that nevertheless the FID-signal contains accurate motion information the correlation to actual motion parameters is subject specific. Hence, the motivation to propose another FIDnav FID_{nav}^{theo} , where the threshold is set dynamically during the acquisition. In order to achieve this two data points from the beginning of the scan have to be sacrificed to assess the statistical behavior of the FIDnav and to initialize the thresholding process. Although, this method eliminates the need of an empirical value for the detection of the motion events it highly relies on the fact that no motion is expected during the initialization time. If motion would be present already at the beginning of the acquisition the dynamic threshold would be set too high and the FIDnav would be blind towards true motion in subsequent scan. Hence, the first approach with the use of a empirical threshold is considered advantageous over the second proposal for reliable motion detection. This, however, would require a training data set to establish such a threshold which includes patient, hardware and sequence specific parameters as demonstrated in (Babayeva et al., 2015b). Nevertheless, it was possible to detect all motion events reliably and also to trigger the motion correction functionality of the sequence in our experiments. The relatively high number of false positive triggering events indicate that our choice of the threshold was set too sensitive to apparently motion non-related FIDnav signal fluctuations as no image artifacts were visible in the corresponding datasets. These additional triggering events prolong the scan-time unnecessarily. For both FIDnav variants false positive motion events occurred such that no conclusion on the sensitivity of them can be derived.

Further, it is to mention that our experiments did not include all motion patterns as continuous motion or non-rigid motion. Non-rigid motion as swallowing would have an influence on the FIDnav and might lead to false positive triggering events. It would be possible to detect slow continuous motion by the FID_{nav}^{slow} but not by FID_{nav}^{theo} as it calculated based on the first temporal derivative of the FID signal. Additionally, FID signal drifts, as also observed in (Babayeva et al., 2015b), cause the FID_{nav}^{slow} to detect a false positive motion event. We observed this to be a rare scenario and the benefit of the ability to detect also slow motion justifies its use.

In order to be able to set the optimal threshold for the chosen FIDnav it would be best to start the sequence with a set of IMGnavs together with FIDnavs which is then used to assess the possible presence of motion. If motion was present during the acquisition of the IMGnav set, then the resulting motion parameters could be used to find the linear combination of the

multi-channel FIDs and be able to predict the motion during the image acquisition without the further need of the IMGnav but based only on the FID signal. Such an approach would even benefit from a wide range of motion. Another, scenario would be when no motion was present during the acquisition of the IMGnav set. This would then allow us to trust into the calculated statistics of the FIDnav and to rely on the 'dynamic' threshold.

6.4.3 Advantages and Limitation of the Proposed Motion Correction Method

The present approach extends recent work on MR-based motion correction (Tisdall et al., 2012) in the sense, that motion is monitored with practically no penalty with fast and low-impact FIDnavs and the imaging navigators are employed only when needed without influencing the magnetization profile of the host sequence. We propose a novel IMGnav which is specifically designed to match the properties of the host MP-RAGE sequence in terms of acoustic noise and magnetization profile i.e., the same number of excitations during a read-out train. The sound during the acquisition of the IMGnav differs slightly from the MP-RAGE read-out and can be considered beneficial as a means of signaling the subject that a motion event was detected and the subject has to remain still. It could be shown that significant improvement in image quality from scans with deliberate subject motion could be achieved. For that we chose to use as markers for image quality the segmentation results as well as a quality index based on image background evaluations. The segmentation discrepancies could be reduced by the proposed motion correction for the total intracranial volume and for white matter but not for grey matter.

While the motion related artifacts could be reduced in all cases achieving the quality of the 'no motion' images was difficult. Residual ringing and ghosting artifacts were visible in images with motion correction. We assume that it is caused by the limited registration accuracy of the IMGnav due to ghosting artifacts in its anterior–posterior direction. We showed in simulated motion experiments that the registration reliability of the IMGnav had a mean absolute error of 0.24 ± 0.34 mm and $0.18 \pm 0.22^\circ$. However, we assume that real motion within the scanner bore could significantly impair this result. At the same time, this experiment was performed on a human such that the reported registration accuracy also includes additional errors due to physiological or unintentional motion of the subject's head during the acquisition. As the main design decision for the IMGnav was the same number of excitations as the MP-RAGE host sequence the settings of the IMGnav have to change in case the number of partitions of the MP-RAGE sequence needs to be adapted.

Also, in the current proof-of-concept implementation we did not set any limit to the reacquisition of the presumably corrupted echo-trains. Theoretically if the subject would continue moving there will be an infinite number of reacquisitions and the sequence would never stop. In (Tisdall et al., 2012) the authors propose to move the reacquisition to the end of the scan and limit it to a preset number of echo-trains with most severe motion. Another reacquisition strategy might be to reacquire the corrupted repetitions immediately but limit

Chapter 6. Prospective Head Motion Correction with FID-Triggered Image Navigators

it to a single reacquisition per repetition to ensure that the sequence would end eventually. The simplest and most efficient solution would be not to reacquire any repetitions at all. Our evaluations showed that reacquisition, while providing visually more appealing images, does not add significant value in terms of volume segmentation discrepancies. Nevertheless, it was possible to show that such a concept towards a motion correction method which utilized the FID-signal can provide valuable improvement in image quality when motion is present during the acquisition.

6.4.4 Future Work

Future work should aim at the implementation of an automated and subject specific FIDnav threshold adaptation and at reducing the scan time overhead due to IMGnav acquisition through a motion prediction approach as proposed in (Babayeva et al., 2013, 2015b). Also, the implementation of an efficient reacquisition strategy would refine the motion correction capability of the proposed method. Furthermore, additional experiments are needed to reveal the reason for imperfect correction results and to set the limits for correctable motion magnitudes similar to PACE (Thesen et al., 2000). It would be also interesting to extend the proposed motion correction strategy, employing FIDnav driven triggering of IMGnavs, to other sequences. Especially 2D might be of interest here (e.g., the turbo-spin-echo sequence (TSE)).

6.5 Acknowledgement

We would like to thank Sebastian M. Waszak, Alexis Roche, Davide Piccini, and Mario Fartaria De Oliveira for valuable discussions and suggestions.

7 Host Sequence Influence on FID Signal

Abstract When acquiring a free induction decay (FID) signal within another sequence, also called host sequence, the FID might be influenced by it. Here, we investigated two different imaging sequences: the gradient-echo (GRE) and the magnetization-prepared rapid gradient-echo (MP-RAGE) sequences and their effects on the FID signal on phantom scans in comparison to an acquisition where only the FID signal (FIDnav only) was acquired without embedding it into another sequence.

In this thesis work we have exploited the ability of the FID signal to detect subject's motion. Therefore, we investigated two different imaging sequences: GRE and the MP-RAGE sequences where an FID acquisition was added to the normal imaging sequence. In this context it was important to investigate to which extent the FID signal is affected by the surrounding gradients and excitations pulses.

In the GRE case the FID acquisition was added every 10^{th} repetition or TR (temporal resolution of 100 ms) and in the MP-RAGE at the end of every read-out train every TR. The acquisition parameters were as shown in Tab. 7.1. In the 'FIDnav only' acquisition only the FID signal was sampled every TR with an excitation pulse of 8° in order to have a reference FIDnav signal without any influence of surrounding gradients of an imaging host sequence. Further, embedded in the MP-RAGE acquisition, noise scans were performed by switching the transmit/receive frequency to zero in order to just acquire the thermal noise without any excitation pulse. All scans were performed on a phantom (spherical water phantom, 175 mm diameter; 1.25g NiSO₄ + 6H₂O per 1000g H₂O) but two 'MP-RAGE + FIDnav' scans were taken from a human subject at rest and while changing the head position three times during the scan. The experiments were done at 3T and with a 32 channel head coil.

When the FID signal is acquired within a gradient-echo '3D GRE+FIDnav' sequence or as a stand alone 'FIDnav only' only a decay towards the steady-state as well as a slow time dependent drift are visible as depicted in Fig. 7.1a and Fig. 4.6. On the other hand when the

Chapter 7. Host Sequence Influence on FID Signal

Parameter	3D GRE + FIDnav	FIDnav only	MP-RAGE + FIDnav
TI	n.a.	n.a.	900 ms
TR	25.0 ms	12.5 ms	2300 ms
TE	3.0 ms	3.0 ms	2.86 ms
α	12°	8°	18°/9°/0°
TA	6:07 min	6:11 min	5:21 min
Band width	240 Hz/Px	240 Hz/Px	
Matrix (ROxPExPAR)	256×256×144	n.a.	256×256×176
Voxel size	1.0×1.0×1.2 mm ³	n.a.	1.0×1.0×1.0 mm ³
GRAPPA	×2, 24 ref. lines	n.a.	×2, 24 ref. lines
Field of view in phase	87.5%	n.a.	100%
Slice partial Fourier	6/8	n.a.	1/1
Total number of FIDnav samples during the scan	1328	29568	139

Table 7.1: Acquisition parameters.

FID signal is acquired within an MP-RAGE sequence then rapid temporal signal fluctuations are noticeable. These signal variations are more prominent at higher excitation angles as can be seen in Fig. 7.1b and then change their temporal frequency depending on the acquired line number of the MP-RAGE image i.e., the FIDnav signals that are acquired with the TR number belonging to reference lines have a different fluctuation pattern. By setting the excitation angle to zero degrees for the 'MP-RAGE+FIDnav' acquisition we aimed at acquiring just the thermal noise. This signal variance is very small compared to the variance caused by the sequence gradients i.e., eddy currents.

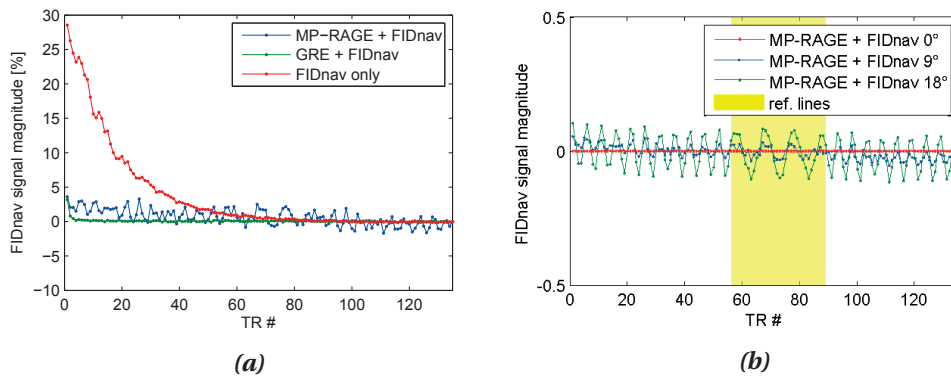


Figure 7.1: a: FIDnav signal magnitude change in % for the different acquisition schemes; 140 TRs are shown. b: FIDnav signal magnitude change for different excitation angles. Influence of the phase encoding gradients is visible.

Further, when looking at the FIDnav magnitude change from a human subject the signal variation due to motion is much stronger compared to signal changes due to host signal influence as seen in Fig. 4.6 and Fig. 7.2, which allows to establish a threshold based on the standard deviation of the FIDnav signal to detect signal changes due to motion. Also,

as already described in Chapter 4.3.3 a temporal signal drift can be observed in all FIDnav acquisitions '3D GRE + FIDnav', 'FIDnav only', and 'MP-RAGE + FIDnav'.

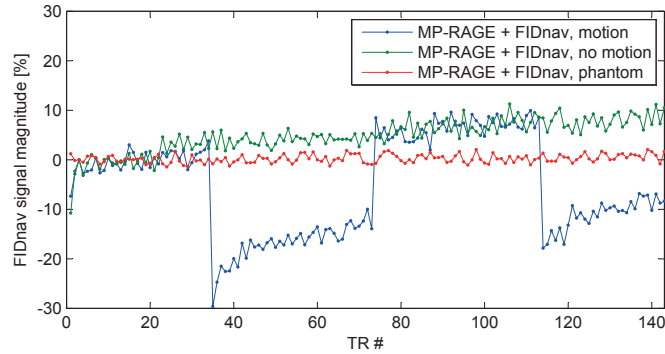


Figure 7.2: FIDnav signal magnitude change in a single coil element for a phantom and human scan. For the human scan the signal is shown for a subject at rest and performing head motion of around 3° rotation 3 mm translation.

Here, we performed some experiments to reveal and describe the influence of the host sequence on the FIDnav signal. We could show that when the FIDnav acquisition is imbedded into an MP-RAGE sequence then signal fluctuations as caused by the phase encoding gradients are visible. Also, we observed temporal signal drifts in all FIDnav acquisitions. As this slow drift is also present in the 'FIDnav only' scans we can conclude that they are not gradient related as no gradients are present during the signal acquisition. The drift might be caused by B_0 drifts due to temperature induced shim changes of the scanner.

These observations are of interest for the use of the FIDnav signal to detect motion within a host sequence. In order to do so, the FIDnav signal is observed over time and if a signal change compared to a reference higher than a preset threshold is detected then the corresponding part of k-space data acquired around the FIDnav signal acquisition can be considered as motion corrupted. This threshold can be set in two ways: either to an empirical value based on a set of scans with the same acquisition scheme but different subjects (training set) and without motion or to a value obtained from FIDnav signal points from the beginning of the acquisition. Both variants have their advantages and disadvantages. In the first case it is hard to trust an empirical value and false positive or negative motion events would be inevitable. In the second case some FIDnav samples must be sacrificed to establish a trustworthy threshold estimation. Moreover, this relies on the scenario that no motion occurs during the acquisition of this threshold data otherwise the threshold would be set too high and the FID based motion detection would be blind to motion events occurring at a later stage. Therefore, the first approach with the use of an empirical threshold which is estimated based on previous scans is considered advantageous over the second proposal for reliable motion detection. This, however, would require a training data set to establish such a threshold which includes patient, hardware and sequence specific parameters as demonstrated in (Babayeva et al., 2015b).

8 Outlook and Conclusion

This is perhaps 5 per cent empirical information and 95 per cent speculation, some of it possibly tainted by wishful thinking.

SIMON S KUZNETS

MRI is a powerful tool in medical imaging allowing to visualize the anatomy of a human body non-invasively. This technology is however highly susceptible to motion as the scanning times are usually on the order of minutes. As of today many motion mitigation strategies have been proposed but with only little success in clinical use. Hence, there was a motivation to examine a new approach to motion detection and correction utilizing the simplest MR signal – a free induction decay (FID) – for motion tracking.

The physical theory behind the ability of the FID signal to react to motion seems natural as stated by the Biot–Savart law: the closer an object is located to the receive coil the higher will be the detected signal. Similar to any other sensor for distance detection e.g., ultrasound or infrared in order to determine a location and its exact motion trajectory of an object in the three dimensional space it is necessary to measure the motion trajectory in six degrees of freedom (three translation and three rotational parameters). Therefore, at least six orthogonal measures of the posture or rigid body motion are needed to determine the objects position and orientation or positional changes. Here, we postulate that the limited motion ability of the human head and a sufficient number of spatially distributed receive coil elements allows us to perform such motion tracking.

In order to show the validity of our hypothesis we performed a set of experiments where the accurate motion of a human head was tracked by a highly precise optical tracking device while the FID signal was acquired with a 32-channel head coil. Five subjects participated in this study performing various types of motions (head nodding, head shaking, moving the head in the head foot direction and drawing a virtual eight with the nose tip). Our results

as shown in Chapter 4 could show that the the FID signal is linearly correlated with the six motion parameters with a sub-millimeter and sub-degree accuracy and precision. However, we were not able to find a closed form solution which would apply to all subjects. Therefore, we assume that in order to be able to find a universal mapping from FID signal changes to exact motion parameters more information is required as the individual shape of the head and its initial position within the head coil.

Computer aided quantitative evaluations of medical MR images have become more popular in the recent years e.g., automatic disease prediction based on volumetric measurements of the brain anatomy. Such techniques rely heavily on high image quality which may be compromised by motion. If an image is corrupted by motion the validity of the segmentation results is questionable. Therefore, it is important to be able to assess the image quality quantitatively before the image is used for further computer based analysis. We proposed to acquire the FID signal along the normal imaging sequence in order to calculate an FID based motion sensitive quality metric. This metric has also the advantage of labeling the acquired data as motion corrupted even if the scan is has not finalized yet in order to terminate the exam to save time and possibly advise the subject to remain still. We called the proposed quality index FIDI (FID index) and could show in Chapter 5 on 109 clinical data sets that it could reliably identify motion corrupted images.

Further, also in Chapter 5, we could show that the FID signal could be used for a retrospective motion correction technique based on autofocusing. This correction method adjusts the already acquired k-space data chunks such that a cost function is optimized according to the underlying motion trajectory. We proposed to extent this cost function by the use of the FID signal as an additional parameter to guide the optimization process. This FID guided approach allows for faster convergence of the algorithm (Babayeva et al., 2014b; Loktyushin et al., 2013). We could also show on clinical data sets which were evaluated by an expert that the FID guided method leads to better correction results compared to the blind autofocusing approach.

To show a method how the FID signal can be used for prospective motion correction in MRI we proposed a technique where the FID is used for binary motion detection to drive another motion estimation mechanism. On an example of an MP-RAGE sequence the FID signal was periodically sampled (every TR) and if head motion was detected according to FID signal changes then an acquisition of a low resolution image (IMGnav) of the whole head was triggered. This IMGnav was used to determine the underlying motion parameters through image registration to a reference IMGnav from the beginning of the scan. This acquisition scheme provides an efficient way of motion correction during and MRI scan as the motion correction mechanism is only active when motion happens. A disadvantage of this technique is the temporal resolution with which the motion can be detected i.e., only every TR. Hence, it is not possible to avoid the acquisition of uncorrected data that has to be discarded resulting in additional scan time overhead. Another bottleneck of this technique is the limited registration accuracy of the IMGnav as a trade-off between scan time and image resolution needs to be

made. We evaluated the registration accuracy and precision of our IMGnav by acquiring successively several volumes of the IMGnav from a human subject and by introducing an artificial motion trajectory through a text file. This approach provided us with a notion of the reliability of our motion correction method. This strategy, however, does not take into account the possible real and involuntary motion of the subject during the experiment. Hence, a moving phantom to prescribe an accurate motion trajectory or a precise motion tracking device (i.e., optical camera system) to track real human subject movements would render this experimental validation more realistic. Another challenge of this motion correction method is the adjustment of the FID threshold when the signal change is considered high enough to correspond to a potential head motion. One way is to set this threshold empirically or to use few FID signal samples from the beginning of the scan as reference to calculate its standard deviation and to set the threshold above a multiple of this value. The drawback of the latter value is that it relies on the fact that no motion was present during the acquisition of the reference FID signal values otherwise the method would be blind to eventual latter motion events. The first approach to set the threshold may lead to many false positives or false negatives if it is set too high or too low. Despite the evident drawbacks of the method we were able to demonstrate the efficacy of our proposed technique with a study on 10 subjects and different motion patterns and presented the results in Chapter 6.

Finally, we performed a study on how the FID signal may be influenced by the host sequence i.e., the imaging sequence which includes the acquisition of the FID. We could show that it is important to consider the 'magnetic' environment of the FID acquisition as it may introduce additional non-motion related signal fluctuations.

8.1 Direction for Future Research

Future work should be focused on further understand which additional information is needed to find a universal mapping of the multi-channel FID signal to exact motion parameters. This could be achieved through collecting more data sets from different subjects but also acquired by head coils of different geometry to extend the search space. Hereby, a clinical dataset containing motion trajectory information, radiological image quality ratings, as well as the FID signal would be of high interest. The motion trajectory could be assessed by introducing the acquisition of an IMGnav throughout all clinical routine scans in either triggered approach or by inserting a fixed number of acquired volumes e.g., every 10 seconds during the scan. The FID signal acquisition could be added to virtually any sequence without or only a small impact on its scan time and magnetization profile. The collection of image quality ratings should be systematically included in all radiological readings as part of the clinical routine.

From our evaluations we think that the most promising approach towards a motion correction method would be to acquire a training data set prior the actual imaging scan to collect the necessary information to obtain a subject, scanner, utilized coil, and sequence specific model. Other models than linear ones can be considered here as well and might provide a

Chapter 8. Outlook and Conclusion

different view on the problem. The acquisition of this training data should, however, take not longer than the imaging scan itself as otherwise a reacquisition of a potentially corrupted data set might be more appealing.

In this thesis we propose to use the FID as a novel technique to calculate a motion sensitive quality index FIDI of the acquired data. In order to set the reliable limits for this index when to label data as motion corrupted it would be advantageous to consider more clinical data sets. These data sets have to be reviewed by experts for motion related artifacts such that these ratings can be correlated to the FID based index FIDI. We investigated the application of FIDI only on MP-RAGE scans. A valuable expansion of this study would be to introduce the FID acquisition to other sequences and perform similar evaluations with expert ratings of clinical images.

In order to understand the real benefit of the FID based prospective and retrospective motion detection and correction as we proposed in Chapters 5 and 6 it is important to bring the implementation to the clinical routine scans. The advantage of the retrospective technique is that the original image is preserved such that the clinicians can choose which image is more suitable for the diagnosis. Hence, introducing the retrospective method to the clinics can be achieved by just providing an efficient implementation of the this retrospective correction technology, which could be the next logical step. Also, such an implementation would allow to conduct a clinical study to assess its potential. The prospective correction technique on the other hand is more challenging in terms of integrating and testing it in a clinical context. With this method it is not possible to retrieve the image without correction. Therefore, the reliability of this methodology has to be assured such that no artifacts are introduced by the method to the final image.

In this work we have gathered an understanding on how the FID signal can be used in two 3D sequences the gradient-echo and the MP-RAGE. To further facilitate the use of the FID for motion detection in correction correction in MRI it is necessary to investigate also other sequences especially the 2D ones. In brief the future research should focus on two orthogonal topics. First the implementation of the proposed motion correction methodologies such that they can be used in clinics to study the impact of motion correction in the daily routine as well as to quantify the prevalence of motion in clinical examinations. Seconds, continue to investigate how the FID signal can be introduced to other sequences as well as how it can complement already existing motion correction methods by establishing a data base with clinical images and corresponding motion trajectories as well as FID signals and radiologists' image quality ratings.

8.2 Conclusion

Motion detection and motion tracking based on the FID signal from a multi-channel head coil array could provide an elegant solution for the motion problem in MRI. It was shown that multi-channel FID signal correlates with underlying motion with sufficient accuracy and several promising approaches on how this technique could be utilized for this purpose and also provide a platform for further investigation was proposed. However, further research is necessary to understand how the exact motion parameters can be extracted from the multi-channel FID signal without relying on other motion tracking methodologies. Additionally, the MR sequence where the acquisition of the FID signal is embedded, has to be taken into consideration as it influences the FID signal. The take-home message of this work is that accurate motion information is contained in the multi-channel FID signal and it can be used in prospective and retrospective motion correction applications if combined with other techniques but bears also the potential for more elaborate use.

Bibliography

- Aksoy, M., Forman, C., Straka, M., Skare, S., Holdsworth, S., Hornegger, J., and Bammer, R., 2011. Real-time optical motion correction for diffusion tensor imaging. *Magnetic Resonance in Medicine*, **66**(2):366–78.
- Alhamud, A., Tisdall, D., Hess, A. T., Hasan, K. M., Meintjes, E. M., and van der Kouwe, A. J. W., 2012. Volumetric navigators for real-time motion correction in diffusion tensor imaging. *Magnetic Resonance in Medicine*, **68**(4):1097–1108.
- Andre, J. B., Bresnahan, B. W., Mossa-basha, M., Hoff, M. N., Smith, C. P., Anzai, Y., and Cohen, W. A., 2015. Toward Quantifying the Prevalence, Severity, and Cost Associated With Patient Motion During Clinical MR Examinations. *J Am Coll Radiol*, **12**(7):689–95.
- Atkinson, D., Hill, D. L. G., Stoye, P. N., Summers, P. E., Clare, S., Bowtell, R., and Keevil, S. F., 1999. Automatic compensation of motion artifacts in MRI. *Magnetic Resonance in Medicine*, **41**(1):163–70.
- Atkinson, D., Hill, D. L. G., Stoye, P. N., Summers, P. E., and Keevil, S. F., 1997. Automatic correction of motion artifacts in magnetic resonance images using an entropy focus criterion. *IEEE transactions on medical imaging*, **16**(6):903–10.
- Babayeva, M., Falkovskiy, P., Hilbert, T., Bonnier, G., Maréchal, B., Meuli, R., Thiran, J.-p., and Gruetter, R., 2015a. Prospective motion correction with FID-triggered image navigators. *Proc. Intl. Soc. Mag. Reson. Med.*, **23**:683.
- Babayeva, M., Kober, T., Herbst, M., Hennig, J., Seeger, M., Gruetter, R., Zaitsev, M., and Krueger, G., 2013. Can Multi-Channel FID Navigators Quantify Head Motion? *Proc. Intl. Soc. Mag. Reson. Med.*, **21**:306.
- Babayeva, M., Kober, T., Knowles, B., Herbst, M., Zaitsev, M., and Krueger, G., 2015b. Accuracy and Precision of Head Motion Information in Multi-Channel Free Induction Decay Navigators for Magnetic Resonance Imaging. *IEEE transactions on medical imaging*, **34**(9):1–11.
- Babayeva, M., Loktyushin, A., Falkovskiy, P., Kober, T., Mueli, R., Gruetter, R., and Krueger, G., 2014a. FID navigator triggered acquisition of imaging navigators for retrospective head motion correction. *ISMRM Workshop on Motion Correction*, **3703**.

Bibliography

- Babayeva, M., Loktyushin, A., Kober, T., Granziera, C., Nickisch, H., Gruetter, R., and Krueger, G., 2014b. FID-guided retrospective motion correction based on autofocusing. *Proc. Intl. Soc. Mag. Reson. Med.*, **22**:2227.
- Brau, A. C. S. and Brittain, J. H., 2006. Generalized self-navigated motion detection technique: Preliminary investigation in abdominal imaging. *Magnetic Resonance in Medicine*, **55**(2):263–70.
- Busse, R. F. and Riederer, S. J., 2001. Steady-state preparation for spoiled gradient echo imaging. *Magnetic Resonance in Medicine*, **45**(4):653–61.
- Dantendorfer, K., Amering, M., Bankier, A., Helbich, T., Prayer, D., Youssefzadeh, S., Alexandrowicz, R., Imhof, H., and Katschnig, H., 1997. A study of the effects of patient anxiety, perceptions and equipment on motion artifacts in magnetic resonance imaging. *Magnetic Resonance Imaging*, **15**(3):301–306.
- Delattre, B. M., Heidemann, R. M., Crowe, L., Vallée, J.-P., and Hyacinthe, J.-N., 2010. Spiral demystified. *Magnetic resonance imaging*, **28**(6):862–81.
- Ehman, R. L. and Felmlee, J. P., 1989. Adaptive technique for high-definition MR imaging of moving structures. *Radiology*, **173**(1):255–263.
- Erasmus, L., Hurter, D., Naudé, M., Kritzing, H., and Acho, S., 2004. A short overview of MRI artefacts. *South African Journal of Radiology*, **8**(2):13–17.
- Falkovskiy, P., Brenner, D., Feiweier, T., Kannengiesser, S., Maréchal, B., Kober, T., Roche, A., Thostenson, K., Meuli, R., Reyes, D., *et al.*, 2016. Comparison of accelerated T1-weighted whole-brain structural-imaging protocols. *NeuroImage*, **124**, Part A:157 – 167.
- Falkovskiy, P., Kober, T., Reyes, D., Steinert, K., Seeger, M., Bernstein, M., and Krueger, G., 2013. Segmented Multi-Echo MPRAGE Acquisition for Accelerated T1-Weighted Brain Imaging. *Proc. Intl. Soc. Mag. Reson. Med.*, **21**:3703.
- Fries, P., Runge, V. M., Kirchin, M. A., Stemmer, A., Naul, L. G., Williams, K. D., Reith, W., Bückner, A., and Schneider, G., 2009. Diffusion-weighted imaging in patients with acute brain ischemia at 3 T: current possibilities and future perspectives comparing conventional echoplanar diffusion-weighted imaging and fast spin echo diffusion-weighted imaging sequences using BLADE (PROPELLER). *Investigative radiology*, **44**(6):351–359.
- Gedamu, E. and Gedamu, A., 2012. Subject movement during multislice interleaved MR acquisitions: prevalence and potential effect on MRI-derived brain pathology measurements and multicenter clinical trials of therapeutics for multiple sclerosis. *Journal of magnetic resonance imaging*, **36**(2):332–43.
- Gumus, K., Keating, B., White, N., Andrews-Shigaki, B., Armstrong, B., Maclaren, J., Zaitsev, M., Dale, A., and Ernst, T., 2015. Comparison of optical and mr-based tracking. *Magnetic Resonance in Medicine*, **74**(3):894–902.

- Haacke, E. M., Brown, R. W., Thomson, M. R., Venkatesan, R., E. H., R. B., M. T., and R. V., 1999. *Magnetic resonance imaging: physical principles and sequence design*. Wiley, New York, NY, USA.
- Haeberlin, M., Kasper, L., Barmet, C., Brunner, D. O., Dietrich, B. E., Gross, S., Wilm, B. J., Kozerke, S., and Pruessmann, K. P., 2014. Real-time motion correction using gradient tones and head-mounted NMR field probes. *Magnetic Resonance in Medicine*, **74**(3):647–60.
- Herbst, M., Maclaren, J., Lovell-Smith, C., Sostheim, R., Egger, K., Harloff, A., Korvink, J., Hennig, J., and Zaitsev, M., 2014. Reproduction of motion artifacts for performance analysis of prospective motion correction in MRI. *Magnetic Resonance in Medicine*, **71**(1):182–190.
- Herbst, M., Maclaren, J., Weigel, M., Korvink, J., Hennig, J., and Zaitsev, M., 2012. Prospective motion correction with continuous gradient updates in diffusion weighted imaging. *Magnetic Resonance in Medicine*, **67**(2):326–38.
- Hess, A. T., Tisdall, D., Andronesi, O. C., Meintjes, E. M., and van der Kouwe, A. J. W., 2011. Real-time motion and B(0) corrected single voxel spectroscopy using volumetric navigators. *Magnetic Resonance in Medicine*, **323**(66):314–323.
- Hu, X. P. and Kim, S.-G. S., 1994. Reduction of signal fluctuation in functional MRI using navigator echoes. *Magnetic Resonance in Medicine*, **31**(5):495–503.
- Jack, C. R., Bernstein, M. A., Fox, N. C., Thompson, P., Alexander, G., Harvey, D., Borowski, B., Britson, P. J., Whitwell, J. L., Ward, C., *et al.*, 2008. The Alzheimer’s Disease Neuroimaging Initiative (ADNI): MRI Methods. *Journal of magnetic resonance imaging : JMRI*, **27**(4):685–691.
- Johnson, K. O., Robison, K. R., and Pipe, J. G., 2011. Rigid body motion compensation for spiral projection imaging. *IEEE transactions on medical imaging*, **30**(3):655–665.
- Kaufman, L., Kramer, D. M., Crooks, L. E., and Ortendahl, D. A., 1989. Measuring signal-to-noise ratios in MR imaging. *Radiology*, **173**(1):265–267.
- Kim, B., Boes, J. L., Bland, P. H., Chenevert, T. L., and Meyer, C. R., 1999. Motion correction in fMRI via registration of individual slices into an anatomical volume. *Magnetic Resonance in Medicine*, **41**(5):964–72.
- Kober, T., Gruetter, R., and Krueger, G., 2012. Prospective and retrospective motion correction in diffusion magnetic resonance imaging of the human brain. *NeuroImage*, **59**(1):389–98.
- Kober, T., Marques, J., Gruetter, R., and Krueger, G., 2010. Motion Characterisation using FID navigators and Spatial Pattern of MRI Coil Arrays. *Proc. Intl. Soc. Mag. Reson. Med.*, **18**:3047.
- Kober, T., Marques, J., Gruetter, R., and Krueger, G., 2011. Head motion detection using FID navigators. *Magnetic resonance in medicine*, **66**(1):135–43.

Bibliography

- Liao, J. R., Pauly, J. M., Brosnan, T. J., and Pelc, N. J., 1997. Reduction of motion artifacts in cine MRI using variable-density spiral trajectories. *Magnetic Resonance in Medicine*, **37**(4):569–75.
- Lin, W., Ladinsky, G. a., Wehrli, F. W., and Song, H. K., 2007. Image metric-based correction (autofocusing) of motion artifacts in high-resolution trabecular bone imaging. *Journal of magnetic resonance imaging* ;, **26**(1):191–7.
- Lin, W., Nielsen, T., Qin, Q., Mostofsky, S. H., Wei, J., Huang, F., and Duensing, G. R., 2014. Real-time motion correction in two-dimensional multislice imaging with through-plane navigator. *Magnetic Resonance in Medicine*, **71**(6):1335–2005.
- Loktyushin, A., Babayeva, M., Gallichan, D., Krueger, G., Scheffler, K., and Kober, T., 2015a. Retrospective rigid motion correction of undersampled MRI data. *Proc. Intl. Soc. Mag. Reson. Med.*, :2334.
- Loktyushin, A., Nickisch, H., Pohmann, R., and Schölkopf, B., 2013. Blind retrospective motion correction of MR images. *Magnetic Resonance in Medicine*, **70**(6):1608–1618.
- Loktyushin, A., Nickisch, H., Pohmann, R., and Schölkopf, B., 2015b. Blind multirigid retrospective motion correction of MR images. *Magnetic Resonance in Medicine*, **73**(4):1457–68.
- Maclaren, J., Armstrong, B. S. R., Barrows, R. T., Danishad, K., Ernst, T., Foster, C. L., Gumus, K., Herbst, M., Kadashevich, I., Kusik, T. P., *et al.*, 2012. Measurement and Correction of Microscopic Head Motion during Magnetic Resonance Imaging of the Brain. *PLOS ONE*, **7**(11):e48088.
- Maclaren, J., Bones, P., Millane, R., and Watts, R., 2008. MRI with TRELIS: a novel approach to motion correction. *Magnetic Resonance Imaging*, **26**(4):474–483.
- Maclaren, J., Herbst, M., Speck, O., and Zaitsev, M., 2013. Prospective motion correction in brain imaging: A review. *Magnetic Resonance in Medicine*, **69**(3):621–636.
- Maclaren, J., Speck, O., Stucht, D., Schulze, P., Hennig, J., and Zaitsev, M., 2010. Navigator accuracy requirements for prospective motion correction. *Magnetic resonance in medicine*, **63**(1):162–70.
- Malamateniou, C., Malik, S., Counsell, S., Allsop, J., McGuinness, A., Hayat, T., Broadhouse, K., Nunes, R., Ederies, A., Hajnal, J., *et al.*, 2013. Motion-Compensation Techniques in Neonatal and Fetal MR Imaging. *American Journal of Neuroradiology*, **34**(6):1124–36.
- Manduca, A., McGee, K. P., Welch, E. B., Felmlee, J. P., Grimm, R. C., and Ehman, R. L., 2000. Autocorrection in MR imaging: adaptive motion correction without navigator echoes. *Radiology*, **215**(3):904–9.
- Maréchal, B., Kannengiesser, S., Thostenson, K., Kollasch, P., Falkovskyi, P., Thiran, J.-p., Meuli, R., and Bernstein, M. A., 2015. A generalized method for automated quality assessment in brain MRI. In *Proc. Intl. Soc. Mag. Reson. Med.*, volume 1335, page 23.

- Maréchal, B., Kober, T., Hilbert, T., Ribes, D., Chevrey, N., Roche, A., Thiran, J.-P., Meuli, R., and Krueger, G., 2012. Automated quality control in MR-based brain morphometry. In *Proc. Intl. Soc. Mag. Reson. Med.*, volume 20, page 757, Melbourne.
- Maréchal, B. M., 2011. *Toward Reliable MR-Based Brain Structure Morphometry: Importance of Rigorous Quality Control*. Phd, ÉCOLE POLYTECHNIQUE FÉDÉRALE DE LAUSANNE.
- McGee, K. P., Manduca, a., Felmlee, J. P., Riederer, S. J., and Ehman, R. L., 2000. Image metric-based correction (autocorrection) of motion effects: analysis of image metrics. *Journal of magnetic resonance imaging : JMRI*, **11**(2):174–81.
- McRobbie, D. W., Moore, E. A., Graves, M. J., and Prince, M. R., 2006. *MRI from Picture to Proton*. Cambridge University Press, second edition. Cambridge Books Online.
- Mortamet, B., Bernstein, M. A., Jack, C. R., Gunter, J. L., Ward, C., Britson, P. J., Meuli, R., Thiran, J.-P., and Krueger, G., 2009. Automatic quality assessment in structural brain magnetic resonance imaging. *Magnetic Resonance in Medicine*, **62**(2):365–72.
- Munn, Z. and Jordan, Z., 2013. Interventions to reduce anxiety, distress and the need for sedation in adult patients undergoing magnetic resonance imaging: A systematic review. *International Journal of Evidence-Based Healthcare*, **11**(4):265–274.
- Oberstein, A., Meves, M., Bockenheimer, S., and Schlaps, D., 1990. Beeinträchtigte Faktoren in der MR-Routineanwendung-Ergebnisse der "Multicenterstudie zur Evaluierung der Kernspintomographie". *Digit. Bilddiagn.*, **10**:10–16.
- Ooi, M. B., Aksoy, M., Maclaren, J., Watkins, R. D., and Bammer, R., 2013. Prospective motion correction using inductively coupled wireless RF coils. *Magnetic Resonance in Medicine*, **70**(3):639–647.
- Ooi, M. B., Krueger, S., Thomas, W. J., Swaminathan, S., and Brown, T. T., 2009. Prospective real-time correction for arbitrary head motion using active markers. *Magnetic Resonance in Medicine*, **62**(4):943–954.
- Ordidge, R., Helpert, J., Qing, Z., Knight, R., and Nagesh, V., 1994. Correction of motional artifacts in diffusion-weighted MR images using navigator echoes. *Magnetic Resonance Imaging*, **12**(3):455–460.
- Peshkovsky, A., Knuth, K. H., and Helpert, J., 2003. Motion correction in MRI using an apparatus for dynamic angular position tracking (ADAPT). *Magnetic resonance in medicine*, **49**(1):138–43.
- Pfeuffer, J., Van de Moortele, P.-F., Ugurbil, K., Hu, X. P., and Glover, G., 2002. Correction of physiologically induced global off-resonance effects in dynamic echo-planar and spiral functional imaging. *Magnetic resonance in medicine*, **47**(2):344–53.
- Pipe, J. G., 1999. Motion correction with PROPELLER MRI: application to head motion and free-breathing cardiac imaging. *Magnetic resonance in medicine*, **42**(5):963–969.

Bibliography

- Qin, L., Schmidt, E. J., Tse, Z. T. H., Santos, J. M., Hoge, W. S., Tempany-Afdhal, C., Butts-Pauly, K., and Dumoulin, C. L., 2013. Prospective motion correction using tracking coils. *Magnetic resonance in medicine*, **69**:749–759.
- Qin, L., van Gelderen, P., Derbyshire, J. A., Jin, F., Lee, J., de Zwart, J. a., Tao, Y., and Duyn, J. H., 2009. Prospective head-movement correction for high-resolution MRI using an in-bore optical tracking system. *Magnetic Resonance in Medicine*, **62**(4):924–34.
- Reuter, M., Tisdall, M. D., Qureshi, A., Buckner, R. L., van der Kouwe, A. J., and Fischl, B., 2015. Head motion during MRI acquisition reduces gray matter volume and thickness estimates. *NeuroImage*, **107**:107–115.
- Sachs, T., Meyer, C. R., Hu, B., Kohli, J., Nishimura, D., and Macovski, A., 1994. Real-time motion detection in spiral MRI using navigators. *Magnetic Resonance in Medicine*, **32**(5):639–645.
- Schmitter, D., Roche, A., Maréchal, B., Ribes, D., Abdulkadir, A., Bach-Cuadra, M., Daducci, A., Granziera, C., Klöppel, S., Maeder, P., *et al.*, 2014. An evaluation of volume-based morphometry for prediction of mild cognitive impairment and Alzheimer’s disease. *NeuroImage Clin*, **7**:7–17.
- Smith, T. B. and Nayak, K. S., 2010. MRI artifacts and correction strategies. *Imaging in Medicine*, **2**(4):445–457.
- Splitthoff, D. N. and Zaitsev, M., 2009. SENSE shimming (SSH): A fast approach for determining B(0) field inhomogeneities using sensitivity coding. *Magnetic Resonance in Medicine*, **62**(5):1319–25.
- Thesen, S., Heid, O., Mueller, E., and Schad, L. R., 2000. Prospective acquisition correction for head motion with image-based tracking for real-time fMRI. *Magnetic Resonance in Medicine*, **44**(3):457–65.
- Tisdall, D., Hess, A. T., Reuter, M., Meintjes, E. M., Fischl, B., and van der Kouwe, A. J. W., 2012. Volumetric navigators for prospective motion correction and selective reacquisition in neuroanatomical MRI. *Magnetic Resonance in Medicine*, **68**(2):389–399.
- van der Kouwe, A. J. W., Benner, T., and Dale, A. M., 2006. Real-time rigid body motion correction and shimming using cloverleaf navigators. *Magnetic Resonance in Medicine*, **56**(5):1019–32.
- Welch, E. B., Manduca, A., and Grimm, R. C., 2002. Spherical navigator echoes for full 3D rigid body motion measurement in MRI. *Magnetic Resonance in Medicine*, **47**(1):32–41.
- White, N. S., Roddey, J. C., Shankaranarayanan, A., Han, E. T., Rettmann, D., Santos, J. M., Kuperman, J. M., Dale, A. M., Roddey, C., Shankaranarayanan, A., *et al.*, 2010. PROMO: Real-time prospective motion correction in MRI using image-based tracking. *Magnetic Resonance in Medicine*, **63**(1):91–105.

- Wood, M. L. and Henkelman, M. R., 1985. MR image artifacts from periodic motion. *Medical Physics*, **12**(2):143–151.
- Zaitsev, M., Dold, C., Sakas, G., Hennig, J., and Speck, O., 2006. Magnetic resonance imaging of freely moving objects: prospective real-time motion correction using an external optical motion tracking system. *NeuroImage*, **31**(3):1038–50.
- Zaitsev, M., Maclaren, J., and Herbst, M., 2015. Motion Artifacts in MRI: A Complex Problem With Many Partial Solutions. *J Magn Reson Imaging*, **42**(4):887–901.

Maryna Waszak

✉ maryna.waszak@gmail.com



PERSONAL INFORMATION

Birth 30 July, 1984 in Charkiv, Ukraine
Formerly Maryna Babayeva
Nationalities German, Ukrainian
Languages German, English, Russian

EDUCATION

04/2012-03/2016 **Ph.D., Electrical Engineering,**
Swiss Federal Institute of Technology Lausanne, Switzerland.
Thesis Title Motion Correction in Magnetic Resonance Imaging Using the Signal of Free-Induction-Decay
Thesis Advisors Prof. Rolf Gruetter (EPFL), Dr. Gunnar Krueger (Siemens)

10/2009-09/2011 **M.Sc., Computational Science and Engineering,**
Technical University of Munich, Germany.
GPA 1.9 (on a scale from 1–5; 1 is best; 5 is failed)
Thesis Title Efficient Sampling for Accelerated Diffusion Magnetic Resonance Imaging
Thesis Advisors Prof. Nassir Navab (TUM), Prof. Dimitri Van De Ville (EPFL)

10/2005-09/2009 **Dipl.-Ing. (FH), Electrical Engineering and Information Technology,**
University of Applied Sciences Munich, Germany.
GPA 1.9 (on a scale from 1–5; 1 is best; 5 is failed)
Thesis Title Development and Implementation of an Automotive Diagnostic System on an Electronic Control Unit Prototype According to ISO 14229
Thesis Advisor Prof. Alfred Irber

TEACHING EXPERIENCE

2012-2015 **Swiss Federal Institute of Technology Lausanne,** Lausanne, Switzerland.
General Physics I, General Physics II, Physics Laboratory Experiments

WORK EXPERIENCE

10/2011-03/2016 **Siemens,** Lausanne, Switzerland.
Siemens Advanced Imaging Technology – *Development of a motion correction strategy for magnetic resonance imaging.*

09/2010-01/2011 **General Electric,** Zeist, Netherlands.
Healthcare IT – *Software development and unit testing of a medical data archiving system.*

- 09/2009-07/2010 **Brainlab**, Munich, Germany.
Research & Development Surgery – *Test and development of a surgical documentation and visualization system.*
- 03/2009-08/2009 **Gigatronik**, Munich, Germany.
Automotive Diagnostics – *Project on an automatic diagnostic analysis and reporting hard- and software system.*
- 10/2008-02/2009 **Infineon Technologies**, Munich, Germany.
Automotive System Applications Engineering – *Development and verification of embedded software for microcontrollers.*
- 03/2008-08/2008 **Infineon Technologies**, Singapore.
Automotive System Applications Engineering – *Development and verification of software drivers for microcontrollers.*
- 01/2007-02/2008 **Qimonda**, Munich, Germany.
Quality Management – *Documentations and quality reports for customers on production and packaging specifications for wafer manufacturing.*
- 05/2006-12/2006 **Siemens**, Munich, Germany.
Environmental Protection and Product Safety – *Maintaining databases and assisting in administrative data processing.*

INTERNATIONAL EXPERIENCE

- 03/2011-08/2011 **Swiss Federal Institute of Technology Lausanne**, Switzerland.
M.Sc. thesis project at the Electrical Engineering faculty.
- 09/2010-01/2011 **Utrecht University**, Netherlands.
Study semester within the Mathematics and Computer Science faculty.
- 03/2008-08/2008 **Infineon Technologies**, Singapore.
Full-time industrial internship.
- 07/2004-07/2005 **EurAuPair**, USA.
Intercultural exchange program.

FELLOWSHIPS

- 03/2010-09/2011 Siemens Masters Program, Germany.
- 03/2011-08/2011 DAAD PROMOS, Germany.
- 09/2010-01/2011 ERASMUS, Germany.
- 03/2008-08/2008 InWEnt – Capacity Building International, Germany.

VOLUNTARY WORK

- 09/2011-03/2016 Committee member of the EPFL alpine club *Club Montagne* being responsible for organizing weekly rock climbing outings as well as for private club sponsorships (Mammut, Stöckli).
- 01/2006-11/2007 Mentor within the *Cascading Mentoring Project* of the University of Applied Sciences Munich. Support of female students in their first year of studies.
- 03/2007-06/2007 Teaching in a youth center *Jugendprogrammierer - Centrum München e. V* (www.jpccm.de) graphical design and computer architecture for kids.

INTERESTS

Climbing, road biking, winter sports, arts, and traveling.

Publications

Journals

Babayeva M, Kober T, Knowles B, Herbst M, Meuli R, Zaitsev M, Krueger G. (2015). Accuracy and Precision of Head Motion Information in Multi-Channel Free Induction Decay Navigators for Magnetic Resonance Imaging. In: *IEEE Transactions on Medical Imaging* 34(9):1-11.

Conferences

Babayeva M, Falkovskiy P, Hilbert T, Bonnier G, Maréchal B, Meuli R, Thiran J-P, Gruetter R, Krueger G, Kober T. (2015). Prospective motion correction with FID-triggered image navigators. In: *ISMRM*, 23:583, Toronto, Canada.

Loktyushin A, **Babayeva M**, Gallichan D, Krueger G, Scheffler K, Kober T. (2015). Retrospective rigid motion correction of undersampled MRI data. In: *ISMRM*, 23:2334, Toronto, Canada.

Babayeva M, Loktyushin A, Falkovskiy P, Kober T, Mueli R, Gruetter R, Krueger G. (2014). FID navigator triggered acquisition of imaging navigators for retrospective head motion correction. In: *ISMRM Workshop on Motion Correction*, July 11-14, Tromsø, Norway.

Babayeva M, Kober T, Granziera C, Nickisch H, Gruetter R, Krueger G. (2014). FID-guided retrospective motion correction based on autofocusing. In: *ISMRM*, 22:2227, Milan, Italy.

Babayeva M, Kober T, Herbst M, Hennig J, Seeger M, Gruetter R, Zaitsev M, Krueger G. (2013). Can Multi-Channel FID Navigators Quantify Head Motion? In: *ISMRM*, 21:306, Salt Lake City, USA.

In Preparation

Waszak M, Loktyushin A, Falkovskiy P, Kober T, Roche A, Marechal B, Granziera C, Mueli R, Gruetter R, Krueger G. Blind and FID-guided Retrospective Motion Correction Based on Autofocusing for Clinical Magnetic Resonance Images.

Waszak M, Kober T, Falkovskiy P, Roche A, Marechal B, Granziera C, Mueli R, Gruetter R, Krueger G. FID-based Motion Sensitive MR Image Quality Metric.

Waszak M, Falkovskiy P, Kober T, Marechal B, Mueli R, Gruetter R, Krueger G. Prospective Head Motion Correction with FID-Triggered Image Navigators.